C9orf72 expansion creates the unstable folate-sensitive fragile site FRA9A

Mila Mirceta[1,2], Monika H.M. Schmidt[1,2], Natalie Shum[1,2], Tanya K. Prasolava[1], Bryanna Meikle[1,2], Stella Lanni[1], Mohiuddin Mohiuddin[1], Paul M. Mckeever[3], Ming Zhang[3-6], Minggao Liang[1,2], Ilse van der Werf[7], Stefaan Scheers[7], Patrick A. Dion[8,9], Peixiang Wang[1], Michael D. Wilson[1,2], Theresa Abell[10], Elliot A. Philips[10], Łukasz J. Sznajder[11,12], Maurice S. Swanson[11], Mustafa Mehkary[1,2], Mahreen Khan[1,2], Katsuyuki Yokoi[1], Christine Jung[13], Pieter J. de Jong[13], Catherine H. Freudenreich[10], Philip McGoldrick[3], Ryan K.C. Yuen[1,2], Agessandro Abrahão[14], Julia Keith[14], Lorne Zinman[14], Janice Robertson[3], Ekaterina Rogaeva[3], Guy A. Rouleau[8,9,15], R. Frank Kooy[7], Christopher E. Pearson[1,2]*

[1] Program of Genetics & Genome Biology, Peter Gilgan Centre for Research and Learning, The Hospital for Sick Children; Toronto, Canada.

[2] Department of Molecular Genetics, University of Toronto; Toronto, Canada.

[3] Tanz Centre for Research of Neurodegenerative Diseases, University of Toronto; Toronto, Canada.

[4] The First Rehabilitation Hospital of Shanghai, Department of Medical Genetics, School of Medicine, Tongji University; Shanghai, China.

[5] Institute for Advanced Study, Tongji University; Shanghai, China.

[6] Clinical Center for Brain and Spinal Cord Research, Tongji University; Shanghai, China.

[7] Department of Medical Genetics, University of Antwerp; Edegem, Belgium.

[8] Montreal Neurological Institute, McGill University; Montreal, Canada.

[9] Department of Neurology & Neurosurgery, McGill University; Montreal, Canada.

[10] Department of Biology, Tufts University; Medford, USA.

[11] Department of Molecular Genetics and Microbiology, Center for NeuroGenetics and the Genetics Institute, College of Medicine, University of Florida; Gainesville, USA.

[12] Currently at Department of Chemistry and Biochemistry, University of Nevada, Las Vegas, NV, USA.

[13] BACPAC Resource Center, Children's Hospital Oakland Research Institute; Oakland, USA.

[14] Sunnybrook Health Sciences Centre; Toronto, Canada.

[15] Department of Human Genetics, McGill University; Montreal, Canada.

* To whom correspondence should be addressed. Tel: (647) 388-5151; Email: cepearson.sickkids@gmail.com

ABSTRACT

The hyper-unstable Chr9p21 locus, harbouring the interferon gene cluster, oncogenes and *C9orf72*, is linked to multiple diseases. *C9orf72* (GGGGCC)n expansions (*C9orf72*Exp) are associated with incompletely penetrant amyotrophic lateral sclerosis, frontotemporal dementia and autoimmune disorders. *C9orf72*Exp patients display hyperactive cGAS-STING-linked interferon immune and DNA damage responses, but the source of immuno-stimulatory or damaged DNA is unknown. Here, we show *C9orf72*Exp in pre-symptomatic and ALS-FTD patient cells and brains cause the folate-sensitive chromosomal fragile site, FRA9A. FRA9A centers on >33kb of *C9orf72* as highly-compacted chromatin embedded in an 8.2Mb fragility zone spanning 9p21, encompassing 46 genes, making FRA9A one of the largest fragile sites. *C9orf72*Exp cells show chromosomal instability, heightened global- and Chr9p-enriched sister-chromatid exchanges, truncated-Chr9s, acentric-Chr9s and Chr9-containing micronuclei, providing endogenous sources of damaged and immunostimulatory DNA. Cells from one *C9orf72*Exp patient contained highly-rearranged FRA9A-expressing Chr9 with Chr9-wide dysregulated gene expression. Somatic *C9orf72*Exp repeat instability and chromosomal fragility are sensitive to folate-deficiency. Age-dependent repeat instability, chromosomal fragility, and chromosomal instability can be transferred to CNS and peripheral tissues of transgenic *C9orf72*Exp mice, implicating *C9orf72*Exp as the source. Our results highlight unappreciated effects of *C9orf72* expansions that trigger vitamin-sensitive chromosome fragility, adding structural variations to the disease-enriched 9p21 locus, and likely elsewhere.

GRAPHICAL ABSTRACT

***C9orf72* expansion creates the unstable folate-sensitive fragile site FRA9A**

Graphical Abstract

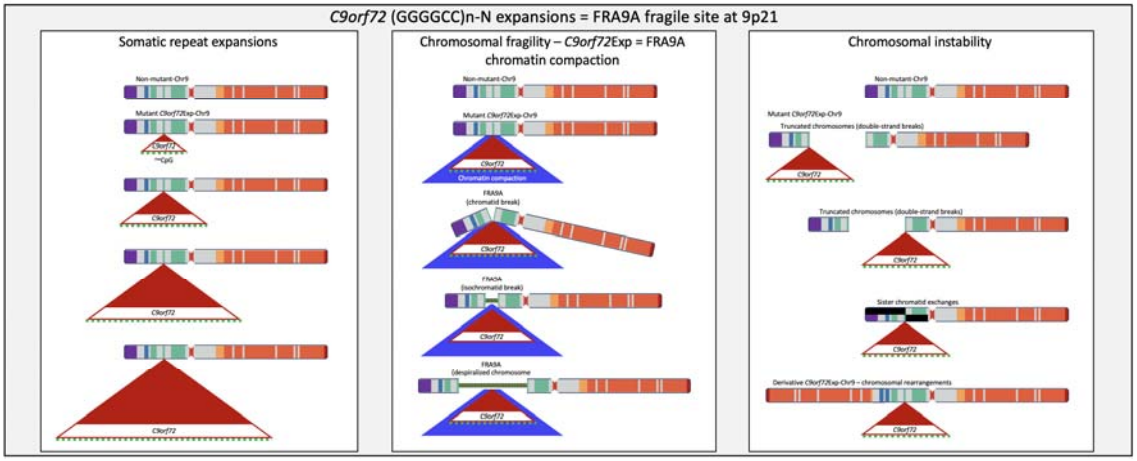

INTRODUCTION

Expansions of 30-7950 GGGGCC repeats in the *C9orf72* gene, which resides in 9p21 (*C9orf72*Exp), are the most common cause of ALS, FTD, and numerous seemingly unrelated diseases including inflammation dysregulation, autoimmune diseases, over-expression of type I *IFN* genes (1–6), and melanoma (7). Most *C9orf72*Exp carriers are asymptomatic at 40-years of age, some will develop amyotrophic lateral sclerosis (ALS), frontotemporal dementia (FTD), another co-occurring disease, or a mixture of these, while many can be disease-free into their 80s-90s (8,9). This incomplete penetrance and clinical diversity suggests the involvement of genetic and environmental modifiers and/or cumulative events.

Many studies on *C9orf72*Exp disease have focused upon the expanded repeat RNA and repeat-associated non-AUG RAN-peptides, where many model systems are devoid of the endogenous chromosomal expanded repeat. Repeat expansions downregulate *C9orf72*Exp expression leading to reduced C9ORF72 protein levels (10, 11). *St*imulator of *In*terferon *G*enes (STING), which with cGAS activates the innate immune response following sensing of cytosolic double-stranded DNA that could arise from viruses, damaged mitochondria, or damaged chromosomes leaked from micronuclei. In *C9orf72*Exp individuals, decreased C9ORF72 leads to STING-hyperactivated *IFN* expression and inflammation in vulnerable neurons (12), but the source of the immunostimulatory DNA is unknown (4, 13, 14). Accumulating evidence supports a role of an activated DNA damage response (DDR) in *C9orf72*Exp disease (15–25), yet the source of the damaged DNA is unknown. Massive post-natal inter- and intra-tissue repeat length instability is evident in post-mortem tissues of *C9orf72*Exp individuals with the largest somatic expansions in the brain (26–30). Surprisingly, there have been no prior cytogenetic or chromosomal instability studies of *C9orf72*Exp. The recent discontinued clinical programs of antisense oligonucleotides

targeting the sense-strand *C9orf72* mRNA, which successfully reduced the RAN-peptides, but resulted in no clinical benefit or trended toward greater clinical decline for the cohort, highlight our poor understanding of *C9orf72*Exp (31–36). A recent meeting focused on the post-trials path forward for *C9orf72*Exp highlighted key areas needing attention: "*Critical information in our understanding of the biology around the C9orf72 expansion is still lacking, including what molecular and cellular changes occur at presymptomatic stages…studies of genetics and lifestyles might be useful"* (31). Unknown biology of the *C9orf72*Exp has been highlighted as a focus arena (31–36). Factors that may determine disease penetrance, clinical variation, disease onset, progression and severity, are indispensable for family life decisions as well as clinical trial design (6, 9, 31, 37–41).

Genomic context is important, as *C9orf72*Exp occurs on a risk haplotype, which could influence repeat length instability, leading to reduced transcription and its retention of the intron containing the expanded GGGGCC repeat (42–45) (Fig. 1). Many of the co-occurring *C9orf72*Exp symptoms can arise independent of a *C9orf72*Exp and are associated with other 9p21 genes. For example, the type I interferon (*IFN*) cluster of 17 genes, including *IFNk* adjacent to *C9orf72*, are linked to autoimmune diseases (e.g., dysregulated inflammation, lupus, rheumatoid arthritis, diabetes, multiple sclerosis) (1, 3–5, 7). The enhancer-rich 9p21 gene desert is associated with *IFN* signaling (46, 47). *CDKN2A/B*, *EMICERI*, and *IFN*s are linked to melanoma (48), a cancer recently associated with *C9orf72*Exp (7). *LINGO2*, *TOPORS*, *APTX*, and *DNAJA1* have been associated with neurodevelopmental, neurodegenerative, and motoneuron disease (49).

The 9p21 locus is hyper-prone to various recurrent structural rearrangements (50–54) (Fig. 1). 9p deletion/duplication syndrome includes 9p21.2 as a breakpoint hotspot (55, 56). Instability in cancers is suspected to involve chromosomal fragile sites although the hyper-

unstable 9p21 has no mapped fragile site (57). “Rare” fragile sites can be present in as few as a single individual, as initially reported for FRA9A (58), to ≤5% of individuals and are linked to partially penetrant neurological disorders, as reviewed (59). Most rare fragile sites are folate-sensitive fragile sites (FSFS), induced in the absence of folate or by the antimetabolite 5-fluorodeoxyuridine (FUdR). Ten of the ~30 FSFS have been mapped to gene-specific expanded (CGG)n repeats, including FRAXA, FRAXE, FRAXF, FRA2A, FRA7A, FRA10A, FRA11A, FRA11B, FRA12A, and FRA16A. FSFS are prone to DNA breaks making them mutation hotspots — mutations that can alter clinical presentation, which is well-characterized for the CGG-expanded FRAXA/*FMR1*, reviewed in (59). Through >75 years of study, many isolated case reports, diverse mutation forms (varying CGG expansion sizes, contiguous gene deletions, gene duplications, intra- and inter-chromosomal recombination, point mutations), and *FMR1* mosaic epimutations have been identified as the cause of numerous seemingly unrelated diseases, many incompletely penetrant (59). Individual case studies with deep clinical, neuropathological and molecular phenotyping can be informative of disease etiology. Thus, instability of FSFS can impact disease manifestation and clinical presentation. Our objective was to better understand the biology of the endogenous expanded *C9orf72* repeat in the context of 9p21 in presymptomatic and disease states. We assessed whether the expanded *C9orf72* repeat, GGGGC***CGG***GGC***CGG***GGC***CGG***GGCC…, which contains the CGG-motif common to all mapped FSFS, is a FSFS.

Figure 1

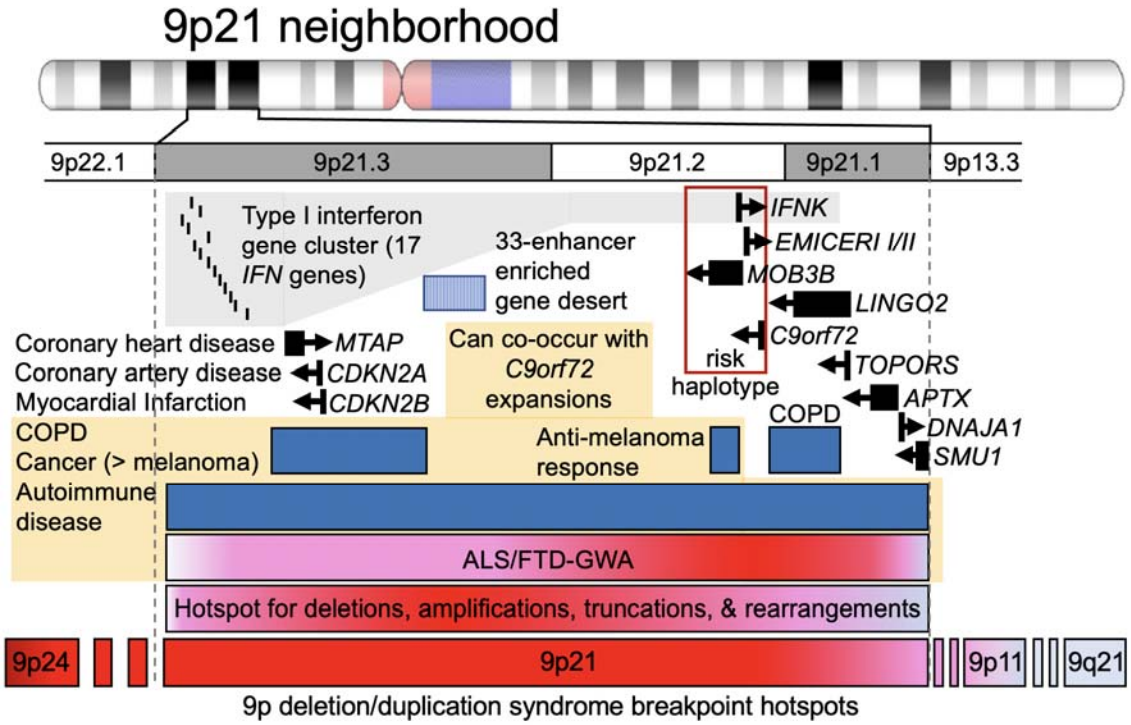

Figure 1 Legend:
The 9p21 neighborhood, associated genes, diseases, and instability hotspots. See text.

RESULTS

9p21 shares sequence and epigenetic features with (CGG)n FSFS

The *C9orf72* locus and each of the CGG-expanded FSFS share many sequence, structural, functional, and epigenetic features (Fig. 2A-D, Fig. S1A-J). Nine of the 10 CGG-FSFS plus *C9orf72* colocalize to boundaries between topologically associating domains and were enriched with CTCF sites and CpG-islands (Fig. 2D). Thus, *C9orf72* and CGG-FSFS share with 22 other disease-associated repeat expansion loci these epigenetic features (60). Unlike other disease-associated repeats, both the *C9orf72* GGGGCC and all CGG-FSFS share G4-quadruplex forming repeats (61–63).

Variations in *C9orf72* repeat expansion size, CpG-methylation, and disease state permit assessment of contribution to fragility

To study the connection between *C9orf72*Exp and fragility, we characterized lymphoblastoid cells from *C9orf72*Exp families, where some carriers were presymptomatic and some presented with ALS or ALS/FTD (Fig. 3A). Sizing *C9orf72* expansions by Southern blots shows repeat length heterogeneity within and between individuals, with expansions ranging from ~300 to ~4400 repeats (Fig. 3B, Table S1). All individuals carried (GGGGCC)2 on the non-expanded allele.

Most of our cell lines were CpG methylated in the expanded repeat, with varying levels in flanking CpG-islands, and no methylation in the non-expanded allele (Fig. 3B, Fig. S2), consistent with previous findings of aberrant methylation and levels of methylation mosaicism in *C9orf72*Exp carriers (64, 65). We found an absence of methylation, likely arising from methylation mosaicism, in cells of a presymptomatic *C9orf72*Exp (P1) and ALS-affected individuals (P7 & P8). No obvious differences were observed between cells from presymptomatic and affected *C9orf72*Exp individuals. Methylation status was stable,

consistent with longitudinally collected samples from *C9orf72*Exp carriers (66). Control cells from individuals without *C9orf72*Exp had no methylation at *C9orf72*. Thus, our *C9orf72*Exp cell line collection permitted assessing fragility in the presence/absence of methylation and with/without disease of donors (Fig. 3A, see right-hand chart).

Figure 2

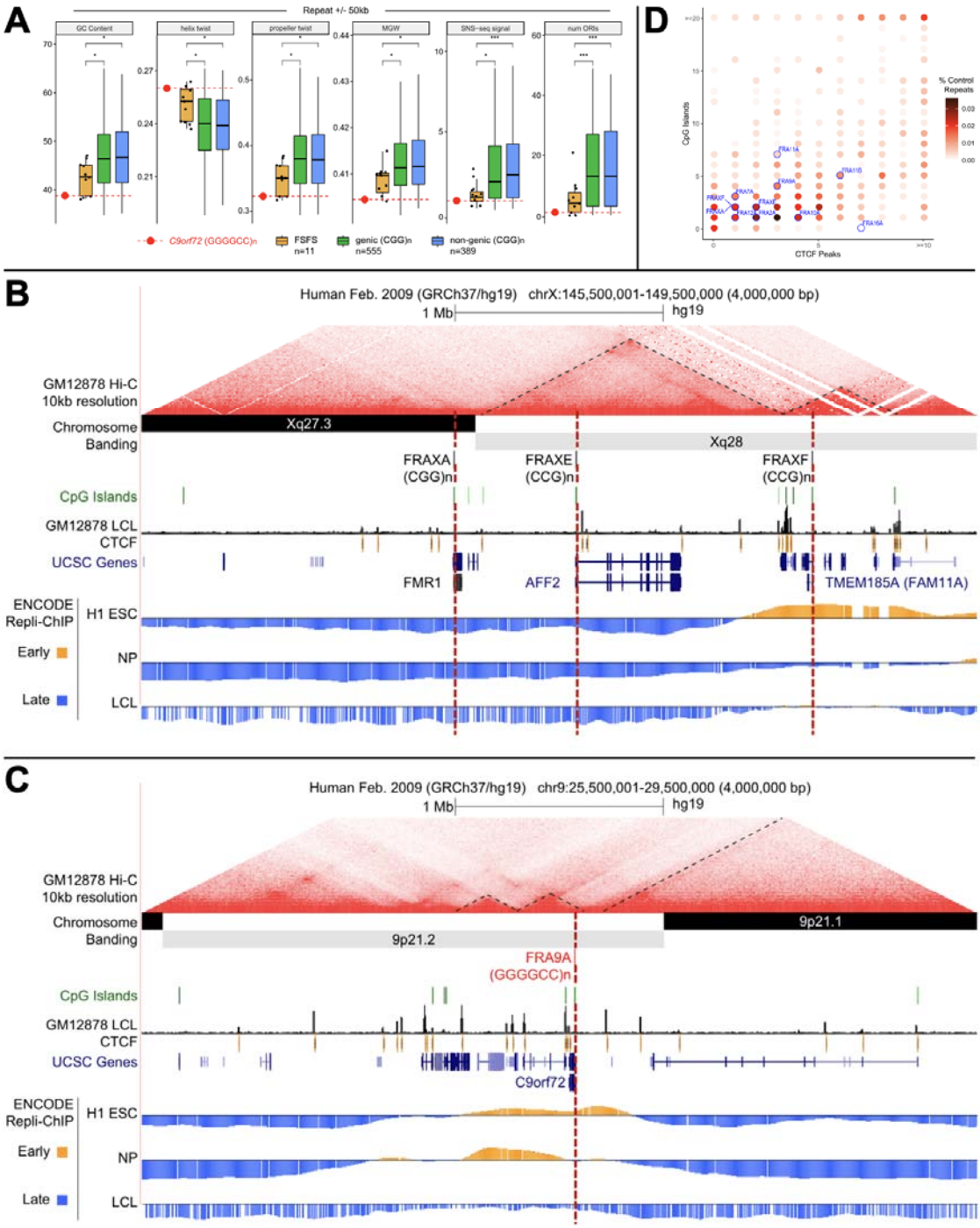
A
Repeat +/- 50kb
GC Content
helix twist
propeller twist
MGW
SNS-seq signal
num ORs
C9orf72 (GGGGCC)n
FSFS n=11
genic (CGG)n n=555
non-genic (CGG)n n=389
D
CpG Islands
CTCF Peaks
% Control Repeats
B
Human Feb. 2009 (GRCh37/hg19) chrX:145,500,001-149,500,000 (4,000,000 bp)
1 Mb
hg19
GM12878 Hi-C 10kb resolution
Chromosome Banding
Xq27.3
Xq28
FRAXA (CGG)n
FRAXE (CCG)n
FRAXF (CCG)n
CpG Islands
GM12878 LCL
CTCF
UCSC Genes
FMR1
AFF2
TMEM185A (FAM11A)
ENCODE Repli-ChIP
H1 ESC
Early
NP
Late
LCL
C
Human Feb. 2009 (GRCh37/hg19) chr9:25,500,001-29,500,000 (4,000,000 bp)
1 Mb
hg19
GM12878 Hi-C 10kb resolution
Chromosome Banding
9p21.2
9p21.1
FRA9A (GGGGCC)n
CpG Islands
GM12878 LCL
CTCF
UCSC Genes
C9orf72
ENCODE Repli-ChIP
H1 ESC
Early
NP
Late
LCL

Figure 2 Legend: DNA sequence, structure, topological associated domain (TAD), CpG island, and Repli-Chip analysis for all 10 CGG-folate-sensitive fragile sites. (A) Boxplots comparing average %GC, helix twist, propeller twist, major groove width (MGW), SNS-seq (short nascent strand sequencing) signal and number of origins of replication initiation (ORIs) at CGG/CCG-mapped FSFS and *C9orf72* versus 944 control genome-wide CGG/GGC repeats, calculated for windows +/- 50kb and +/- 500kb from the repeat center. Control repeat regions were further separated as genic or non-genic based on overlap with an annotated transcript. Median repeat length for FSFS is 8.7; all FSFS have GC content of 100% (AT=0 except FRAXF, GC=0.826). Repeat length req of >4.5 for 944 CGG/CCG control regions yieded a median length of 8.7, same as mapped FSFS. Asterix denotes significance based on a two-sided Wilcoxon test (* $p<0.05$; ** $p<0.01$). Each individual FSFS is represented as a black dot. The *C9orf72* (GGGGCC)n is represented by a red dot. (B & C) Topological domain, DNA replication timing tracks, CpG islands, and CTCF sites for the contiguous FRAXA, FRAXE, and FRAXF compared to same for *C9orf72*. Shown are the contour density plots depicting the number of CTCF sites and CpG-islands in 100 kb windows centered on the repeat, representing boundaries with normal-length, matched repeats. Repli-seq data were obtained in bigwig format (GSE61972). H1 ESC = H1 Embryonic Stem Cells; accession:ENCFF000KUF; NP = Neuronal progenitor cells (BG01 Fibroblast-derived); accession:ENCFF907YXU; LCL = GM06990 lymphoblastoid cells; accession:ENCFF000KUA. Early (positive) and late (negative) replication was determined by subtracting the genome-wide median score from all values. To conserve space, only the FSFS gene is indicated, while other UCSC genes are condensed into one line. (D) Summary of enrichment of each fragile site (indicated in blue fonts) for CpG islands and CTCF sites. Points are colored according to density. For analyses of FRA2A, FRA7A, FRA10A, FRA11A, FRA11B, FRA12A, and FRA16A see Fig. S1.

Figure 3

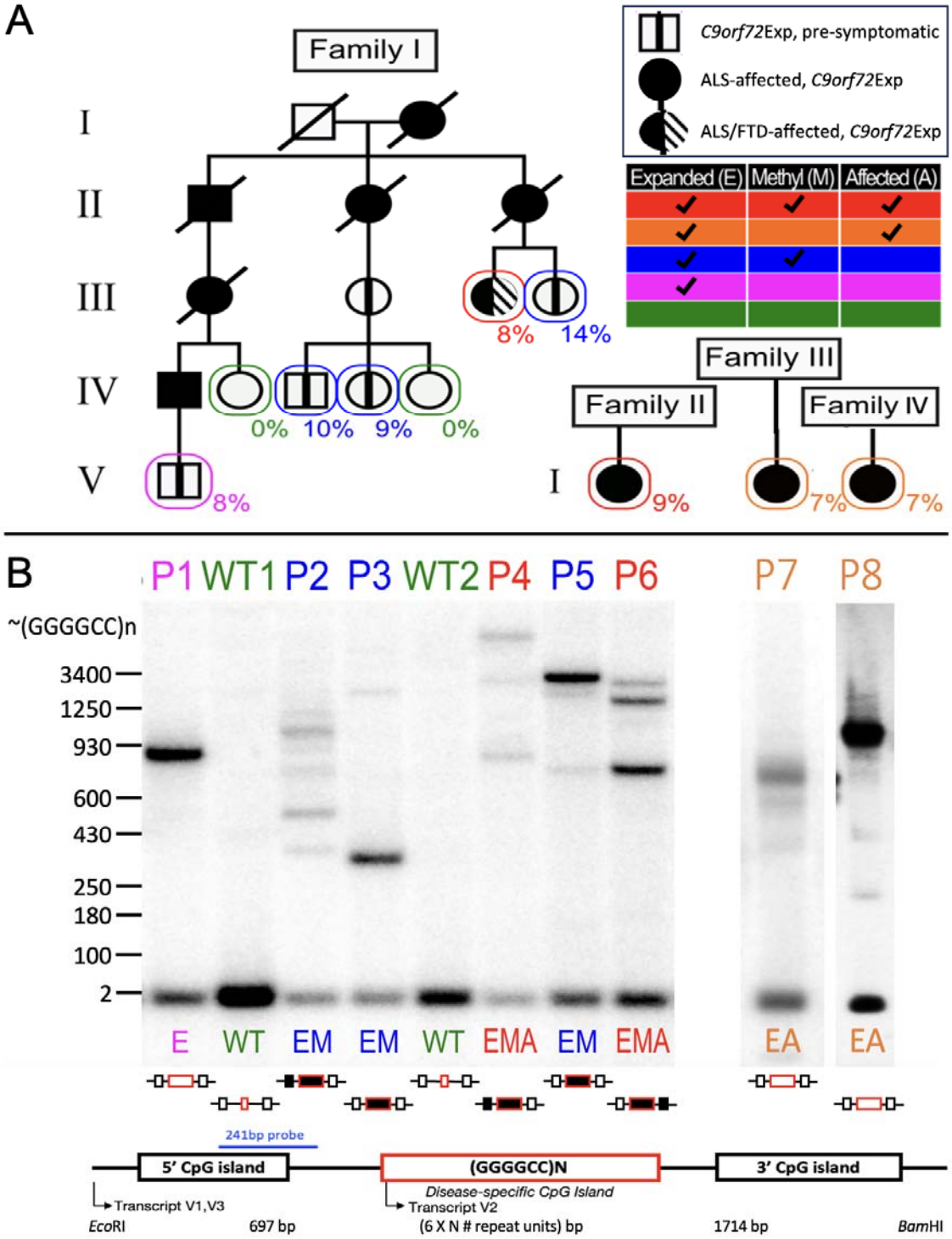
A
Family I
I
II
III
IV
V
8%
14%
0%
10%
9%
0%
8%
C9orf72Exp, pre-symptomatic
ALS-affected, C9orf72Exp
ALS/FTD-affected, C9orf72Exp
Expanded (E)
Methyl (M)
Affected (A)
Family III
Family II
Family IV
I
9%
7%
7%
B
P1 WT1 P2 P3 WT2 P4 P5 P6 P7 P8
~(GGGGCC)n
3400
1250
930
600
430
250
180
100
2
E WT EM EM WT EMA EM EMA EA EA
241bp probe
5' CpG island
(GGGGCC)N
3' CpG island
Disease-specific CpG Island
Transcript V1,V3
Transcript V2
EcoRI
697 bp
(6 X N # repeat units) bp
1714 bp
BamHI

Figure 3 Legend. *C9orf72*Exp cells, repeat lengths, CpG-methylation, and disease state.

(A) ALS/FTD families with Southern blot vertically aligned for each individual. Females are represented by circles, males by squares, disease state is as per the insert legend. Colors of text and boxes around symbols indicate the expansion, methylation, and affected status for each sample. Percentage of cells showing FRA9A expression are indicated for each individual in the pedigree. "P#" refers to patient number, "E", "M", and "A" refer to *E*xpanded, *M*ethylated, and *A*ffected, is summarized at right and this coding system is used throughout the text. Southern blot of *C9orf72* (GGGGCC)n repeat expansion (Methods) used *Eco*RI/*Bam*HI to release the repeat-containing fragment leaving 697 and 1714 bp upstream and downstream of the (GGGGCC)n/N repeat. (B) Schematic of Southern blot probe location, CpG-methylation status at the GGGGCC repeat and CpG-islands (filled boxes denote methylation). For raw CpG methylation data see Figure S2.

C9orf72 expansion is the molecular cause of a FSFS at 9p21 (FRA9A)

Fragility was assessed cytogenetically (Fig. 4A-D). FUdR-induced fragile sites were observed and localized to 9p21 by fluorescent *in situ* hybridization (FISH), in all eight *C9orf72*Exp cell lines. Fragility was only observed in *C9orf72*Exp cells, with FUdR-treatment and only on one Chr9, consistent with FRA9A (58). Fragility presented in various forms including gaps (isochromatid and chromatid), constrictions, and despiralized regions (Fig. 4A). Full metaphase spreads and zoomed-in versions, with greater resolution are available upon request. With the exception of the despiralized form, these are similar to forms of FRAXA (59). The despiralized Chr9 was similar to the despiralized heterochromatin in immunodeficiency, centromeric instability, and facial anomalies (ICF) syndrome (67). Lengthening of the despiralized FRA9A is evident when compared to the non-fragile Chr9 from the same metaphase spread (Fig. 4A, control Chr9 in lower left is from the same metaphase as the leftmost stretched FRA9A). These cytogenetic observations reveal a fragile site, FRA9A, at 9p21.

We next quantified fragility. Established FXS/FRAXA diagnostic guidelines (68, 69) dictate that fragile site frequencies of 3% or 5% within 100 metaphases yields confidence levels of 95% or 99%. Typically, FXS individuals show fragility at 3-15%, but never >50% of CGG expanded ChrXs (69, 70). We observed 9p21 fragility at 7-14% across *C9orf72*Exp cell lines (Fig. 4E). Fragility was evident in *C9orf72*Exp cells of presymptomatic and ALS/FTD-affected individuals. Chromosomal assignment and band location of fragility was confirmed by Giemsa-banding, trypsinization, and karyotyping (Fig. S3). Fragility at 9p21 was observed on only one of the Chr9 homologs in a given metaphase of any one *C9orf72*Exp cell line, consistent with each being heterozygously expanded. Fragility at 9p21 was only detected with FUdR treatment. Similar levels of fragility arose using folate-free

media (M199) as for FUdR, revealing induction by different methods of folate stress (Fig. S3A). Fragility could not be induced without *C9orf72* expansions in two control cell lines (100 metaphases each). Thus, fragility depends on folate perturbation and the presence of the expanded repeat. As few as 300 repeats (P3, 9%) could express FRA9A at similar levels as 4400 repeats (P4, 8%). The localized fragility, limited to one Chr9, in *C9orf72*Exp cells is consistent with previous FS mapping to autosomes that concluded fragility arises on the expanded allele (71, 72). We validated that the *C9orf72* repeat expansion is the molecular cause of FRA9A fragility through gene-transfer experiments (below).

We further mapped fragility using seven FISH probes spanning the outer edges of 9p21, in eight *C9orf72*Exp cell lines, >100 metaphases each, with probe signals being telomeric, spanning, or centromeric to the break (Fig. 4B, 4D & 4F). Breaks were detected across 9p21.1-9p21.3 chromosomal bands, ~8.2Mb, with ≥83% of breaks at a ~1Mb stretch of 9p21.2 encompassing *C9orf72* (Fig. 4D). Splitting of the FISH signal to both sides of the break was evident for the GGGGCC-containing probe 4, supporting that the expanded repeat causes fragility (Fig. 4C). Probes telomeric to *C9orf72* preferentially fluoresced telomeric of the break, with the same trend for centromeric probes (Fig. 4F). The telomeric boundary could be considered at probe 2, which straddles 9p21.2-9p21.3, with fluorescence both telomeric and spanning fragility. A centromeric boundary could not be defined, as probe 7 was detected telomeric, spanning, and centromeric to breaks, suggesting fragility extended centromeric of probe 7. Additional centromeric probes, being pericentromeric, hampered break detection. Thus, within the limits of FISH resolution, FRA9A maps most intensely to *C9orf72*, but has a wide zone of breakage (summarized in Fig. 4D). FRA9A's fragility core of enriched breakage includes *C9orf72* covering ~500kb (plus the repeat), spanning the *C9orf72*Exp risk haplotype, where breaks can extend ~2Mb and ~6.2Mb telomerically and

centromerically (Table 1). This makes FRA9A one of the largest fragile sites, spanning ~8.2Mb over 9p21.1-21.3, encompassing 46 genes (Table 1), similar in size to FRA1H, FRA3B, FRA4F, FRA7B, FRA9E, FRA11G, and FRAXF, spanning up to 12.2Mb over multiple chromosome bands, encompassing 10-110 genes (Table 1) (73–82). Moreover, CpG-methylation of *C9orf72*Exp was not required, as fragility was observed in cells +/- methylation (Fig. 4E). Thus, neither symptomatic state of blood donors nor CpG-methylation were required for FRA9A expression. That we detected FRA9A fragility at 9p21 in *C9orf72*Exp, lymphoblastoid cells, confirms previous observations that FRAXA expression was similarly detected lymphoblastoid cells as in freshly-collected peripheral blood lymphocyte cultures (83). Thus, FRA9A and FRAXA are distinct from the fragility at 11q23, which depends upon the EBV encoded protein EBNA1 (84–87).

Figure 4

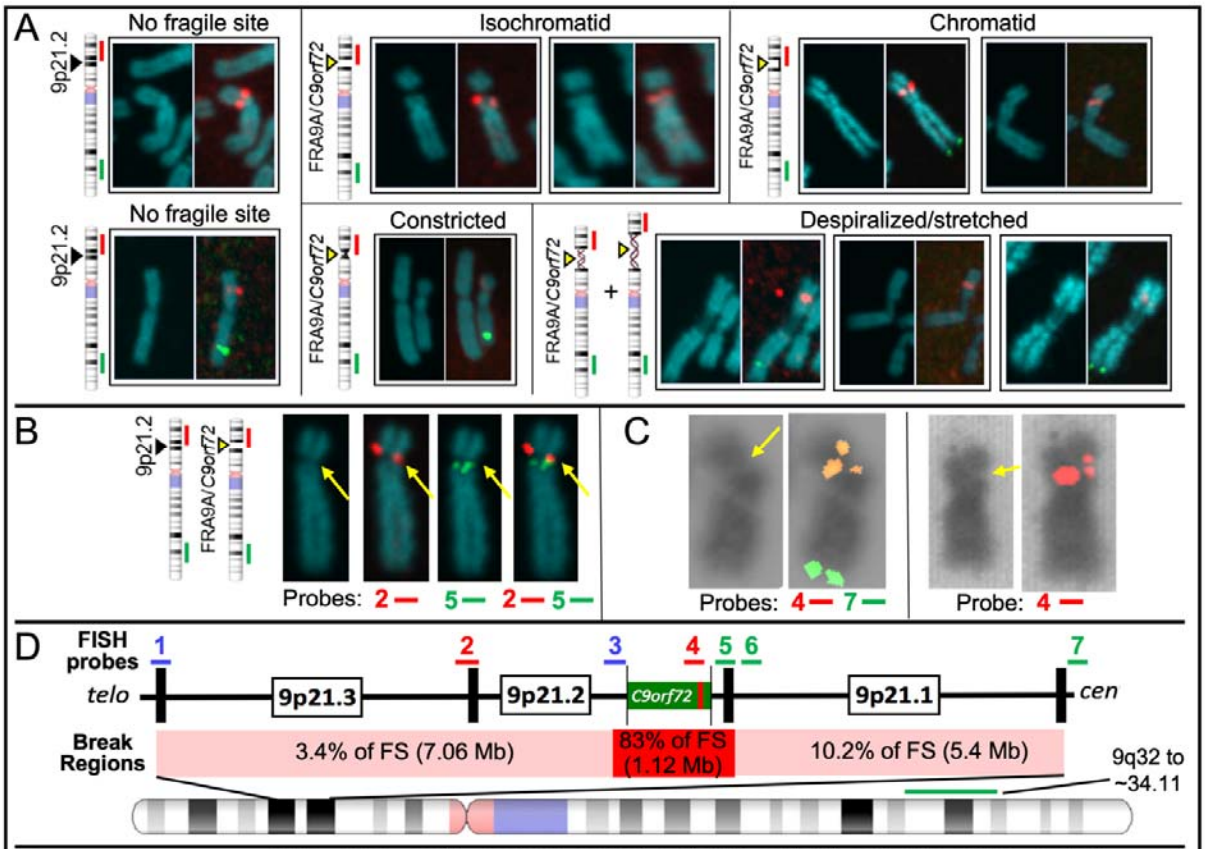

E

		WT1	WT2	P1 (E)	P2 (EM)	P3 (EM)	P4 (EMA)	P5 (EM)	P6 (EMA)	P7 (EA)	P8 (EA)	
0.1 µM FUdR		0%	0%	8%*	10%*	9%*	8%*	14%*	9%*	7%*	7%*	
Folate-free 199 media					7.5%*		10%*					
Break type	Gap/break	-	-	4	6	2	4	8	5	2	4	48.6%
	Constriction	-	-	1	2	3	4	5	2	2	3	30.6%
	Stretched	-	-	3	2	4	0	1	2	3	0	20.8%

*Confidence interval of 99%, following FXS diagnostic recommendations (Hecht F & Sutherland GR, 1984, *ClinGenet*. **26**, 301-303; Veenema H, *et al.*, 1988, *ClinGenet*. **33**, 410-417), assessing ≥100 metaphases per sample.

F

	Probe 1 RP11-15P13	Probe 2 RP11-274I21	Probe 3 RP11-1149M23	Probe 4 (GGGGCC)n RP11-491J7	Probe 5 RP11-945G22	Probe 6 RP11-1079P2	Probe 7 RP11-360B21
Centromeric	0	0	0	0	9	3	8
Spanning	0	1	3	5	8	2	6
Telomeric	2	24	29	4	10	1	3
TOTAL:	2	25	32	9	27	6	17
% Telomeric	100% (2/2)	96% (24/25)	91% (29/32)	44% (4/9)	37% (10/27)	17% (1/6)	18% (3/17)

Figure 4 Legend: *C9orf72*Exp causes FRA9A folate-sensitive fragile site that maps across 9p21.

(A) Fragile site forms (indicated), with examples of non-fragile chromosomes from the same metaphase spreads. Showing DAPI-stained and paired FISH-probed chromosomes from FUdR-treated cells. 9q-arm FISH probe (9q32~34.11; RP11-696J10) in green. FISH probe #2 at *C9orf72* (panel D-F) in red. Magnification is the same for all chromosome images within each panel, facilitating comparison within the panel. Control Chr9 in upper left of panel A is from the same metaphase as the leftmost isochromatid Chr9. Full metaphase spreads can be provided upon request. Notably, the control "No fragile site" Chr9 in lower left of panel A is from the same metaphase as the leftmost "Despiralized/stretched" Chr9, revealing the lengthening of the stretched Chr9. (B) Representative example of the same chromosome (same magnification) with or without indicated FISH probes. (C) Two representative examples (same magnification) of isochromatids with FISH signal of *C9orf72*-containing probe 4 split over the fragile site. (D) 9p21 location of FISH probes with regional summary of fragile site location. (E) Quantification of fragility for 100 metaphases under two folate-stressed conditions. (D) Cells were described in Figure 3. (F) Fragile site breakage regions calculated from number of breaks relative to FISH signal found centromeric, telomeric, or spanning across probes used. Percentage of telomerically located FISH signal relative to the break is on the bottom row. Frequencies of probes found spanning or on each side the break were used to calculate the percent breakage within each region in panel D.

Table 1: Large fragile sites with variably located fragility cores (increased breakage) and gene numbers

Fragile site	location	fragility size	fragility core size	core location	# genes*	schematic; ▬ = 1 Mb (TEL … CEN)	citation
FRA1H	1q41-42.1	10 Mb	4 Mb	asymmetric	49		75
FRA3B	3p14.1-14.2	4 Mb	500 kb	asymmetric	24		77
FRA4F	4q22	7 Mb	4 Mb	broad	12		76
FRA7B	7p21.3-22.3	12.2 Mb	5 Mb	asymmetric	79		73
FRA9E	9q32-33	9.8 Mb	5 Mb	broad	63		74
FRA9A	9p21	8.2 Mb + repeats**	500 kb + repeats**	asymmetric	46		this study
FRA11G	11q23.3	4.5 Mb	2.32, 1.37 Mb	broad	38		78
FRAXA	Xq27.3	20-600 kb + repeats**	20 kb + repeats**	centric	10		79, 80
FRAXF	Xq27-q28	1-2.5 Mb + repeats**	1 Mb + repeats**	asymmetric	110		81, 82

*The number of genes in the fragile region was determined for protein-coding genes as of 01-2024 as per FISH probes used.

**Schematic of FRA9A, FRAXA, and FRAXF is shown with (GGGGCC)4000, (CGG)900, and (CCG)600 repeats, respectively (red bars).

fragile
fragility core
dispersed fragility
repeat

_C9orf72_Exp allele assumes a compact chromatin conformation, which is enhanced by expansion size and CpG-methylation

Since constricted fragile sites on metaphase chromosomes may be the result of localized unusual chromatin condensation, we next determined whether the mutant *C9orf72*Exp locus assumes an unusual chromatinized state relative to the non-mutant allele using micrococcal nuclease (MNase) accessibility, which is widely used as an indication of regional chromatin compaction. We were able to electrophoretically resolve MNase accessibility on the mutant from the non-mutant alleles by Southern blotting. MNase can directly reveal both inaccessible and accessible regions for each allele, while sequencing-based methods of chromatin accessibility, like ATAC-seq, must impute inaccessibility and cannot resolve alleles. Permeabilized cells were exposed to MNase, which preferentially cuts DNA between nucleosomes; DNA was de-proteinized, isolated, restriction digested releasing the repeat-containing fragment, electrophoretically resolved, and detected by Southern blotting (Fig. 5A-B, blue probe). Over-digestion by MNase to mono-, di-, and tri-nucleosome sized DNA fragments was evident by ethidium staining (Fig. 5C, left panel). A striking resistance to MNase accessibility is seen exclusively for the *C9orf72*Exp allele, contrasting the non-expanded allele, which serves as an internal equimolar control, completely degraded at low MNase concentrations (Fig. 5C, compare lanes 4 & 5). The expanded allele resisted digestion at much higher MNase concentrations (Fig. 5, compare lanes 5-10). MNase resistance extended beyond the expansion into the flanking regions of the mutant allele. Increasing concentrations of MNase (>50 Units) led to partial and progressive degradation of the expanded allele to a distinct shorter size, losing ~1 kb of flanks from the full-length *Eco*RI-*Bam*HI restriction fragment, which subsequently digested the probed region (Fig. 5C, schematic). Conversely, on the non-mutant allele, the same flanking regions and non-

expanded repeat were completely digested at low MNase concentrations, along with the rest of the genome (<10 Units, Fig. 5C, lanes 5-10). The poor digestion of the *C9orf72*Exp mutant allele relative to the internal sequence control of the equimolar non-mutant allele, strongly suggests the formation of an unusual chromatinized state of the mutant *C9orf72* allele. Control experiments confirmed that the inaccessibility of MNase to the *C9orf72*Exp allele was due to its chromatinized state, and not due to an inherent inability of MNase to cleave the expanded non-chromatinized (GGGGCC)n sequence (Fig. S4A & S4B, Methods). Six cell lines showed MNase resistance of the *C9orf72*Exp allele, regardless of presymptomatic or symptomatic state of the blood donors (Fig. 5C-E).

Mapping the boundaries of MNase-resistance using multi-probe and multi-restriction digests revealed the extent and distribution of MNase inaccessibility over the *C9orf72*Exp allele. Maximal MNase resistance spanned a total of >33kb for an allele with 4400 repeats (P4), with MNase inaccessibility extending ~3300bp upstream and ~3700bp downstream of the repeat (summarized in Fig. 5A to scale, Fig. S4C, see Methods). Mapping in six *C9orf72*Exp cell lines showed little variation of the absolute boundaries of MNase inaccessibility with expansion size or presence of disease. Together, these data confirm that the *C9orf72*Exp allele assumes a large region of compact chromatin. Maximal MNase inaccessibility covers the upstream CpG-island, the *C9orf72* promoter, transcription start sites (sense and anti-sense), the expanded repeat, cryptic splice sites C1-4, the downstream CpG-island, beyond exon 2, and falls within FRA9A's fragility core.

Repeat length and CpG-methylation enhanced MNase-resistance. Analysis of a cell line that harbored a mosaic heterogenous mixture of expansion sizes ranging between ~300–4400 repeat units demonstrated that repeat expansion size directly correlates with MNase resistance (Fig. 5D, P4). Longer expansions were more resistant to MNase than shorter

expansions, which were more resistant than the non-expanded alleles (Fig. 5D, lanes 3 & 4, quantified in Fig. 5D). CpG-methylation exacerbated inaccessibility. Two cell lines with similar expansion sizes (~770 repeats) with or without aberrant methylation at the mutant *C9orf72* (P6 [isolated single cell clone] and P7, respectively) showed that methylation further enhanced MNase resistance of the expanded allele (Fig. 5E, S4A-iii). Larger expansions and methylation enhance chromatin compaction of the *C9orf72* locus.

We assessed chromatin compaction of post-mortem brains of two *C9orf72*Exp individuals, previously deep-phenotyped for lifestyle choices, clinical, neuropathological, molecular and genetic biomarkers (29, 88). One was a 90-year old male asymptomatic for ALS or FTD, with a distinct ~70 repeats in blood, no signs of neurodegeneration, overexpression of *C9orf72*/C9ORF72, and devoid of TDP-43 neuropathology (summarized in Table S2). The other was his daughter with 300-3000 repeats in blood who had ALS at age 57 and died at 59 and autopsy showing neurodegeneration and TDP-43 inclusions (29) (detailed in Table S2). The asymptomatic father had a striking heterogenous mosaic range of 13-3500 and 13-1500 repeats in the frontal cortex and cerebellum, respectively, with CpG-methylation likely triggered by large (>70 repeats) expansions (Fig. 5F, lanes 0). In contrast, the affected daughter showed very large distinct expansions of mostly ~4400 and ~1600 CpG-methylated repeats in the frontal cortex and cerebellum, respectively, where the intensity of the expansions matched that of the non-expanded allele (Fig. 5F, lanes 0). Chromatin was MNase inaccessible on only the expanded *C9orf72* alleles in both brain regions of both individuals, while the non-expanded (GGGGCC)2 allele was rapidly digested by MNase (Fig. 5F). MNase inaccessibility for both individuals appeared more severe in the cerebellum relative to the frontal cortex, which contrasts the expectation that the longer expansions in the frontal cortex would make it more MNase resistant, but may reflect the longer expansions and/or the

increased levels of deacetylated and trimethylated histone modifications in the frontal cortex over the cerebellum, relative to the acetylated histones on the non-expanded allele of *C9orf72*Exp carriers (89). The shorter expansions in the father's brain were more MNase sensitive than the larger expansions. Quantifying MNase inaccessibility between asymptomatic and symptomatic brains is hampered by the repeat length variations they presented, which we have shown to affect chromatin accessibility (Fig. 5D). Expression of the *C9orf72* transcript in the asymptomatic *C9orf72*Exp father was dramatically increased 2.5-7-fold in the frontal cortex, cerebellum, spinal cord, blood, and four other tissues compared to the affected daughter's tissues, whose *C9orf72* levels were twice less than an individual devoid of expansions (29, 88). We suggest that the increased transcription in the father's brain arose from the shorter range of expansion sizes (13-1200 repeats) which were less MNase resistant than the longer expansions, which is consistent with both the over expression in the father's blood, which contained predominantly 70 repeats, and with the low transcription in the daughter's brain that contained only very large expansions. This interpretation is consistent with the 2.5-5-fold increased expression of intermediate *C9orf72* repeats in human brains, blood, and knockin iPSC-derived neural progenitor cells (66, 90). This parallels the 5- to 10-fold increased expression from the premutation CGG expansions at the *FMR1* repeat in hemizygous males, which also show compact chromatin (91, 92). We conclude that *C9orf72* expansions and flanks assume a highly compact chromatin in cells and brain regions of *C9orf72*Exp carriers. MNase resistance is evident on *all C9orf72*Exp alleles in a given sample, which differs from the 7-14% of *C9orf72*Exp cells cytogenetically showing FRA9A-Chr9s, like FXS, only a portion of the CGG-expanded ChrXs show FRAXA (69, 70). In this manner, MNase resistance might be considered a proxy for fragility. Towards assessing whether MNase resistance was linked to the unusual chromatin compaction of cytogenetic fragility or merely linked to expanded repeats, we assessed the

MNase accessibility of the *HTT* locus in Huntington's disease patient cells with $(CAG)_{21/180}$, which is known to not be a cytogenetically detectable fragile site (93). MNase treatment and Southern blotting resolved the mutant and non-mutant *HTT* alleles and both showed the same MNase accessibility when most of the genome was sensitive (Fig. S5, lanes 3-5), suggesting that MNase inaccessibility does not extend to this non-fragile mutant locus. As part of another study, we extended the MNase inaccessibility to the CGG-expanded *FMR1* gene the molecular cause for the fragile site FRAXA. We find MNase resistance of only the CGG expanded allele (in cells from male and female carriers of the CGG expansion) (not shown). That the CGG expanded *FMR1*, which forms FRAXA, but not the non-fragile CAG expanded *HTT*, forms an MNase resitant region supports our suggestion that MNase inaccessibility of the *C9orf72*Exp can be considered a proxy for chromosomal fragility. We suggest that the MNase resistance of the *C9orf72*Exp locus in human brains is a reflection of chromosomal fragility (Fig. 5F).

Figure 5

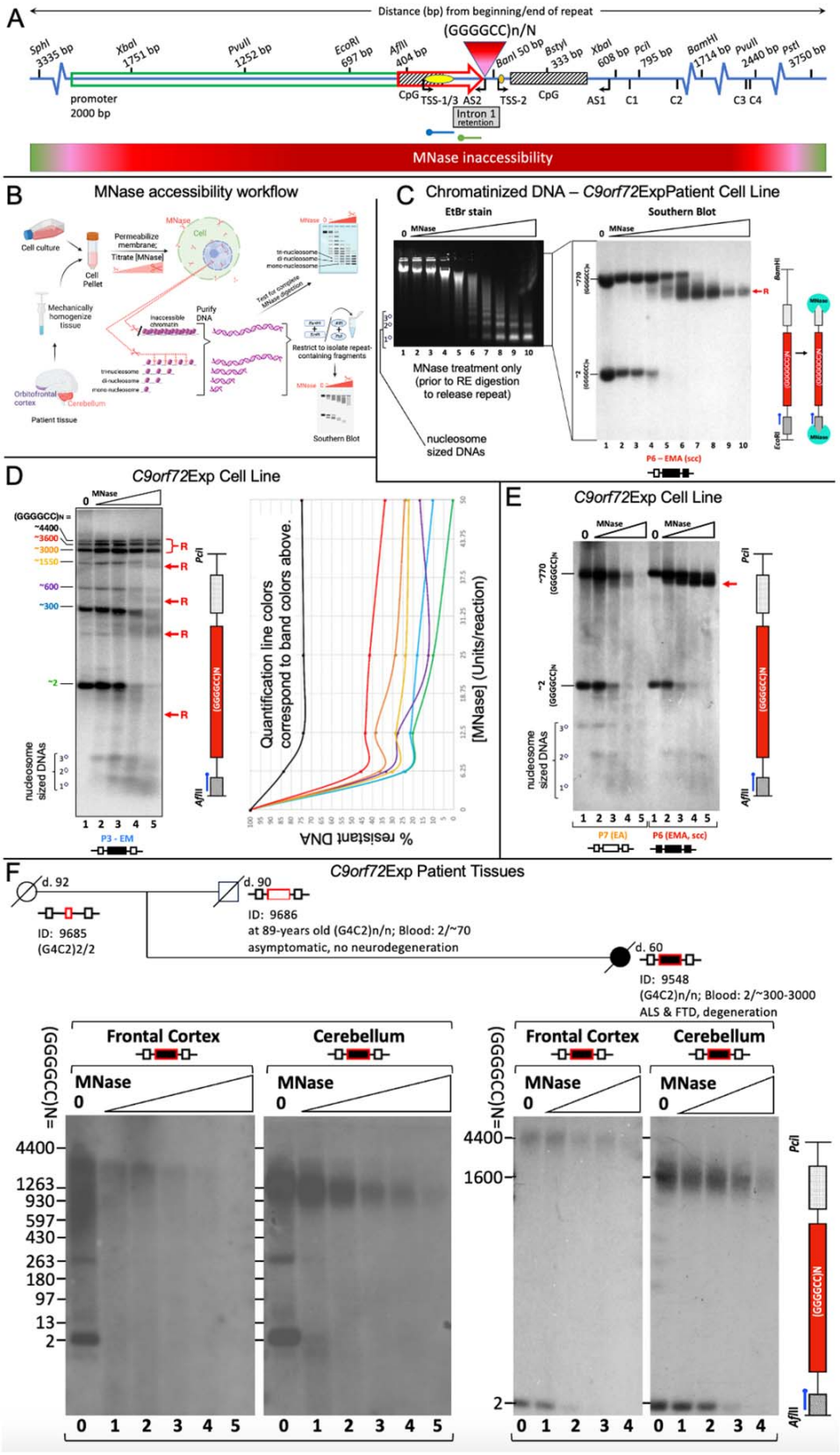
A
Distance (bp) from beginning/end of repeat
(GGGGCC)n/N
SphI 3335 bp
XbaI 1751 bp
PvuII 1252 bp
EcoRI 697 bp
AflII 404 bp
BanI 50 bp
BstyI 333 bp
XbaI 608 bp
PstI 795 bp
BamHI 1714 bp
PvuII 2440 bp
PstI 3750 bp
promoter 2000 bp
CpG
TSS-1/3
AS2
TSS-2
CpG
AS1
C1
C2
C3 C4
Intron 1 retention
MNase inaccessibility
B
MNase accessibility workflow
Cell culture
Cell Pellet
Permeabilize membrane; Titrate [MNase]
Mechanically homogenize tissue
Orbitofrontal cortex
Cerebellum
Patient tissue
Inaccessible chromatin
Purify DNA
Test for complete MNase digestion
Restrict to isolate repeat-containing fragments
Southern Blot
C
Chromatinized DNA – C9orf72ExpPatient Cell Line
EtBr stain
Southern Blot
MNase treatment only (prior to RE digestion to release repeat)
nucleosome sized DNAs
P6 – EMA (scc)
D
C9orf72Exp Cell Line
(GGGGCC)N =
~4400
~3600
~3000
~1550
~600
~300
~2
nucleosome sized DNAs
P3 - EM
Quantification line colors correspond to band colors above.
% resistant DNA
[MNase] (Units/reaction)
E
C9orf72Exp Cell Line
~770 (GGGGCC)N
~2 (GGGGCC)N
nucleosome sized DNAs
P7 (EA)
P6 (EMA, scc)
F
C9orf72Exp Patient Tissues
d. 92
ID: 9685
(G4C2)2/2
d. 90
ID: 9686
at 89-years old (G4C2)n/n; Blood: 2/~70
asymptomatic, no neurodegeneration
d. 60
ID: 9548
(G4C2)n/n; Blood: 2/~300-3000
ALS & FTD, degeneration
Frontal Cortex
Cerebellum
MNase
(GGGGCC)N =
4400
1263
930
597
430
263
180
97
13
2
1600
0 1 2 3 4 5
0 1 2 3 4

Figure 5 Legend: *C9orf72*Exp locus is MNase-inaccessible.

(A) Schematic of the region of unusual chromatin organized as determined by MNase accessibility analysis in *C9orf72*-ALS patient cells and brain regions. *C9orf72* (GGGGCC)n-N repeat, CpG-islands (hatched boxes), long-2kb and intermediate 435bp promoters (green and red arrows, respectively), exons 1a (yellow dot) and 1b (orange dot), sense and antisense transcription start sites, restriction sites with distances from the beginning and end of the (GGGGCC)N tract, and probes for upstream (green) and downstream (blue) mapping of MNase accessibility. Cryptic splice site transcripts C1-C4 derived from the *C9orf72*Exp allele are indicated with their distance from the end of the repeat tract (42, 45). (B) Workflow for MNase assay. (C) MNase treatment of chromatinized DNA from a cell line (P6) with a large methylated *C9orf72*Exp that had undergone single-cell cloning (scc) to isolate a single expanded allele, ensuring a single expansion size and facilitating clarity. Ethidium bromide (EtBr) staining of the MNase-treated DNA reveals over-digestion of the DNA to mono-, di-, tri-nucleosomal, sized fragments. The same DNA was digested with *Eco*RI/*Bam*HI, to release the repeat fragment having 697 bp upstream and 1714 bp downstream of the repeat, then assessed by Southern blotting using the blue probe. Resistance of only the expanded allele occurs, even at high concentration of MNase (200U). Red "R" indicates the region with reduced MNase accessibility that is about to lose the probed region indicated in the schematic at right. (D) Sample P3 with a mixture of heterogeneous repeat allele lengths shows that with increasing repeat size, MNase accessibility is decreased, as quantified by densitometric analysis for each allele size (colours coordinate between graph and Southern blot). In panels D-F the repeat was released with *Afl*II/*Pci*I, leaving 404 bp upstream and 689 bp downstream allowing increased resolution. NB, van Blitterswijk uses *Xba*I/*Xba*I to release the repeat, leaving 1751 bp upstream and 608 bp downstream of the repeat, the greater amount of flanking sequence reduces electrophoretic resolution. (E) Methylation is associated with increased MNase inaccessibility as assessed in cell lines (P6 (ssc) and P7) containing similar sized repeats but differing methylation status. The non-expanded allele is digested at the same rate in both lines. (F) MNase treatment of post-mortem (orbito)frontal cortex and cerebellum from an asymptomatic 90-year-old father and his ALS-FTD-affected daughter, previously deep-phenotyped for lifestyle choices, clinical, neuropathological, and molecular biomarkers (29, 88) (summarized in Table S2). MNase concentrations are doubled between each lane (2.5U in lane 2 up to 40U). Expanded allele in both tissues is MNase resistant relative to the equimolar non-expanded allele, which serves as an internal control. See Figure S4 for MNase controls and mapping experiments.

Increased Chr9-containing micronuclei in *C9orf72*Exp cells

Micronuclei (MN) are indicators of chromosomal double-strand breaks (DSBs) including fragile sites (94–97), where MN often harbor broken chromosomes to be eliminated or reintegrated. Nuclear buds (NBuds) are chromatin-containing protrusions linked to the nucleus by a nucleoplasmic stalk (95, 97). Both MN and NBuds can arise from chromosome breaks. NBuds can become MN (95). These subnuclear structures can be enriched with tandem gene amplifications and satellite repeats (67, 98, 99). Cytoplasmic release of MN DNA triggers an immune response via DNA sensing by cGAS-STING that activates *IFN* expression (94), a pathway hyperactivated in vulnerable neurons of *C9orf72*Exp carriers (4, 12–14). Given these connections, we assessed MN and NBuds and whether they contained Chr9 in *C9orf72*Exp cells. *C9orf72*Exp cells showed elevated MN/NBud levels compared to control cells, which were further increased with folate stress (Fig. 6A). More NBuds over MNs contained Chr9 in *C9orf72*Exp cells compared to control cells. The modest increase in MN with Chr9 could be due to loss of fragile chromosome-containing MN during folate-perturbation, as suggested for FRAXA cells (Fig. 6B) (100, 101). Depending upon whether the breakpoint is centromeric or telomeric of *C9orf72*, the presence of the *C9orf72*-containing FISH signal alone or the 9q-arm FISH signal alone, supports subnuclear inclusion of an acentric or truncated Chr9, respectively, while the presence of both *C9orf72*- and q-arm signals supports the inclusion of truncated Chr9 or the full-Chr9 (Fig. 6B). An absence of either FISH signal could reflect an absence of any Chr9, or an acentric Chr9 broken telomeric of *C9orf72*. When Chr9 signals were present in MN/NBuds, the proportion of the *C9orf72* signal alone, 9q-arm alone, or the two together occurred at 1:1:5, respectively. Increased Chr9-containing MN/NBuds were evident in *C9orf72*Exp cells of presymptomatic and

symptomatic individuals. Cumulatively, these data support increased chromosomal damage in *C9orf72*Exp cells.

We also observed increased nuclear blebs (NBlebs) in *C9orf72*Exp compared to control cells (Fig. 6A). NBlebs are chromatin-containing nuclear herniations (95, 97, 102, 103), without an obvious constriction between the nucleus and the protruding nuclear material. NBlebs may in some instances lead to NBuds, which may lead to MN (95). NBlebs are hallmarks of the DNA damage accumulating progeroid syndromes and can be enriched with genomic regions with perturbed chromatin and DNA damage (γH2AX) (102–106). In *C9orf72*Exp cells, NBlebs contained Chr9 at higher levels than in cells without expansions (Fig. S6A), which is consistent with reports of NBlebs being enriched with regions having altered chromatin compaction and damaged DNA (102–104).

421 **Figure 6**

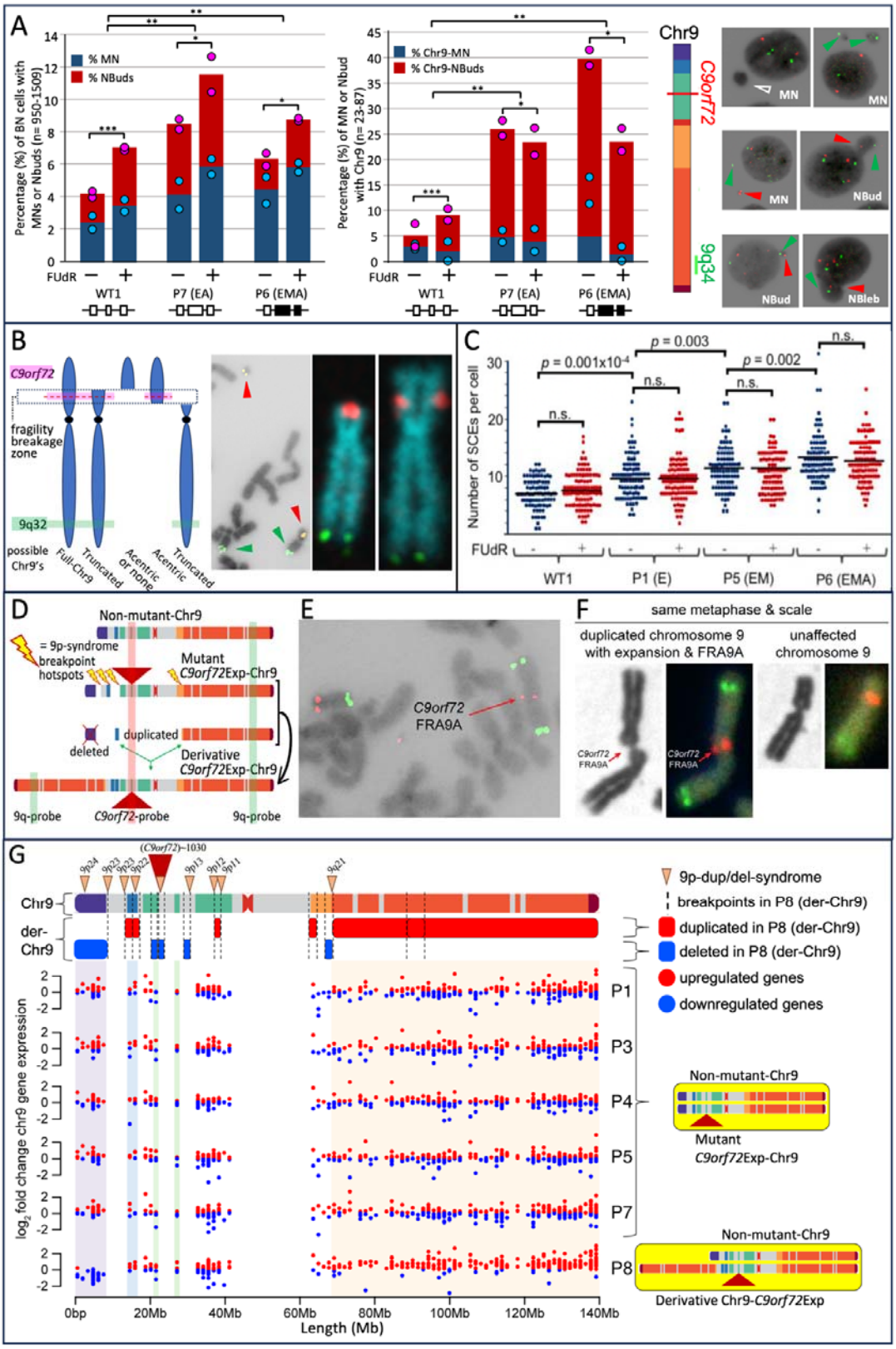
A
% MN
% NBuds
Percentage (%) of BN cells with MNs or Nbuds (n= 950-1509)
FUdR
WT1
P7 (EA)
P6 (EMA)
% Chr9-MN
% Chr9-NBuds
Percentage (%) of MN or Nbud with Chr9 (n= 23-87)
Chr9
C9orf72
9q34
MN
NBud
NBleb
B
C9orf72
fragility breakage zone
9q32
possible Chr9's
Full-Chr9
Truncated
Acentric or none
Acentric
Truncated
C
Number of SCEs per cell
p = 0.001x10-4
p = 0.003
p = 0.002
n.s.
FUdR
WT1
P1 (E)
P5 (EM)
P6 (EMA)
D
Non-mutant-Chr9
= 9p-syndrome breakpoint hotspots
Mutant C9orf72Exp-Chr9
duplicated
deleted
Derivative C9orf72Exp-Chr9
9q-probe
C9orf72-probe
9q-probe
E
C9orf72
FRA9A
F
same metaphase & scale
duplicated chromosome 9 with expansion & FRA9A
unaffected chromosome 9
C9orf72
FRA9A
G
(C9orf72)-1030
9p24
9p23
9p22
9p13
9p12
9p11
9q21
Chr9
der-Chr9
9p-dup/del-syndrome
breakpoints in P8 (der-Chr9)
duplicated in P8 (der-Chr9)
deleted in P8 (der-Chr9)
upregulated genes
downregulated genes
log2 fold change chr9 gene expression
P1
P3
P4
P5
P7
P8
Non-mutant-Chr9
Mutant C9orf72Exp-Chr9
Non-mutant-Chr9
Derivative Chr9-C9orf72Exp
0bp
20Mb
40Mb
60Mb
80Mb
100Mb
120Mb
140Mb
Length (Mb)

Figure 6 Legend: *C9orf72*Exp cells display chromosomal instability.

(A) Quantification of micronuclei (MN) and nuclear buds (NBud) in binucleated cells without FISH, left, and with *C9orf72* and 9q-FISH probes, middle, in WT and *C9orf72*Exp cells (P6 (ssc) and P7) containing similar sized repeats (~770) but differing methylation status. Data are means of two independent experiments. Dots show data of each experiment. Statistical analyses using Fisher's exact test (*P<0.05, **P<0.01, ***P<0.001). Representative images of MN and NBuds in cytokinesis-blocked cells treated with FUdR for 24 hours, that contain no FISH signal (hollow arrows), a *C9orf72*-signal (red arrows), or 9q-signal (green arrows). (B) Depending upon site of breakage, *C9orf72*-FISH probes can have varying interpretations, left. Example of *bona fide* chromosome breaks in *C9orf72*Exp line P4 with acentric terminal *C9orf72*-containing fragment in same metaphase spread as a truncated-Chr9 that is free of *C9orf72*-signal, middle. Example of truncated-Chr9 with *C9orf72*-signal, and control Chr9 from same spread, right. (C) Levels of global sister chromatid exchanges (SCEs) in WT and *C9orf72*Exp cells +/-FUdR. Methylation/clinical status is as per Figure 3. Each datapoint represents a single metaphase. At least 100 mitotic cells were analyzed per condition in each experiment. Statistical analyses were performed by student's t-test (P<0.01). NS: not significant. See also Figure S5B-E. (D) *C9orf7*Exp line P8 with complex highly rearranged derivative-Chr9, schematic, see text and Figure S7A. (E) Example of FRA9A-expressing derivative-Chr9 and control Chr9 in same spread with *C9orf72*- (red) and 9q-FISH probes (green) (100%=100/100 metaphases). (F) Only the derivative-Chr9 expresses FRA9A coincident with the *C9orf72*-FISH signal, revealing derivative-Chr9 to be the *C9orf72*Exp-Chr9, (+FUdR, 7%=7/100, 99% confidence). (G) Breakpoint analysis (top) and gene expression (binned/gene) along Chr9 in each of the *C9orf72* Exp cells with trisomic (red dots) and monosomic (blue dots) in duplicated and deleted regions of the derivative-Chr9 (P8). Breakpoint and copy number change analysis in P8 was by whole genome sequencing, see Table S3. An interactive html file detailing mis-expressed genes can be accessed here: https://data.cyverse.org/dav-anon/iplant/home/ljsznajder/FRA9A/Chromosome9.html), also presented in Table S4. See Figure S7B-D for statistical significance of differential gene expression.

***C9orf72*Exp and double-strand breakage**

Direct support that fragile sites are prone to DNA breakage is the cytogenetic manifestation of a truncated chromosome or acentric chromosome fragment broken at the fragile site (107, 108). We observed truncated Chr9s broken at 9p21, where the truncated p21→pter acentric arm, containing the *C9orf72*-FISH signal, remained within the *same* metaphase spread (Fig. 6B). We observed numerous instances of truncated Chr9s with the *C9orf72* signal at the broken end, in the absence of their acentric p21→pter acentric arms, which had likely been lost. 9p21-truncated Chr9s without *C9orf72*-signal were also observed, consistent with FRA9A's broad ~8.2Mb breakage zone (Fig. 6B, see truncated Chr9 broken centromeric and telomeric of the *C9orf72*-FISH signal). Our cytogenetic findings, coupled with the increased Chr9-containing MN/NBuds, is convincing evidence that double-strand DNA breaks occur at FRA9A, consistent with the γ-H2AX foci in cells, spinal cord, and brains of *C9orf72*Exp carriers (23, 24).

We further explored the susceptibility of GGGGCC repeats to double-strand DNA breaks using a yeast system that quantifies rates of chromosome end-loss (109). A (GGGGCC)60 inserted into a yeast chromosome was extremely unstable, yielding mixed populations with 15-60 repeat units (Fig. S7A-D). Rates of breakage showed a significant length-dependent increase: Tracts of 35-60 repeats broke 6-16-fold compared to (GGGGCC)15, which incurred breaks at 10-fold higher rates than a (CAG)85 tract analyzed in the same assay (Fig. S7B and Fig. S7C). Thus, even short GGGGCC repeats can be highly prone to DNA breakage. Instability of a (GGGGCC)70 tract in humans was reported (29).

Sister-chromatid exchange and recombinant events in *C9orf72* expansion cells

An increased incidence of sister-chromatid exchanges (SCEs) occurs at rare and common fragile sites (110). We analyzed SCE formation in *C9orf72*Exp. Unexpectedly, *C9orf72*Exp cells exhibit an increase, up to 2-fold, in spontaneous genome-wide SCEs/cell (~7 up to 10-15/metaphase), compared to control cells without expansions (Fig. 6C). Increased SCEs were evident in *C9orf72*Exp cells from presymptomatic and symptomatic individuals (Fig. 6C, compare P1, P5 with P6, all greater than WT). The increased SCEs did not require FUdR. This increase is significant, yet modest relative to 10-fold increased SCE/metaphase in individuals with the chromosome instability Bloom syndrome. Bloom individuals present high SCEs (111–114), increased MN (112, 115), a self-DNA cGAS-STING-mediated *IFN* over-expression (115), and often succumb to cancer before age 30 due to a coincident 10-fold increased mutation rate (114, 116, 117). Chemical and genetic factors can drive SCEs (114, 118, 119). In all instances, SCEs predominantly occur at common (120–122) and rare fragile sites (110, 123–126), regardless of whether the fragile site is being induced or not (122, 127). Consistent with this, the SCEs levels in *C9orf72*Exp cells were mildly but not significantly increased by FUdR (Fig. 6C). Through FISH mapping SCEs were significantly enriched on Chr9p, where *C9orf72* resides (Fig. S6B-D). Thus, the GGGGCC-expanded FRA9A, like the CGG-expanded FRAXA, the AT-repeat-expanded FRA16B, and the EBNA1-motif repeat 11q23 fragile site, incurs increased SCEs (85, 87, 110, 126, 128). These findings extend the forms of genetic instability and the sources of DNA damage in *C9orf72*Exp cells to include global and focal SCEs.

Unexpectedly, one of the *C9orf72*Exp cell lines (P8) showed complex rearrangements restricted to one Chr9, clearly evident in every metaphase (100/100 observed) (Fig. 6D-F). Specifically, one Chr9 showed a duplication of nearly the entire 9q-arm (9qter-q21.11 fused to 9p23, Fig. 6C), a terminal deletion of 9pter-p23, and duplications of 9p23, 9p12, 9p11.2,

9q13, 9q21.11, and deletions in 9q13, making a derivative-Chr9 (see CNV and whole-genome sequencing analysis, Fig. 6D-E, Fig. S8A, Table S3). Breakpoint pattern was reminiscent to 9p deletion/duplication syndrome (Fig. 6G top) (55, 129). Importantly, only the derivative-Chr9 expressed FRA9A with FUdR in 7% (7/100) metaphases (Fig. 6F), indicating it arose from the *C9orf72*Exp Chr9. Strikingly every metaphase showed the same rearrangements, which were evident prior to FUdR treatment. In our previous examinations of thousands of metaphases from control cells, we have not observed such homogeneity of rearrangements, making it highly unlikely that this derivative-Chr9 arose by cell line establishment or culturing. It is also highly unlikely that this individual, who was neurotypical until presenting with bulbar onset ALS at age 56, had inherited this complex set of rearrangements constitutionally in all tissues, as congenitally such rearrangements would be incompatible with neurotypical life (55, 129). Rather than inherited, it is likely the rearrangements arose somatically in the blood of the *C9orf72*Exp individual, which is supported by our observation of similar rearrangements of the *C9orf72* transgene-containing Chr6 in mouse tissues (below). Whole genome sequencing revealed the derivative-*C9orf72*Exp-Chr9 presented a unique state with ≥13 breakpoints clustered on 9p, with direct and inverted junctions, confined to a single chromosome, as such, fulfilling the criteria of chromothripsis (130–132). It is possible the FRA9A-expressing *C9orf72*Exp-Chr9 isolated in a micronucleus, was shattered and reassembled as the derivative-Chr9 (133). A single experimentally targeted double-strand break can induce chromothripsis to the targeted chromosome (134, 135). The derivative-Chr9 may have arisen by stepwise alterations. The origin of the derivative-*C9orf72*Exp-Chr9 could not be discerned as the patient was deceased. The complex chromosomal rearrangements of the mutant *C9orf72*Exp FRA9A-expressing Chr9 could have downstream impact.

While we cannot exclude the possibility that the highly rearranged derrivarive-Chr9 in the *C9orf72*Exp cell line (P8) arose during cell line establishment or passage, it is difficult to argue away the coincidences that the rearrangements we observe were limited to only one Chr9 – the Chr9 with the *C9orf72*Exp expressing FRA9A (Fig. 6D-F), and that the breakpoints were non-random but aligned with the breakpoints of 9p-duplication/deletion syndrome (Fig. 6G) (55). We also observed numerous forms of chromosome rearrangements of murine chromosomes harboring the human *C9orf72* expansion, including one reminiscent of the der-Chr9 we observed in the human cell (see murine cytogenetics described below). Moreover, the cytogenetic observation of thousands of human EBV-transformed cells have not presented such chromosomal instability (59), asides from the EBV-induced fragility at 11q23, which depends upon the EBV protein EBNA1 (84–87).

Gene expression across most of the derivative-Chr9 is dysregulated. Expression analysis by RNA-seq comparing P8 to other *C9orf72*Exp cells, revealed trisomic and monosomic expression levels of many genes corresponding to the large duplicated and deleted regions (Fig. 6G, see red and blue dots, for significance see Fig. S8B-D, an interactive html file detailing mis-expressed genes can be accessed here: https://data.cyverse.org/dav-anon/iplant/home/ljsznajder/FRA9A/Chromosome9.html), also presented in Table S4. Amongst the dysregulated genes along the der-Chr9 in P8, many are also dysregulated in vulnerable neurons of *C9orf72*Exp ALS patients, including ALS- and inflammation-linked genes (https://www.biorxiv.org/content/10.1101/2023.12.22.573083v1, Table S4). Breakpoint and copy number changes analyzed in P8 are presented in Table S4.

Cell culture in FUdR increases repeat instability

We tested whether repeat length instability could be generated in *C9orf72*Exp patient cells under fragile site inducing conditions. We observed that expansion tracts shifted towards

shorter repeat lengths over culture time in FUdR-treated cells (Fig. S9). In contrast, under uninduced conditions, the expanded repeat showed a general shift towards *longer* repeat sizes or the more predominant repeat length (Fig. S9). FUdR affected the length of only the mutant *C9orf72*Exp allele. FUdR-induced changes were consistent in three different *C9orf72*Exp cell lines and did not appear to depend upon methylation or clinical status (Fig. S9). These results support repeat size variations being generated under folate-perturbing fragile site inducing conditions.

Tissue-specific somatic repeat expansions, chromosomal fragility, and chromosomal instability in *C9orf72*Exp mice

Tissue-specific somatic repeat instability, FRA9A chromosome fragility, and chromosome instability, was recapitulated in *C9orf72*Exp-Transgenic(Tg) mice (*C9orf72*Exp-Tg) harboring a single copy of the human *C9orf72* with a GGGGCC expansion integrated into murine Chr6 (136). Using this mouse as a tool for instability, we isolated cells from various organs of *C9orf72*Exp-Tg and control non-Tg mice, aged 5-months, when cell proliferation in the CNS and peripheral organs had ceased at 2-months of age (137–139) (see Methods). To retain as close a representation of cell types, harvested tissues were cultured for short periods sufficient for chromosome preparation (1-4 weeks, with no storage). Tissues from three mice inheriting ~620-690 repeats (tail at two-weeks, aged 5-months) showed a heterogenous smear of 586-1488 repeat sizes, with some of the greatest expansions in the CNS (Fig. 7A). This supports massive post-natal inter- and intra-tissue repeat expansions in non-proliferating murine tissues, as observed in *C9orf72*Exp humans (26–30). Expansions were evident as early as 2-weeks (Shum *et al.*, in preparation).

Chromosomal fragility of the *C9orf72*Exp transgene occurred in all tissues at frequencies of 5% to >35% (99% confidence, Fig. 7Bi-iii). Fragility presented as despiralized regions,

constrictions, chromatid, and isochromatid, breaks, with split transgene-specific *C9orf72* FISH signals, as we observed in human *C9orf72*Exp cells (Fig. 5Bi). Only chromosomes from the transgenic mice showed FUdR-induced fragile sites, where fragility localized to the expanded repeat of the integrated transgene, but never to the non-transgenic Chr6 (Fig. S10). Thus, FRA9A fragility can be transferred to this Tg-mouse thereby validating the *C9orf72* repeat expansion as the molecular cause of FRA9A.

Chromosomal instability was evident on the *C9or72*Exp-Tg-containing Chr6, including acentrics, truncations, duplications, translocations, deletions, and multi-branched chromosomes (Fig. 7C). In one instance the *C9orf72*Exp-Tg translocated itself from murine Chr6 to another chromosome (Fig. 7C), and in another the *C9orf72*Exp-Tg was deleted (Fig. 7C). We observed a rearranged chromosome with a large duplication (Fig. 7C), reminiscent of the derivative-*C9orf72*Exp-Chr9 in ALS patient, P8 (Fig. 6D-G). Chromosomal fragility and instability were observed in all tissues of all three *C9or72*Exp-Tg mice.

While rearranged chromosomes were rare relative to fragility, neither were ever observed in the non-transgenic murine Chr6 at 6qE3, the site of transgene integration, or in any control non-transgenic tissues (three replicate mice). The absence of fragility at 6qE3 in control non-transgenic tissues is consistent with 6qE3 not being an endogenous fragile site in mice (140).

Together our data support the ability of the *C9orf72*Exp-Transgene to incur post-natal somatic tissue-specific repeat expansions, display chromosomal fragility and chromosomal instability, as in humans. Our findings provide insight into fragile site expression and rearrangement in the CNS and periphery.

591 **Figure 7**

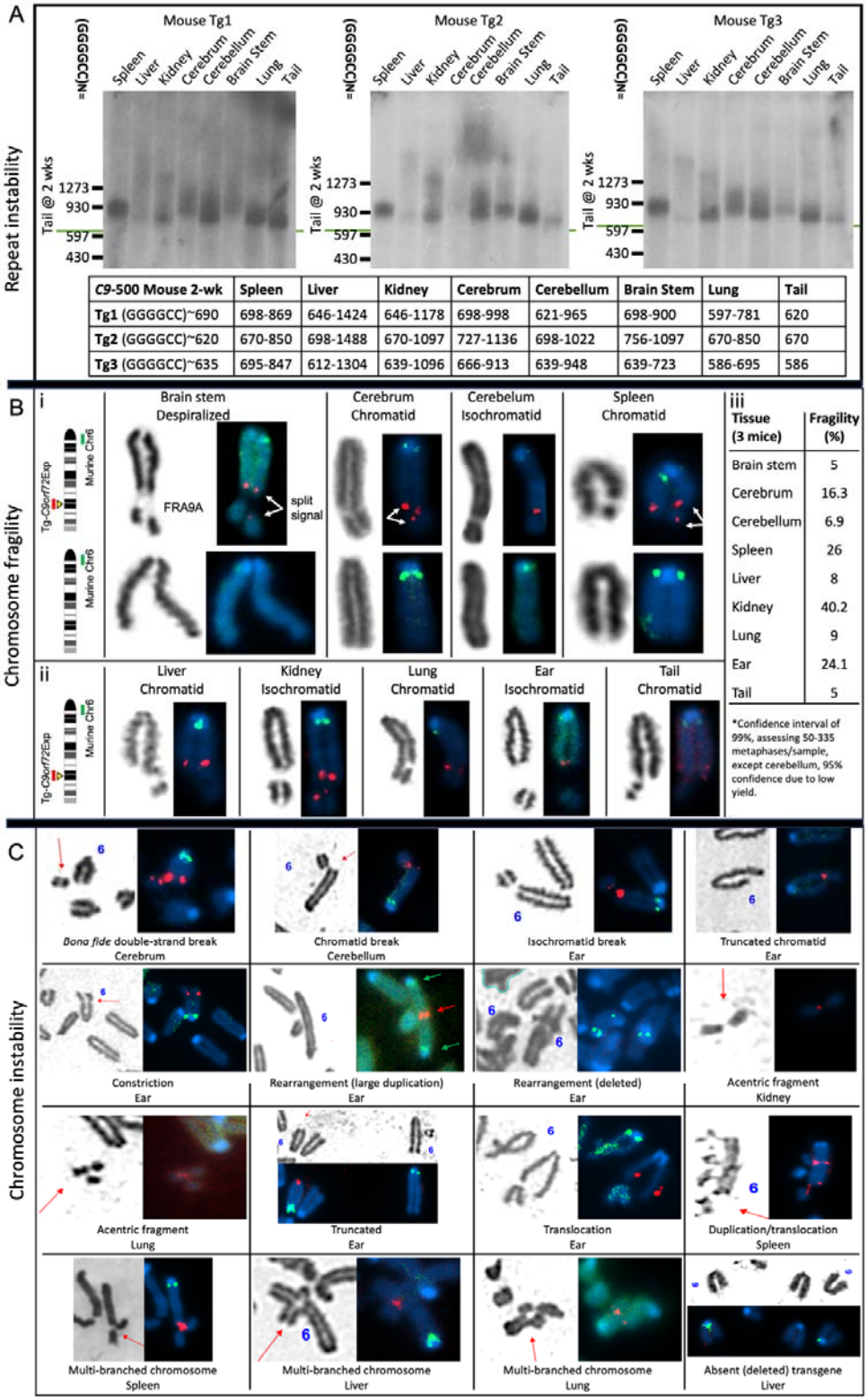

C9-500 Mouse 2-wk	Spleen	Liver	Kidney	Cerebrum	Cerebellum	Brain Stem	Lung	Tail
Tg1 (GGGGCC)~690	698-869	646-1424	646-1178	698-998	621-965	698-900	597-781	620
Tg2 (GGGGCC)~620	670-850	698-1488	670-1097	727-1136	698-1022	756-1097	670-850	670
Tg3 (GGGGCC)~635	695-847	612-1304	639-1096	666-913	639-948	639-723	586-695	586

Figure 7 Legend: *C9orf72* repeat instability, chromosomal fragility and chromosomal instability in *C9orf72*Exp-Tg-mice

Southern blots for *C9orf72* transgene in C9-500 mouse tissues. C9-500 mouse tissues were sized for repeat size via Southern blot in three *C9orf72*Exp Tg-mice. The tail was the most stable tissue. (A) Somatic repeat instability by Southern blots in tissues of three 5-month-old *C9orf72*Exp-Transgenic mice harboring a single copy of the human *C9orf72* gene with a GGGGCC expansion integrated into murine Chr6 (136). (B) Cells isolated from tissues of the mice shown in panel A were grown for 1-4 weeks sufficient for metaphase spreads for fragility analysis with 1µM FUdR with FISH analysis. A murine-specific green probe identified mouse Chr6, and human-specific red probe identified the *C9orf72*Exp transgene. Pictured are FSFS in the CNS (i), the periphery (II), and quantified in panel iii. (C) Chromosomal instability at the *C9orf72*Exp transgene was assessed in the same tissues used in panel C, using the same FISH probes.

DISCUSSION

Here we demonstrate that *C9orf72*Exp is the molecular cause of the rare folate-sensitive FRA9A, cytogenetically observed more than 4 decades ago (58, 141). This reveals previously unconsidered avenues to study genotype-phenotype relationships for co-occurring disease states associated with *C9orf72*Exp and attributes linked to the 9p21 region. First, folate-sensitivity suggests a possible gene-environment interaction. Second, FRA9A may serve as a DNA source to activate DDR and *IFN* pathways. Third, FRA9A chromosomal instability and global SCEs may increase somatic mutations at 9p21 and beyond.

Disease penetrance & gene-environment

Gene-environment interactions have long been suspected for ALS, FTD, and the incompletely penetrant co-occurring phenotypes of *C9orf72*Exp (142). Folate-sensitive induction of *C9orf72*Exp repeat instability, brain region-specific repeat expansions, FRA9A fragility, chromosomal instability, and methylation-sensitive chromatin compaction, which we have shown can arise in cells and tissues of both presymptomatic and symptomatic individuals, may have clinical implications. Lifestyle, including nutritional choices, of *C9orf72*Exp carriers can affect disease onset and progression (40). Proper levels of the linked vitamins B9 (folate) and B12 are protectors from ALS (143). Individuals with folate deficiencies, nutritionally-, pharmaceutically-, or genetically-induced, are associated with chromosomal fragility, localized chromosomal rearrangements (144–153), megaloblastic/pernicious anemia, ALS- and FTD-like symptoms (154, 155), reviewed (59). In such cases these presentations were reversed upon B12 supplementation – indicating that chromosomal instability was induced by folate-stress. Somatic GGGGCC repeat instability, FRA9A fragility, and global increase of SCEs depend upon *C9orf72* expansion and are folate-sensitive and can occur in cells from presymptomatic *C9orf72*Exp individuals.

*C9orf72*Exp carriers, in folate-deficient states, may be predisposed to repeat instability, FRA9A fragility, and chromosomal instability, which if exacerbated over time may impact gene dysregulation, altering the susceptibility of phenotypic variations amongst *C9orf72*Exp carriers. Fragile sites and SCEs can be induced in the blood and myeloid cells by lifestyle choices, including cigarette smoking, alcohol consumption, and diet (59, 156–160). Tobacco and alcohol consumption by presymptomatic *C9orf72*Exp carriers affected disease age-of-onset (40). Various clinically used agents (161), including some considered for use in ALS/FTD, *C9orf72*Exp (162), and fragile X syndrome (163), like phenytoin or decitabine can induce fragile sites (59, 164), induce sister-chromatid exchanges (165, 166), and modify chromosome condensation (167, 168). Age-dependent ongoing repeat expansions in the brain have been suggested as a contributor to disease (26, 88, 169, 170), could be folate sensitive. Additionally, CpG-methylation of *C9orf72*Exp (169, 171) and acceleration of genome-specific DNA methylation age (epigenetic clock) are modifiers of disease onset and progression in *C9orf72*Exp carriers (172, 173). Chromatin compaction of *C9orf72*Exp is sensitive to the degree of expansion and CpG-methylation (Fig. 5). Efforts to prophylactically slow the epigenetic clock are a central focus (174–176). The *C9orf72* expansion was recently reported to be bound by the chromatin remodeler DAXX (177). Coincidentally, DAXX, is known to associate with satellite and telomere repeats and its downregulation led to a global increase in MNase sensitivity (178–180). Environmental contributions to *C9orf72*Exp diseases must be considered.

Various genetic, molecular, and environmental aspects have been demonstrated to modify disease presentation in *C9orf72*Exp carriers (3, 4, 7, 8, 40, 42, 45, 181–188). The 90-year old male *C9orf72*Exp carrier presented herein (Fig. 5) is likely to be truly asymptomatic, as a long presymptomatic phase with evident degeneration often detected decades before ALS or

FTD symptom manifestation (238, 239), pathology that was not present in his brain (88). Clinical differences between the truly asymptomatic father and symptomatic daughter studied herein could not be explained by either genetic modifiers (*TMEM106B*, *ATXN2*, Finnish haplotype), both expressed similar burdens of p62 inclusions, similar burdens of sense and antisense RNA foci, similar burdens of all five types of RAN-peptides (GA > GP > GR > PA/PR, except for the cerebellum, which showed more RAN-peptide inclusions (~7-fold) and sense RNA foci (~2-fold) in the asymptomatic father compared to the ALS/FTD-affected daughter) (29, 88) (summarized in Table S2). Also, neither lifestyle choices, life events, nor autoimmunity, could explain their phenotypic differences (29, 88) (Table S2). However, compared to the daughter, in the brain the father showed extreme repeat length mosaicism (13-3500 repeats) (Fig. 5D), with increased MNase accessibility of shorter expansions, increased *C9orf72* expression (mRNA and C9ORF72-long, but not C9ORF72-short protein) (29, 88), increased TDP-43 inclusions (29, 88), and an epigenetic age ~9 years younger than his chronologic age (the daughter was 3 years older) (88, 172) (summarized in Table S2). Thus, these somatic variations deserve further attention in pre-, asymptomatic, and symptomatic *C9orf72*Exp carriers.

FRA9A as a DNA source to activate the DDR and *IFN* pathways

Both a spontaneous activated DNA damage response (DDR) (15–25) and a hyperactivated *IFN* cGAS-STING-associated immune response occur in *C9orf72*Exp patient cells and brains (4, 12–14). The source of the damaged DNA or DNA-immunostimulant to activate either DDR or *IFN* response is unknown. DDR in cells and brains of *C9orf72*Exp, evident as increased γ-H2AX, phosphorylated-ATM, cleaved PARP-1, and 53BP1, is coincident with DSBs (22–24). We reveal that DSBs arise at *C9orf72*Exp via heightened FRA9A fragility, broken/rearranged Chr9s, increased genome-wide SCEs, increased MN, and Chr9-containing

MN. The increased C9ORF72 protein levels in multiple tissues of the asymptomatic father shown to have massive mosaic somatic expansions (Fig. 5F, Table S2 and (29, 88)) may suppress an autoimmune response by increasing STING levels. Models of the *C9orf72*Exp-linked DDR activation involve RAN-peptide induced p53-target gene activation, inhibition, or mislocalization of the DSB DNA repair proteins ATM, 53BP1, TDP-43, FUS, Ku80, and PARP-1 (15–25). Other non-RAN-peptide DDR paths have received little attention.

The unusual >33kb of compact chromatin at FRA9A's core fragility zone (Fig. 5A), could be susceptible to DSBs, which would contribute to DDR activation. Supporting this possibility is that experimentally-induced locus-specific compacted chromatin of an artificial ~10kb stretch of ~250 tandem arrays of LacO, which becomes a fragile site, has been demonstrated to activate a DDR in the absence of damage (189–192). A contribution of FRA9A fragility to DDR can act in parallel to RAN-peptide induced DDR (23, 24). Disruption of higher-order chromosomal organization may also contribute to DDR and *IFN* responses. Long-range chromosomal interactions involving 9p21 are activated in the inflammatory response. All *IFN* genes at 9p21 are transcriptionally inactive until immunostimulated by viral infection or cytosolic self-DNAs, whereupon dramatic chromatin (193) and multiple intra-9p21, inter-arm (9p21-9q34.2), and inter-chromosomal (9p21-4p14 and 9p21-18q21.1) interactions arise to activate *IFN* cluster expression and inflammation (47, 194). Reduced levels of the C9ORF72 protein in *C9orf72*Exp patients, being unable to supress STING, leads to a sustained hyperactivation of *IFN* in brains (195). Upon FRA9A breakage the *C9orf72*Exp-Chr9 activates DDR and is then sequestered to MN whose contents can be released to the cytosol to activate *IFN* through cGAS-STING, and this sequestration may disrupt other inter- and intra-Chr9 interactions (196). That disruption of intra-/inter-chromosomal associations can drive DDR and *IFN* cascades is supported by the experimental

disruption of such interactions leading to chromosome sequestration to MN (197, 198). CGG expansions at *FMR1*, the cause of FRAXA, disrupt intra- and inter-chromosome interactions (199). The 2-fold increase in global SCEs in *C9orf72*Exp cells we observe may contribute to DDR and MN. MN enriched with the DSB repair protein, TDP-43, have been detected in brains of ALS patients (200). Our suggestion that DNA damage induced by FRA9A fragility can serve as a DNA-immunostimulant in the CNS is consistent with reports of *in vivo* DNA damage by ATM-deficiency or brain trauma that activates an *IFN* response in motor neurons (201–203). Our working model that the *C9orf72*Exp acts as a chromatin compacted FSFS and is an inducer of DNA damage at many locations including on Chr9, is suited to non-cycling neurons.

We suggest that the cytoplasmic release of DNA from FRA9A-enhanced MN, may further tip the balance by exacerbating the stimulation of the aberrantly hyperactive cGAS-STING initiated *IFN* expression in *C9orf72*Exp carriers (4, 13, 14) – which may explain the co-morbid partially-penetrant autoimmunity (1–6). FRA9A broken-Chr9s and increased global SCEs might also further exacerbate the DDR cascade, as DNA-immunostimulation enhances sense and antisense transcription from *C9orf72* (42) whose RAN-peptide products would feedback upon the DDR by suppressing DSB DNA repair proteins ATM, p53, TDP-43, FUS, Ku80, and PARP-1 (15–25). The neuroinflammatory and autoimmune phenotypes of *C9orf72*Exp carriers is complex (14), and the effects of either FRA9A altered chromatin, or MNs containing broken Chr9s upon the *IFN* response is unknown.

FRA9A chromosomal instability, mosaic somatic mutations, and 9p21-associated diseases

A reasonable prediction from our findings is that the *C9orf72*/FRA9A fragile site may, like other fragile sites, predispose to mosaic deletions, duplications, or rearrangements resulting in

altered expression of genes on 9p21 or throughout Chr9. Such mosaic chromosomal variations may vary between tissues, accumulate with age, and lead to phenotypic variability. In the case of *FMR1*/FRAXA, phenotypic variability can arise through mosaic genetic or chromosomal instability (deletions, duplications, and rearrangements) extending beyond the *FMR1* CGG-repeat, as revealed through decades of isolated case reports (59). Similar phenomena may arise at the mutant *C9orf72*, as suggested by our observation of truncated-Chr9s broken at *C9orf72*, acentric-Chr9s, chromosomal instability of the *C9orf72*Exp allele, and heightened levels of genome-wide SCEs. Detection of somatic mosaic levels of chromosomal instability will likely require more focused studies. For example, the dramatic Chr9 rearrangements, evident by FISH in every metaphase of the ALS/*C9orf72*Exp line P8, escaped detection by repeat-primed PCR and by Southern blot assessment of the repeat size (compare Fig. 3B with Fig. 6F). Indeed, mosaic mutations at various loci (reviewed in (204–206)) including *FMR1* (207–212) required focused attention. Mosaic mutations may be confined to specific cell types, as recently revealed for Purkinje cells with large somatic CAG-expansions, amongst stable tracts in the cerebellum of Huntington's disease patients (213, 214). One might expect an increase in somatic mutation rates throughout the genome in *C9orf72*Exp patients, as the increased 2-fold global SCEs we observed may have a coincident increase in mutation rate, similar to the 10-fold increased mutation rates in BLM individuals who show a 10-fold increase of SCEs (111, 112, 116, 117). *C9orf72*Exp cells from presymptomatic individuals show folate-sensitive repeat instability, FRA9A fragility, chromosomal instability, MNase-resistance, increased levels of micronuclei/NBuds, and global sister chromatid exchanges. Long-term display of these features may exacerbate disease-onset and affect penetrance. Our findings support that the *C9orf72*Exp patients may incur mosaic mutations at under-appreciated levels, and recent findings support increased

somatic mutations in brains of *C9orf72*Exp individuals (https://www.biorxiv.org/content/10.1101/2023.11.30.569436v1).

Knowledge gaps remain for FRA9A/*C9orf72*. In particular, the co-occurrence of many diverse phenotypes in *C9orf72* expansion carriers is unclear. That FRA9A encompasses the *IFN* cluster, *CDKN2A*, *IFNk*, *LINGO2*, *TOPORS*, *APTX*, *DNAJA1*, and *SMU1* genes, each independently associated with symptoms that can co-occur in *C9orf72*Exp carriers, provide new insights into the possible involvement of chromosomal instability (Fig. 1). An increase in ALS occurring in cancer survivors, particularly melanoma, has been repeatedly reported (7, 215–219). While a correlation of *C9orf72*Exp in cancer predisposition has not been studied in large populations, *C9orf72*Exp carriers have a significantly higher risk of melanoma (7). *C9orf72*Exp carriers may succumb to cancer prior to onset or awareness of ALS. That both *CDKN2A* and the *IFN* gene cluster, frequently deleted in melanoma, are encompassed in FRA9A's fragility zone introduces the possible involvement of *C9orf72*Exp. Mosaic somatic mutations that extend beyond the *C9orf72* repeat, may affect expression of genes encompassed by FRA9A or beyond. Thus, revisiting the *C9orf72*/9p21 locus with the awareness that it is, and can share the attributes of, a chromosomal fragile site should provide key insights into the genotype-phenotype relationships for the many and varied presentations associated with the 9p21 region.

MATERIAL AND METHODS

In silico datasets and analyses

Sequence feature and epigenetic datasets used in Figure 2 and Figure S1 are described as follows. Repeat annotations and %GC tracks were obtained from the UCSC genome browser (hg19). Wavelet-summarized repliseq data (ENCODE) was obtained in bigWig format from GEO:GSE34399. Erythroblast SNS-seq data and replication origins were obtained in bedGraph and bed format, respectively, from GEO:GSE6197. Imputed %DNA methylation for GM12878 was obtained from the roadmap epigenomics data portal: (https://egg2.wustl.edu/roadmap/data/byFileType/signal/consolidatedImputed/DNAMethylSBS/E116-DNAMethylSBS.imputed.FractionalMethylation.signal.bigwig). Pre-calculated 2nd-order DNA shape features were obtained from the Rohs lab GBShape database.

Cell culture and fragile site induction

All cytogenetic studies were performed using Epstein-Barr virus transformed lymphoblastoid cell lines from *C9orf72*-ALS patients, expansion carriers, and control individuals provided by Dr. Guy Rouleau (McGill University). One of the patients, P4, displayed signs of FTD. All patients provided written informed consent. Cells were cultured in RPMI 1640 media supplemented with 15% FBS (ThermoFisher Scientific), 2 mM L-glutamine, Pen/Strep (100 IU/mL, 100 µg/mL), and 1 mM sodium pyruvate. Two modes of FSFS induction were used to demonstrate fragility at 9p21.2: i) 24 hours with 0.1 µM 5-fluorodeoxyuridine (FUdR) or ii) 14 days with Media 199 (Gibco, Cat #: 11150-059) supplemented with 2% FCS, 2 mM L-glutamine, and Pen/Strep (100 IU/mL, 100 µg/mL). Cells in 199 media were treated with 100 nM methotrexate for 16 hours, washed and then treated with 0.01 µM bromodeoxyuridine (BrdU) for a total of 3 hours prior to harvest. All cells were treated with 6 µg/mL ethidium bromide (EtBr) and 0.05 µg/mL KaryoMAX (Gibco; Cat #: 15212012) prior to harvest. Cells

were then centrifuged and resuspended in 0.075 M KCl solution for 30 minutes at 37ºC followed by several washes with fixative solution (3:1 methanol:acetic acid). Long-term FUdR culture experiments were performed in either RPMI 1640 media (as described above) or RPMI 1640 media + 0.1 µM FUdR for a total of 8 weeks. Media and FUdR was replaced every 2-3 days. Cells were harvested at 1, 2, 4, 6, 8-week time points for DNA purification and Southern blot was run as described below.

Metaphase chromosome and FISH analysis

Slide preparation for both cytogenetic and FISH analysis of metaphase spreads were made from fixed cell suspensions using a Model CDS 5 Cytogenetic Drying chamber according to standard methods. For 199 media conditions, breaks and gaps were quantified on total Giemsa stained metaphases and subsequently G-banded to karyotype each metaphase and confirm fragile site on 9p-arm. SpectrumGreen & SpectrumOrange-conjugated dUTP probes (RP11-15P13, RP11-274I21, RP11-1149M23, RP11-491J7, RP11-945G22, RP11-1079P2, RP11-360B21, RP11-696J10) from RPCI-11 human BAC library were generated by The Centre for Applied Genomics (TCAG, PGCRL, Toronto, Canada) using the Vysis nick translation kit (Cat #07J00-001; Abbott Molecular, Illinois, USA) in accordance with manufacturer's instructions. Chromosomes were counterstained with DAPI. One hundred metaphases per sample were scored for each condition using either brightfield microscopy, Olympus IX81 quorum spinning disk confocal microscope, or Zeiss Axioplan 2 fluorescence microscope. Images were collected using a CCD camera (Hamamatsu C9100-13 EM-CCD, Hamamatsu, Japan) (Princeton Instruments Pentamax, Roper Scientific, New Jersey, USA) and analyzed using Volocity (Perkin Elmer, Massachusetts, USA) or CytoVision (Leica Biosystems, Germany) software.

Southern blot analysis of *C9orf72* repeat expansion size

Southern blot analysis was performed to size *C9orf72* repeat expansions as this method is the gold standard for sizing large (GGGGCC)n repeat expansions (220). Southern blotting provides an estimate of non-bias expansion sizes (221). We used Southern blotting method (220, 222) with 241 bp probe, which anneals 153 bp upstream of the (GGGGCC)n repeat tract, and used selected restriction-endonuclease digestions of genomic DNA (as noted in the figures) – which permit sensitive detection of repeat size and length heterogeneity at molar levels. The 241 bp probe was produced by PCR using primers (Fwd: 5'–AGAACAGGACAAGTTGCCCC–3' and Rev: 5'–AACACACACCTCCTAAACCC–3') as published (220, 222). For mapping boundaries of MNase accessibility an additional probe was used (see below). Molecular weight markers were used to estimate the size of repeats. Distances between molecular weight markers were measured using ImageLab software (BioRad) and plotted against the known number of base pairs for each marker. A best-fit linear regression was calculated in Microsoft Excel and the equation of this line was used to calculate the size of each band on the blot. Different restriction enzyme combinations were used to cut the genomic DNA, as noted in each figure, hence resulting in different flank repeat sizes.

Methylation analysis of the *C9orf72* repeat

Methylation analyses were done in blinded experiments using the same DNA prep as for Southern blot. Genomic DNA was bisulfite converted using the EZ DNA Methylation-Lightning™ Kit (Zymo). We estimated the number of methylated CpG-sites at the CpG-island 5′ of the (GGGGCC)n repeat using bisulfite sequencing as reported previously (64). To estimate the methylation of the (GGGGCC)n repeat itself, we used a qualitative GGGGCC-methylation assay, sensitive enough to detect repeat methylation in a mixture containing ~5% high-methylated DNA standard (60). We always observed methylation mosaicism for

expanded repeat samples, revealed by presence of the amplification product of the expansion in both methylated (blue) and unmethylated (green) channels (223).

Micronucleus and nuclear bud detection

Micronuclei and nuclear bud analyses were done as previously described with some modifications (95, 97, 224). Briefly, cells were treated with 0.5 µM FUdR for a total of 24 hours, with cytochalasin B (4 µg/mL) being added 3 hours after addition of FUdR. Cells were briefly incubated in 0.075 M KCl, fixed with Carnoy's fixative and slides with sparsely spread cells were prepared using a Model CDS 5 Cytogenetic Drying chamber (Thermotron, Michigan, USA). SpectrumGreen (RP11-696J10) & SpectrumOrange (RP11-672M4)-conjugated dUTP probes from RPCI-11 human BAC library were generated by The Centre for Applied Genomics (TCAG, PGCRL, Toronto, Canada) using the Vysis nick translation kit (Cat #07J00-001; Abbott Molecular, Illinois, USA) in accordance with manufacturer's instructions. Nuclei were counterstained with DAPI. At least 950 binucleated cells were scored per condition for the presence of micronuclei and nuclear buds and Chr9 signals, as previously described (97). Two blinded and independent experiments were carried out for each data asset. Statistical analyses were done using Fisher's exact test for the combined values of micronuclei and nuclear bud events as they are believed to arise from the same phenomenon (97, 225). Images were captured using an Olympus BX61 fluorescence microscope. Images were collected using a CCD camera (Hamamatsu C9100-13 EM-CCD, Hamamatsu, Japan) (Princeton Instruments Pentamax, Roper Scientific, New Jersey, USA) and analyzed using ASI SpotScan software (Applied Spectral Imaging, California, USA).

Sister-chromatid exchange (SCE) assay

Cells were incubated in the presence of 10 µM BrdU for two cell cycle periods and pulsed with 0.1 µg/mL of KaryoMAX (Gibco; Cat #: 15212012) for the last 2 hours before being

harvested. FUdR (0.1 μM) was added for the last cell cycle. Harvested cells were treated with 0.075 M KCl for 20 min and subsequently fixed with methanol:acetic acid (3:1) for at least 30 minutes. Cells were fixed onto glass slides. Dried slides were incubated with 10 μg of Hoechst 33258 per ml in phosphate buffer (pH 6.8) for 20 minutes, followed by rinsing with MacIlvaine solution (164 mM Na_2HPO_4, 16 mM citric acid [pH 7.0]). Slides were irradiated with UV light for 2 hours and incubated in 2X SSC solution at 62°C for 1 h before staining with 5% Giemsa solution and subsequent microscopy. At least 100 metaphase cells were evaluated for SCE events genome-wide per genotype. For Chr9-specific SCEs, slides were destained with xylene solution followed by methanol:acetic acid (3:1) and then standard FISH procedures, as described above were followed using SpectrumOrange-dUTP conjugated RP11-696J10 probe. At least 30 of the same Giemsa-stained metaphases were relocalized using fluorescence microscopy and imaged to allow for quantification of SCEs specifically on the 9p- and 9q-arms.

Construction of plasmids and yeast strains

An *Xba*I-*Hin*dIII fragment containing a region of the human *C9orf72* gene containing an expanded (GGGGCC)n repeat and 547 bp of flanking sequence (from pcDNA3.1(+)c9-200+ obtained from R.H. Brown; CF stock #435) was cloned into the MCS of plasmid pEP1 to create plasmids pEP1-(GGGGCC)n. pEP1 was made by cloning the *ADE2* gene from pRS402 into the *Bsa*AI and *Nsi*I sites of pHZ1; pHZ1 was made by cloning the G4T4 sequence into the *Sma*I site of pYIP5. The CAG repeat was cloned into pEP1 *Xho*I and *Xba*I sites. Repeat lengths in plasmid clones were confirmed by sequencing. Repeat lengths of the (GGGGCC)n plasmids were approximately 16, 29, and 36 for plasmids 504, 484, and 485, respectively; exact number of repeats varied with different sequencing runs. Plasmids were linearized with *Xcm*I and recombined into the *URA3* marked yeast artificial chromosome

(YAC) CF1 in strain VPS105 (CFY #289) to create the new GGGGCC-*ADE2-URA3* and CAG-*ADE2-URA3* YACs (see Fig. S7A & S7D), which were confirmed for YAC structure by PCR. CAG tract lengths were confirmed by sequencing of PCR amplicons but (GGGGCC)n tract lengths could only be determined approximately by Southern blot since amplification from genomic DNA was unsuccessful, and are therefore reported to the nearest 5 bp.

YAC fragility assay

End loss of the repeat-*ADE2-URA3* YACs was determined by an established protocol (109) except that 1 ml of an overnight culture inoculated with a specific colony was plated on media containing FOA and a low amount of adenine but lacking leucine (FOA-Leu low Ade) to determine the number of mutants, and a dilution was plated on yeast complete media lacking leucine (YC-Leu) for a total cell count. Rates were determined by the method of the median. Another 1 ml of the same culture was used to isolate genomic DNA for Southern blot to assess repeat length. For reasons not completely understood, but that could include reduction of transcription through the repeat tract, the insertion of the *ADE2* marker resulted in a lower rate of FOA^R compared to previously published values for the CAG-85 YAC without the *ADE2* gene. End loss was confirmed in a subset of colonies (usually one from each FOA-Leu plate) by PCR (retention of the sequence to the left of the G_4T_4 telomere seed and loss of sequence to the right of the repeat tract; Fig. S7).

Southern blot - yeast

Yeast genomic DNA was digested with *Nhe*I and *Xba*I restriction enzymes, separated by horizontal gel electrophoresis, and blotted to a nylon membrane using a standard Southern protocol. Either the Roche Molecular Weight Marker VI or VII was run as a size marker. For the preparation of the probe, a 301 bp fragment adjacent to the (GGGGCC)n repeat was PCR

amplified from DNA of plasmid #485 as template, using Primers #1402 (ALSsouthernFOR) and #1403 (ALSsouthernREV). Probes were labeled using the DIG High-Prime DNA Labeling and Detection Starter Kit I (Cat #: 11745832910; Roche). Repeat tract estimation was performed as previously described (Southern blot analysis of repeat expansion size).

Chromatin accessibility *in cellulo* with MNase

Human lymphoblast cell lines from *C9orf72*-expansion carriers were assessed for MNase accessibility, as outlined in Figure 5B. Briefly, cell pellets were washed in ice-cold 1X PBS, re-pelleted, and permeabilized by ice-cold NP-40 lysis buffer (10 mM Tris pH 7.4, 10 mM NaCl, 3 mM $MgCl_2$, 0.5% NP-40, 0.15 mM spermine, 0.5 mM spermidine) for 5 min on ice. Nuclei were collected at 200 X*g* (10 minutes, 4ºC), washed in 1X MNase digestion buffer (10X stock: 100 mM Tris pH 7.4, 150 mM NaCl, 600 mM KCl, 5 mM spermidine, 1.5 mM spermine), re-pelleted, and subsequently resuspended in 1X MNase digestion buffer supplemented with 1mM $CaCl_2$. Treatment followed with MNase for 5 min. at 22ºC, at differing concentrations (refer to Fig. 5 and Fig. S4A – all serial dilutions). All digestion reactions were stopped with an equal volume of *Stop* solution (0.625 mg/mL proteinase K, 20 mM EDTA, 20 mM EGTA, 1% SDS diluted in 1X MNase buffer) and incubated at 37°C for a minimum of 1 hour. Reaction conditions were optimized to ensure over-digestion by MNase, which diminishes MNase cleavage preference. DNA was purified by phenol/chloroform extraction, RNase A treatment, and ethanol precipitation. A small amount of purified DNA was assessed for completeness of MNase digestion, by its conversion to mono-, di-, tri-nucleosome sized fragments as resolved by electrophoresis stained with ethidium bromide and visualized by UV imaging (Fig. 5B, left panel; S4A). DNA samples were analyzed by Southern blot as described.

Chromatin accessibility in post-mortem tissues with MNase

We conducted MNase accessibility analysis using post-mortem brain tissues (orbito-frontal cortex and cerebellum) of an asymptomatic 90-year-old male and his 59-year-old ALS-FTD-affected daughter, previously deep-phenotyped (summarized in Table S2) (29, 88). The asymptomatic male carried 70-repeat *C9orf72* expansion in the blood and was deceased at 90-years of age. Tissue was Dounce homogenized using 1X MNase digestion buffer, 10% NP-40 was added to final concentration 0.5%, incubated 5 minutes on ice, filtered through a 40 μm strainer, and centrifuged. Nuclei pellets were washed in MNase digestion buffer and incubated with different concentrations of MNase. Remaining steps were performed as described above.

Digestibility of *C9orf72* BAC DNA *in vitro* with MNase

A bacterial artificial chromosome (BAC) containing ~160 (GGGGCC)•(GGCCCC) repeats, prepared in the lab of Piet de Jong, was restricted by *Nhe*I and *Xho*I giving rise to a shorter fragment of approximately 1750 base pairs, which was gel-purified. Half (by volume) of the purified product underwent CpG-methylation by *M.Sss*I methyltransferase supplemented with 640 μM S-adenosylmethionine (New England Biolabs) and purified using the QIAEX II kit (Qiagen). Completeness of methylation was checked by the inability to be digested by the methyl-sensitive *Hpa*II but successful digestion by the methyl-insensitive *Msp*I. Subsequently, in parallel, equal concentrations (~100 ng/reaction) of the non-methylated and methylated fragments were treated with increasing levels of MNase (0U – 0.1U – 1U – 5U – 25 U) for 5 minutes at 22ºC in 1X MNase digestion buffer. The MNase reaction was halted by addition of 6X purple loading dye (New England Biolabs) and electrophoresed immediately on a 1% agarose gel at 50 V for 20 minutes, followed by 100 V for 100 minutes. Gene Ruler Mix (Thermo Scientific) was loaded in the first lane. Electrophoresed products were stained with ethidium bromide, visualized by UV imaging (Fig. S4B, left hand side),

and DNA fragments were transferred to a positively-charged nylon membrane, and probed with a 177 bp probe, annealing just upstream of the GGGGCC repeat tract (Table S1). To maximize our ability to assess that loss of signal corresponded to MNase digestion of the GGGGCC repeat fragment, we developed the 177 bp probe which anneals immediately adjacent to the repeat. (The 177 probe anneals 7 bp upstream of the GGGGCC repeat tract, while the 241 bp probe anneals 153 bp upstream). The 177 bp probe was produced by PCR using primers (Fwd: 5'–GAGCAGGTGTGGGTTTAGGA–3' and Rev: 5'–CGACTCCTGAGTTCCAGAGC–3') (Table S1). A phosphor image of the Southern blot was obtained using the Typhoon system (Fig. S4B, right hand side), and the rate of digestion of probed sequence was calculated using densitometric analysis in ImageJ. The percentage of DNA resistant to MNase (therefore, the fraction of undigested 'starting fragment' BAC DNA) was plotted as a function of MNase units of activity (concentration) in GraphPad Prism 8 (Fig. S4B).

MNase controls

The MNase resistance we observe is not a reflection of the sequence preference of MNase or the sequence composition of the *C9orf72* region. The MNase resistance spanning the mutant *C9orf72* locus supports altered chromatin packaging of the non-repetitive flanks, as the 241 bp probe anneals 153 bp upstream of the (GGGCC)n repeat, and resistance is still evident (Fig. 5). The relative resistance of the expanded allele compared to the internal control of the non-mutant *C9orf72* allele, provides strong support for altered chromatin accessibility. MNase is known to display a cleavage sequence preference, preferring 5′-NpT and 5′-NpA sites (226, 227), yet is capable of digesting G-C only sequences and can digest most calf thymus DNA with over-digestion, which diminishes MNase cleavage preference(226). All of our nuclear digests were completed to over-digestion. The *C9orf72* sequences flanking the

repeat, that are probed herein, contain an extensive number of the preferred 5′-NpT and 5′-NpA sites (Fig. S2B, green font). That protein-free genomic DNA from *C9orf72* expansion carriers is digested at an equal rate relative to the internal equimolar control of the non-expanded *C9orf72* allele, supports that the flanks can be digested (Fig. S4A). The MNase digest of the purified (GGGGCC)160 repeat DNA further confirms that the pure GC-rich repeat can be digested by MNase as evidenced by the ethidium bromide-stained gel (Fig. S4B). As such, the reduced digestion of the expanded allele in its native chromatinized state represents a chromatin-mediated inaccessibility.

To rule-out possible artefacts such as differences in the sensitivity between ethidium bromide staining and Southern probe hybridization, or loss of DNA during Southern transfer, or an uneven transfer or membrane retention of DNA, an aliquot of the same samples were run on a high-resolution gel, ethidium-stained, hybridized with the *C9orf72*-specific probe, imaged, and then the blot was stripped and re-probed using radiolabeled total genomic DNA as the probe (Fig. S4A). The hybridization pattern from total genomic DNA probe is very similar to the ethidium bromide-stained gel: most of the genome has been digested to completion to mono-, di-, tri-, and tetra-nucleosome sized fragments (Fig. S7A). In contrast, hybridization with the *C9orf72* probe shows dramatic MNase resistance of the expanded allele, while the non-expanded allele appears to be digested at the same rate as the rest of the genome.

Control MNase digestions of protein-free genomic DNA of unmethylated and methylated *C9orf72*-ALS samples, compared to the chromatinized samples of the same cell lines showed that MNase digestion occurs similarly for both alleles at extremely low MNase concentrations (0.01 Units) in protein-free conditions, yet the expanded allele is strongly

resistant in chromatinized samples, supporting that this resistance is due to an unusual chromatin state (Fig. S4B-C).

There is a striking difference in MNase digestion between the ethidium-stained bulk genomic DNA, and the Southern blot detected *C9orf72* expanded allele, which is internally controlled for by its non-expanded homolog (Fig. 5). See above notes and Figure S4 for controls. The *C9orf72* region showed reduced presence in the mono-, di-, and tri-nucleosomal digested regions, relative to the rest of the genome (compare Southern blot with ethidium stain, Fig. 4A).

Control MNase digests using cloned *C9orf72* expanded (GGGGCC)160 repeat and flanks (+/-CpG-methylation) were performed to assess the impact of MNase sequence selectivity and the influence of CpG-methylation on digestibility. As shown in Figure S4B, the expanded repeat itself can be completely digested by MNase, and under the conditions used, the effect of sequence and CpG-methylation had limited effects on MNase digestibility, as previously reported (226, 227). This is consistent with the extensive number of the MNase-preferred 5′-NpT and 5′-NpA sites (226, 227) in the *C9orf72* sequences flanking the repeat, that are probed in the Southern blot (Fig. S2B, green font). These controls, coupled with the equal rate of MNase digestion of the protein-free *C9orf72* expanded allele in genomic DNA relative to the internal control of the non-expanded *C9orf72* allele (Fig. S4A-ii), demonstrates that the expanded repeat and flanks can be digested. Thus, the inaccessibility of MNase to the chromatinized *C9orf72* expanded allele and flanks (where the Southern probe binds), is due to its unusual chromatin compaction, and is not due to an inherent inability of MNase to cleave the expanded (GGGGCC)n DNA sequence.

Further mapping of the MNase accessibility in the chromatinized *C9orf72* expanded cells, with and without aberrant methylation, was performed. Essentially, for large expansions the

mutant *C9orf72* allele is less accessible to MNase ~3,300 bp upstream and ~2,500 bp downstream of the expanded repeat. Decreased accessibility is further exacerbated by aberrant methylation (detailed in Fig. SD4A-iii). The absolute boundaries of decreased MNase accessibility varied with repeat expansions.

Mapping MNase accessibility boundaries

We mapped the boundaries of MNase resistance in patient cell lines with no expansions (WT), expansions (P1, P7), and expansions with methylation (P3, P6), using a series of post-MNase restriction digests upstream and downstream of the repeat; fragments were detected by Southern blotting using either the 241 bp or 177 bp probe, as indicated. Upstream mapping was carried out with a post-MNase genomic digestion using *Ban*I, which cleaves just downstream of the repeat, in combination with either one of a series of restriction digests progressing along the upstream flank, as far as 3335bp upstream (*Afl*II, *Eco*RI, *Pvu*II, *Sph*I) (Fig. S4C). These samples were assessed by Southern blot, detected with the 177 bp probe (Fig. S4C upper panel, schematic). For each restriction fragment, the non-expanded allele signal was completely lost while the expanded allele was either resistant or partially digested to a shorter, distinct, nearly repeat-only containing fragment. This might suggest that the repeat tract itself is the most resistant to MNase accessibility. The amount of MNase-resistant starting material decreases progressively with increasing distance upstream from the repeat (Fig. S4C). Thus, the MNase resistance of the mutant allele extends upstream of the repeat at least ~1252 bp to the *Pvu*II site, where some of the full-length fragment is still inaccessible to MNase, but diminishes further upstream ~3335 bp to the *Sph*I site (Fig. S4C). Downstream mapping was conducted using a post-MNase genomic digestion with *Afl*II, which cleaves upstream of the repeat and beside the region detected by the 241 bp probe. *Afl*II digestion was paired with one of a series of restriction digests progressing along the downstream flank, as

far as 3750 bp downstream (*Ban*I, *Bst*YI, *Bam*HI, *Pvu*II, or *Psi*I) (Fig. S4C lower panel, schematic). For each restriction fragment, the expanded allele was resistant and progressively digested to a shorter, distinct nearly repeat-only containing fragment, again suggesting that the repeat tract is the most MNase resistant region. Resistance in the downstream region was more evident for the methylated allele, and for larger expansions. For the larger methylated sample, P3 (~3000 repeats), the MNase resistance of the mutant allele extends downstream of the repeat at least ~2440bp to the *Pvu*II site, where some of the full-length fragment is still inaccessible to MNase, but diminishes further downstream ~3750 bp to the *Psi*I site (Fig. S4C). For the shorter methylated expansion P6 (~770 repeats), the MNase resistance of the mutant allele extends downstream of the repeat at least ~1714bp to the *Bam*HI site, where some of the full-length fragment is still inaccessible to MNase, but diminishes further downstream ~3750bp to the *Psi*I site (Fig. S4C). Thus, the MNase resistance of the mutant allele extends at least ~2440 bp downstream from the repeat to the *Pvu*II site, where some of the full-length starting fragment is still resistant downstream ~3,750 bp to the distal *Psi*I site (Fig. S4C). The methylated and expanded allele was more resistant than the non-methylated expanded allele. In summary, for large expansions some of the mutant *C9orf72* alleles can be resistant to MNase ~1250 bp, diminishing through to ~3300 bp upstream and downstream resistance is ~2440 bp, diminishing through to ~3700 bp away from the expanded repeat, and resistance is further exacerbated by aberrant methylation.

Southern blot - *HTT*

Southern blotting for the *HTT* allele was followed as described (228), modifying the probe to be 226 bp, which anneals 143 bp upstream of the (CAG)n repeat tract, and used selected restriction-endonuclease digestions of genomic DNA – permitting sensitive detection of repeat size and length heterogeneity at molar levels. The 226 bp probe was produced by PCR using primers (Fwd: 5'-CTTGCTGTGTGAGGCAGAAC-3' and Rev: 5'-

CGCAGGTAAAAGCAGAACCT-3'). Molecular weight markers were run alongside the DNA (Gene Ruler Mix, Thermo Scientific, and Roche Molecular Weight Marker II).

Chromatin accessibility *in cellulo* with MNase

An HD patient fibroblast cell line, with an *HTT* expansion of (CAG)21/180 (GM09197) was assessed for MNase accessibility at *HTT*. Cell pellets were washed in ice-cold 1X PBS, re-pelleted, and permeabilized by ice-cold NP-40 lysis buffer (10 mM Tris pH 7.4, 10 mM NaCl, 3 mM $MgCl_2$, 0.5% NP-40, 0.15 mM spermine, 0.5 mM spermidine) for 5 min. on ice. Nuclei were collected at 200 *xg* (10 minutes, 4ºC), washed in 1X MNase digestion buffer (10 X stock: 100 mM Tris pH 7.4, 150 mM NaCl, 600 mM KCl, 5 mM spermidine, 1.5 mM spermine), re-pelleted, and subsequently resuspended in 1X MNase digestion buffer supplemented with 1mM $CaCl_2$. Treatment followed with MNase for 5 min. at 22ºC, at differing concentrations (0.5-20U). All digestion reactions were stopped with an equal volume of *Stop* solution (0.625 mg/mL proteinase K, 20 mM EDTA, 20 mM EGTA, 1% SDS diluted in 1X MNase buffer) and incubated at 37°C for a minimum of 1 hour. Reaction conditions were optimized to ensure over-digestion by MNase, which diminishes MNase cleavage preference. DNA was purified by phenol/chloroform extraction, RNase A treatment, and ethanol precipitation. A small amount of purified DNA was assessed for completeness of MNase digestion, by its conversion to mono-, di-, tri-nucleosome sized fragments as resolved by electrophoresis stained with ethidium bromide and visualized by UV imaging. 12 ug of each DNA sample was then restriction digested to completion to release the repeat-containing fragment and flanking regions – this increases resolution by electrophoresis. Following neutral transfer, the *HTT* containing regions were detected by Southern blot as described above.

RNA-seq library preparation, sequencing, and analysis

Total RNA from the lymphoblastoid cell lines was isolated using the hot TRIzol extraction protocol (229). Briefly, samples dissolved in TRIzol were incubated in a thermomixer set to 55°C and 1,000 rpm for 10 min. After cooling to ambient temperature, RNA was isolated by using TRIzol Reagent and the Direct-zol RNA MiniPrep Kit with DNase treatment according to manufacturer's provided protocol (Zymo Research). RNA was quantitated using Qubit RNA BR Assay Kit (Thermo Fisher Scientific). Strand-specific, rRNA-depleted RNA-seq libraries were prepared using the KAPA Stranded RNA-seq Kit with RiboErase HMR (Kapa Biosystems) per manufacturer's instructions, except for the use of custom Illumina-compatible index primers to allow multiplexing. Library size distribution was assessed using the High Sensitivity NGS Fragment Analysis Kit (DNF-747) on a Fragment Analyzer (Agilent). 2 × 150 paired-end sequencing was performed using an Illumina NextSeq 500. Reads were aligned to the genome assembly GRCh38 (hg38). Salmon was used for transcript expression quantification and differential gene expression analysis was performed using DESeq2(230, 231). A heat map was generated in R using the ggplot2 package. Graph was generated and statistical analysis was performed by using GraphPad Prism 8.

Developing murine Tissue-Derived Cell Lines

Mouse tissues for cytogenetic analysis of chromosomes followed published protocols (137–140, 232–237). Mouse care, sacrifice, and tissue harvesting was done on the same day, including three wild type and three transgenic mice, all 5 months of age. Mice aged 5-months, when cell proliferation in the CNS and peripheral organs had ceased at 2-months of age (137–139). Ear, lung, tail, cerebrum, cerebellum, brain stem, kidney, liver, and spleen were harvested. A section of each tissue was manually macerated then treated with DMEM + Trypsin-EDTA for 1 hour in a 37°C incubator. Cells were collected, spun down, then seeded in a T25 flask with DMEM media supplemented with 20% FBS and 2 mM L-Glutamate. Two flasks were prepared: One with 1% Pen/Strep added, and one without. Once confluent, cells

were seeded in a new T25 in DMEM (supplemented with 15% Fetal Bovine Serum, Penicillin/Streptomycin (100 IU/mL, 100 µg/mL), and 2 mM L-Glutamate to begin fragile site induction. To avoid cell type selection and cell type loss due to an inability to adapt to cell culture, harvested tissues were purposely cultured for very short terms following tissue harvesting. When possible, cells were grown to 80% confluency. Avoiding high cell densities, or long periods at confluency, has been shown to diminish FRAXA expression (234). Tissues were harvested and immediately made into cultures. These cultures were grown and induced to express the fragile sites and cytogenetically assessed. There was neither transit delays nor storage of cell lines until fragile sites were induced in metaphase. All procedures, including colony housing and tissue harvesting, were done in-house. Precautions were taken to avoid delays following tissue harvesting, tissue freezing, extended culturing and storage of cells, as these have been noted to diminish fragile site expression (234–237).

REFERENCES

1. Atanasio,A., Decman,V., White,D., Ramos,M., Ikiz,B., Lee,H.-C., Siao,C.-J., Brydges,S., LaRosa,E., Bai,Y., *et al.* (2016) C9orf72 ablation causes immune dysregulation characterized by leukocyte expansion, autoantibody production, and glomerulonephropathy in mice. *Sci Rep*, **6**, 23204.

2. Breevoort,S., Gibson,S., Figueroa,K., Bromberg,M. and Pulst,S. (2022) Expanding Clinical Spectrum of C9ORF72-Related Disorders and Promising Therapeutic Strategies: A Review. *Neurol Genet*, **8**, e670.

3. Fredi,M., Cavazzana,I., Biasiotto,G., Filosto,M., Padovani,A., Monti,E., Tincani,A., Franceschini,F. and Zanella,I. (2019) C9orf72 Intermediate Alleles in Patients with Amyotrophic Lateral Sclerosis, Systemic Lupus Erythematosus, and Rheumatoid Arthritis. *Neuromolecular Med*, **21**, 150–159.

4. McCauley,M.E., O'Rourke,J.G., Yáñez,A., Markman,J.L., Ho,R., Wang,X., Chen,S., Lall,D., Jin,M., Muhammad,A.K.M.G., *et al.* (2020) C9orf72 in myeloid cells suppresses STING-induced inflammation. *Nature*, **585**, 96–101.

5. Miller,Z.A., Sturm,V.E., Camsari,G.B., Karydas,A., Yokoyama,J.S., Grinberg,L.T., Boxer,A.L., Rosen,H.J., Rankin,K.P., Gorno-Tempini,M.L., *et al.* (2016) Increased prevalence of autoimmune disease within C9 and FTD/MND cohorts: Completing the picture. *Neurol Neuroimmunol Neuroinflamm*, **3**, e301.

6. van der Ende,E.L., Jackson,J.L., White,A., Seelaar,H., van Blitterswijk,M. and Van Swieten,J.C. (2021) Unravelling the clinical spectrum and the role of repeat length in C9ORF72 repeat expansions. *J Neurol Neurosurg Psychiatry*, **92**, 502–509.

7. Tábuas-Pereira,M., Almendra,L., Almeida,M.R., Durães,J., Pinho,A., Matos,A., Negrão,L., Geraldo,A. and Santana,I. (2019) Increased risk of melanoma in C9ORF72 repeat expansion carriers: A case-control study. *Muscle Nerve*, **59**, 362–365.

8. Chiò,A., Mazzini,L., D'Alfonso,S., Corrado,L., Canosa,A., Moglia,C., Manera,U., Bersano,E., Brunetti,M., Barberis,M., *et al.* (2018) The multistep hypothesis of ALS revisited: The role of genetic mutations. *Neurology*, **91**, e635–e642.

9. Van Wijk,I.F., Van Eijk,R.P.A., Van Boxmeer,L., Westeneng,H.-J., Van Es,M.A., Van Rheenen,W., Van Den Berg,L.H., Eijkemans,M.J.C. and Veldink,J.H. (2024) Assessment of risk of ALS conferred by the GGGGCC hexanucleotide repeat expansion in C9orf72 among first-degree relatives of patients with ALS carrying the repeat expansion. *Amyotroph Lateral Scler Frontotemporal Degener*, **25**, 188–196.

10. Waite,A.J., Bäumer,D., East,S., Neal,J., Morris,H.R., Ansorge,O. and Blake,D.J. (2014) Reduced C9orf72 protein levels in frontal cortex of amyotrophic lateral sclerosis and frontotemporal degeneration brain with the C9ORF72 hexanucleotide repeat expansion. *Neurobiol Aging*, **35**, 1779.e5-1779.e13.

11. Xiao,S., MacNair,L., McLean,J., McGoldrick,P., McKeever,P., Soleimani,S., Keith,J., Zinman,L., Rogaeva,E. and Robertson,J. (2016) C9orf72 isoforms in Amyotrophic Lateral Sclerosis and Frontotemporal Lobar Degeneration. *Brain Res.*, **1647**, 43–49.

1181 12. Marques,C., Held,A., Dorfman,K., Sung,J., Song,C., Kavuturu,A.S., Aguilar,C., Russo,T., Oakley,D.H.,
1182 Albers,M.W., *et al.* (2024) Neuronal STING activation in amyotrophic lateral sclerosis and
1183 frontotemporal dementia. *Acta Neuropathol*, **147**, 56.

1184 13. Pang,W. and Hu,F. (2023) C9ORF72 suppresses JAK-STAT mediated inflammation. *iScience*, **26**,
1185 106579.

1186 14. Masrori,P., Beckers,J., Gossye,H. and Van Damme,P. (2022) The role of inflammation in
1187 neurodegeneration: novel insights into the role of the immune system in C9orf72 HRE-
1188 mediated ALS/FTD. *Mol Neurodegener*, **17**, 22.

1189 15. Wang,Y., Liu,L., Chen,H., Yang,Y., Mu,C., Ren,H., Liu,Y., Yu,L., Fang,Q., Wang,G., *et al.* (2023)
1190 Disrupted phase behavior of FUS underlies poly-PR-induced DNA damage in amyotrophic
1191 lateral sclerosis. *Hum Mol Genet*, **33**, 64–77.

1192 16. Braems,E., Bercier,V., Van Schoor,E., Heeren,K., Beckers,J., Fumagalli,L., Dedeene,L., Moisse,M.,
1193 Geudens,I., Hersmus,N., *et al.* (2022) HNRNPK alleviates RNA toxicity by counteracting DNA
1194 damage in C9orf72 ALS. *Acta Neuropathol*, **144**, 465–488.

1195 17. Konopka,A. and Atkin,J.D. (2022) DNA Damage, Defective DNA Repair, and Neurodegeneration in
1196 Amyotrophic Lateral Sclerosis. *Front Aging Neurosci*, **14**, 786420.

1197 18. Maor-Nof,M., Shipony,Z., Lopez-Gonzalez,R., Nakayama,L., Zhang,Y.-J., Couthouis,J., Blum,J.A.,
1198 Castruita,P.A., Linares,G.R., Ruan,K., *et al.* (2021) p53 is a central regulator driving
1199 neurodegeneration caused by C9orf72 poly(PR). *Cell*, **184**, 689-708.e20.

1200 19. Andrade,N.S., Ramic,M., Esanov,R., Liu,W., Rybin,M.J., Gaidosh,G., Abdallah,A., Del'Olio,S.,
1201 Huff,T.C., Chee,N.T., *et al.* (2020) Dipeptide repeat proteins inhibit homology-directed DNA
1202 double strand break repair in C9ORF72 ALS/FTD. *Mol Neurodegener*, **15**, 13.

1203 20. Nihei,Y., Mori,K., Werner,G., Arzberger,T., Zhou,Q., Khosravi,B., Japtok,J., Hermann,A.,
1204 Sommacal,A., Weber,M., *et al.* (2020) Poly-glycine-alanine exacerbates C9orf72 repeat
1205 expansion-mediated DNA damage via sequestration of phosphorylated ATM and loss of
1206 nuclear hnRNPA3. *Acta Neuropathol*, **139**, 99–118.

1207 21. Lopez-Gonzalez,R., Yang,D., Pribadi,M., Kim,T.S., Krishnan,G., Choi,S.Y., Lee,S., Coppola,G. and
1208 Gao,F.-B. (2019) Partial inhibition of the overactivated Ku80-dependent DNA repair pathway
1209 rescues neurodegeneration in C9ORF72-ALS/FTD. *Proc Natl Acad Sci U S A*, **116**, 9628–9633.

1210 22. Konopka,A. and Atkin,J.D. (2018) The Emerging Role of DNA Damage in the Pathogenesis of the
1211 C9orf72 Repeat Expansion in Amyotrophic Lateral Sclerosis. *Int J Mol Sci*, **19**, E3137.

1212 23. Walker,C., Herranz-Martin,S., Karyka,E., Liao,C., Lewis,K., Elsayed,W., Lukashchuk,V., Chiang,S.-C.,
1213 Ray,S., Mulcahy,P.J., *et al.* (2017) C9orf72 expansion disrupts ATM-mediated chromosomal
1214 break repair. *Nat Neurosci*, **20**, 1225–1235.

1215 24. Farg,M.A., Konopka,A., Soo,K.Y., Ito,D. and Atkin,J.D. (2017) The DNA damage response (DDR) is
1216 induced by the C9orf72 repeat expansion in amyotrophic lateral sclerosis. *Hum Mol Genet*,
1217 **26**, 2882–2896.

1218 25. Lopez-Gonzalez,R., Lu,Y., Gendron,T.F., Karydas,A., Tran,H., Yang,D., Petrucelli,L., Miller,B.L.,
1219 Almeida,S. and Gao,F.-B. (2016) Poly(GR) in C9ORF72-Related ALS/FTD Compromises

1220 Mitochondrial Function and Increases Oxidative Stress and DNA Damage in iPSC-Derived
1221 Motor Neurons. *Neuron*, **92**, 383–391.

1222 26. van Blitterswijk,M., DeJesus-Hernandez,M., Niemantsverdriet,E., Murray,M.E., Heckman,M.G.,
1223 Diehl,N.N., Brown,P.H., Baker,M.C., Finch,N.A., Bauer,P.O., *et al.* (2013) Association between
1224 repeat sizes and clinical and pathological characteristics in carriers of C9ORF72 repeat
1225 expansions (Xpansize-72): a cross-sectional cohort study. *The Lancet. Neurology*, **12**, 978–
1226 988.

1227 27. Nordin,A., Akimoto,C., Wuolikainen,A., Alstermark,H., Jonsson,P., Birve,A., Marklund,S.L.,
1228 Graffmo,K.S., Forsberg,K., Brännström,T., *et al.* (2015) Extensive size variability of the
1229 GGGGCC expansion in C9orf72 in both neuronal and non-neuronal tissues in 18 patients with
1230 ALS or FTD. *Human Molecular Genetics*, **24**, 3133–3142.

1231 28. Akimoto,C., Volk,A.E., van Blitterswijk,M., Van den Broeck,M., Leblond,C.S., Lumbroso,S.,
1232 Camu,W., Neitzel,B., Onodera,O., van Rheenen,W., *et al.* (2014) A blinded international
1233 study on the reliability of genetic testing for GGGGCC-repeat expansions in C9orf72 reveals
1234 marked differences in results among 14 laboratories. *J Med Genet*, **51**, 419–424.

1235 29. Xi,Z., van Blitterswijk,M., Zhang,M., McGoldrick,P., McLean,J.R., Yunusova,Y., Knock,E.,
1236 Moreno,D., Sato,C., McKeever,P.M., *et al.* (2015) Jump from pre-mutation to pathologic
1237 expansion in C9orf72. *Am J Hum Genet*, **96**, 962–970.

1238 30. Xi,Z., Yunusova,Y., van Blitterswijk,M., Dib,S., Ghani,M., Moreno,D., Sato,C., Liang,Y., Singleton,A.,
1239 Robertson,J., *et al.* (2014) Identical twins with the C9orf72 repeat expansion are discordant
1240 for ALS. *Neurology*, **83**, 1476–1478.

1241 31. Sattler,R., Traynor,B.J., Robertson,J., Van Den Bosch,L., Barmada,S.J., Svendsen,C.N., Disney,M.D.,
1242 Gendron,T.F., Wong,P.C., Turner,M.R., *et al.* (2023) Roadmap for C9ORF72 in
1243 Frontotemporal Dementia and Amyotrophic Lateral Sclerosis: Report on the C9ORF72
1244 FTD/ALS Summit. *Neurol Ther*, **12**, 1821–1843.

1245 32. Cammack,A.J., Balendra,R. and Isaacs,A.M. (2024) Failure of C9orf72 sense repeat-targeting
1246 antisense oligonucleotides: lessons learned and the path forward. *Brain*, **147**, 2607–2609.

1247 33. Petri,S. (2024) Targeting C9orf72 in people with ALS. *Lancet Neurol*, **23**, 850–852.

1248 34. van den Berg,L.H., Rothstein,J.D., Shaw,P.J., Babu,S., Benatar,M., Bucelli,R.C., Genge,A., Glass,J.D.,
1249 Hardiman,O., Libri,V., *et al.* (2024) Safety, tolerability, and pharmacokinetics of antisense
1250 oligonucleotide BIIB078 in adults with C9orf72-associated amyotrophic lateral sclerosis: a
1251 phase 1, randomised, double blinded, placebo-controlled, multiple ascending dose study.
1252 *Lancet Neurol*, **23**, 901–912.

1253 35. Wave Life Sciences Announces Topline Results from Phase 1b/2a FOCUS-C9 Study of WVE-004
1254 for C9orf72-associated Amyotrophic Lateral Sclerosis and Frontotemporal Dementia - Wave
1255 Life Sciences.

1256 36. Tran,H., Moazami,M.P., Yang,H., McKenna-Yasek,D., Douthwright,C.L., Pinto,C., Metterville,J.,
1257 Shin,M., Sanil,N., Dooley,C., *et al.* (2022) Suppression of mutant C9orf72 expression by a
1258 potent mixed backbone antisense oligonucleotide. *Nat Med*, **28**, 117–124.

1259 37. Saracino,D. and Le Ber,I. (2022) How can we define the presymptomatic C9orf72 disease in 2022?
1260 An overview on the current definitions of preclinical and prodromal phases. *Rev Neurol*
1261 *(Paris)*, **178**, 426–436.

1262 38. Saracino,D. and Le Ber,I. (2021) Clinical Update on C9orf72: Frontotemporal Dementia,
1263 Amyotrophic Lateral Sclerosis, and Beyond. *Adv Exp Med Biol*, **1281**, 67–76.

1264 39. Mandrioli,J., Zucchi,E., Martinelli,I., Van der Most,L., Gianferrari,G., Moglia,C., Manera,U.,
1265 Solero,L., Vasta,R., Canosa,A., *et al.* (2023) Factors predicting disease progression in
1266 C9ORF72 ALS patients. *J Neurol*, **270**, 877–890.

1267 40. Westeneng,H.-J., van Veenhuijzen,K., van der Spek,R.A., Peters,S., Visser,A.E., van Rheenen,W.,
1268 Veldink,J.H. and van den Berg,L.H. (2021) Associations between lifestyle and amyotrophic
1269 lateral sclerosis stratified by C9orf72 genotype: a longitudinal, population-based, case-
1270 control study. *Lancet Neurol*, **20**, 373–384.

1271 41. Querin,G., Biferi,M.G. and Pradat,P.-F. (2022) Biomarkers for C9orf7-ALS in Symptomatic and
1272 Pre-symptomatic Patients: State-of-the-art in the New Era of Clinical Trials. *J Neuromuscul*
1273 *Dis*, **9**, 25–37.

1274 42. Rizzu,P., Blauwendraat,C., Heetveld,S., Lynes,E.M., Castillo-Lizardo,M., Dhingra,A., Pyz,E.,
1275 Hobert,M., Synofzik,M., Simón-Sánchez,J., *et al.* (2016) C9orf72 is differentially expressed in
1276 the central nervous system and myeloid cells and consistently reduced in C9orf72, MAPT
1277 and GRN mutation carriers. *Acta Neuropathol Commun*, **4**, 37.

1278 43. Niblock,M., Smith,B.N., Lee,Y.-B., Sardone,V., Topp,S., Troakes,C., Al-Sarraj,S., Leblond,C.S.,
1279 Dion,P.A., Rouleau,G.A., *et al.* (2016) Retention of hexanucleotide repeat-containing intron
1280 in C9orf72 mRNA: implications for the pathogenesis of ALS/FTD. *Acta Neuropathol Commun*,
1281 **4**, 18.

1282 44. Sznajder,Ł.J., Thomas,J.D., Carrell,E.M., Reid,T., McFarland,K.N., Cleary,J.D., Oliveira,R.,
1283 Nutter,C.A., Bhatt,K., Sobczak,K., *et al.* (2018) Intron retention induced by microsatellite
1284 expansions as a disease biomarker. *Proc Natl Acad Sci U S A*, **115**, 4234–4239.

1285 45. Ben-Dor,I., Pacut,C., Nevo,Y., Feldman,E.L. and Reubinoff,B.E. (2021) Characterization of C9orf72
1286 haplotypes to evaluate the effects of normal and pathological variations on its expression
1287 and splicing. *PLoS Genet*, **17**, e1009445.

1288 46. Sarkar,M.K., Hile,G.A., Tsoi,L.C., Xing,X., Liu,J., Liang,Y., Berthier,C.C., Swindell,W.R., Patrick,M.T.,
1289 Shao,S., *et al.* (2018) Photosensitivity and type I IFN responses in cutaneous lupus are driven
1290 by epidermal-derived interferon kappa. *Ann Rheum Dis*, **77**, 1653–1664.

1291 47. Harismendy,O., Notani,D., Song,X., Rahim,N.G., Tanasa,B., Heintzman,N., Ren,B., Fu,X.-D.,
1292 Topol,E.J., Rosenfeld,M.G., *et al.* (2011) 9p21 DNA variants associated with coronary artery
1293 disease impair interferon-γ signalling response. *Nature*, **470**, 264–268.

1294 48. Joung,J., Engreitz,J.M., Konermann,S., Abudayyeh,O.O., Verdine,V.K., Aguet,F., Gootenberg,J.S.,
1295 Sanjana,N.E., Wright,J.B., Fulco,C.P., *et al.* (2017) Genome-scale activation screen identifies a
1296 lncRNA locus regulating a gene neighbourhood. *Nature*, **548**, 343–346.

1297 49. Ahel,I., Rass,U., El-Khamisy,S.F., Katyal,S., Clements,P.M., McKinnon,P.J., Caldecott,K.W. and
1298 West,S.C. (2006) The neurodegenerative disease protein aprataxin resolves abortive DNA
1299 ligation intermediates. *Nature*, **443**, 713–716.

1300 50. Lim,G., Karaskova,J., Beheshti,B., Vukovic,B., Bayani,J., Selvarajah,S., Watson,S.K., Lam,W.L.,
1301 Zielenska,M. and Squire,J.A. (2005) An integrated mBAND and submegabase resolution tiling
1302 set (SMRT) CGH array analysis of focal amplification, microdeletions, and ladder structures
1303 consistent with breakage-fusion-bridge cycle events in osteosarcoma. *Genes Chromosomes*
1304 *Cancer*, **42**, 392–403.

1305 51. Fletcher,J.A., Gebhardt,M.C. and Kozakewich,H.P. (1994) Cytogenetic aberrations in
1306 osteosarcomas. Nonrandom deletions, rings, and double-minute chromosomes. *Cancer*
1307 *Genet Cytogenet*, **77**, 81–88.

1308 52. Giollant,M., Bertrand,S., Verrelle,P., Tchirkov,A., du Manoir,S., Ried,T., Mornex,F., Doré,J.F.,
1309 Cremer,T. and Malet,P. (1996) Characterization of double minute chromosomes' DNA
1310 content in a human high grade astrocytoma cell line by using comparative genomic
1311 hybridization and fluorescence in situ hybridization. *Hum Genet*, **98**, 265–270.

1312 53. Satinover,D.L., Vance,G.H., Van Dyke,D.L. and Schwartz,S. (2001) Cytogenetic analysis and
1313 construction of a BAC contig across a common neocentromeric region from 9p. *Chromosoma*,
1314 **110**, 275–283.

1315 54. Jee,K.J., Kim,Y.T., Kim,K.R., Aalto,Y. and Knuutila,S. (2001) Amplification at 9p in cervical
1316 carcinoma by comparative genomic hybridization. *Anal Cell Pathol*, **22**, 159–163.

1317 55. Sams,E.I., Ng,J.K., Tate,V., Claire Hou,Y.-C., Cao,Y., Antonacci-Fulton,L., Belhassan,K., Neidich,J.,
1318 Mitra,R.D., Cole,F.S., *et al.* (2022) From karyotypes to precision genomics in 9p deletion and
1319 duplication syndromes. *HGG Adv*, **3**, 100081.

1320 56. Shapiro,J.A. (2021) How Chaotic Is Genome Chaos? *Cancers (Basel)*, **13**, 1358.

1321 57. Bignell,G.R., Greenman,C.D., Davies,H., Butler,A.P., Edkins,S., Andrews,J.M., Buck,G., Chen,L.,
1322 Beare,D., Latimer,C., *et al.* (2010) Signatures of mutation and selection in the cancer genome.
1323 *Nature*, **463**, 893–898.

1324 58. Sutherland,G.R., Jacky,P.B., Baker,E. and Manuel,A. (1983) Heritable fragile sites on human
1325 chromosomes. X. New folate-sensitive fragile sites: 6p23, 9p21, 9q32, and 11q23. *Am J Hum*
1326 *Genet*, **35**, 432–437.

1327 59. Mirceta,M., Shum,N., Schmidt,M.H.M. and Pearson,C.E. (2022) Fragile sites, chromosomal
1328 lesions, tandem repeats, and disease. *Front Genet*, **13**, 985975.

1329 60. Sun,J.H., Zhou,L., Emerson,D.J., Phyo,S.A., Titus,K.R., Gong,W., Gilgenast,T.G., Beagan,J.A.,
1330 Davidson,B.L., Tassone,F., *et al.* (2018) Disease-Associated Short Tandem Repeats Co-localize
1331 with Chromatin Domain Boundaries. *Cell*, **175**, 224-238.e15.

1332 61. Reddy,K., Zamiri,B., Stanley,S.Y., Macgregor,R.B. and Pearson,C.E. (2013) The disease-associated
1333 r(GGGGCC)n repeat from the C9orf72 gene forms tract length-dependent uni- and
1334 multimolecular RNA G-quadruplex structures. *The Journal of biological chemistry*, **288**,
1335 9860–9866.

1336 62. Zamiri,B., Mirceta,M., Bomsztyk,K., Macgregor,R.B. and Pearson,C.E. (2015) Quadruplex
1337 formation by both G-rich and C-rich DNA strands of the C9orf72 (GGGGCC)8•(GGCCCC)8
1338 repeat: effect of CpG methylation. *Nucleic Acids Res*, **43**, 10055–10064.

1339 63. Fry,M. and Loeb,L.A. (1994) The fragile X syndrome d(CGG)n nucleotide repeats form a stable
1340 tetrahelical structure. *Proc Natl Acad Sci U S A*, **91**, 4950–4954.

1341 64. Xi,Z., Zhang,M., Bruni,A.C., Maletta,R.G., Colao,R., Fratta,P., Polke,J.M., Sweeney,M.G.,
1342 Mudanohwo,E., Nacmias,B., *et al.* (2015) The C9orf72 repeat expansion itself is methylated
1343 in ALS and FTLD patients. *Acta Neuropathol*, **129**, 715–727.

1344 65. Xi,Z., Zinman,L., Moreno,D., Schymick,J., Liang,Y., Sato,C., Zheng,Y., Ghani,M., Dib,S., Keith,J., *et*
1345 *al.* (2013) Hypermethylation of the CpG island near the G4C2 repeat in ALS with a C9orf72
1346 expansion. *Am J Hum Genet*, **92**, 981–989.

1347 66. Jackson,J.L., Finch,N.A., Baker,M.C., Kachergus,J.M., DeJesus-Hernandez,M., Pereira,K.,
1348 Christopher,E., Prudencio,M., Heckman,M.G., Thompson,E.A., *et al.* (2020) Elevated
1349 methylation levels, reduced expression levels, and frequent contractions in a clinical cohort
1350 of C9orf72 expansion carriers. *Mol Neurodegeneration*, **15**, 7.

1351 67. Xu,G.L., Bestor,T.H., Bourc'his,D., Hsieh,C.L., Tommerup,N., Bugge,M., Hulten,M., Qu,X., Russo,J.J.
1352 and Viegas-Péquignot,E. (1999) Chromosome instability and immunodeficiency syndrome
1353 caused by mutations in a DNA methyltransferase gene. *Nature*, **402**, 187–191.

1354 68. Hecht,F. and Sutherland,G.R. (1984) Detection of the fragile X chromosome and other fragile
1355 sites. *Clin Genet*, **26**, 301–303.

1356 69. Veenema,H., Beverstock,G.C., de Koning,T., Pearson,P.L. and van de Kamp,J.J. (1988) The fragile
1357 X-chromosome: an evaluation of the results in a routine cytogenetic laboratory in the period
1358 1981-1986. *Clin Genet*, **33**, 410–417.

1359 70. Cantú,E.S. and Jacobs,P.A. (1984) Fragile (X) expression: relationship to the cell cycle. *Hum Genet*,
1360 **67**, 99–102.

1361 71. Yu,S., Mangelsdorf,M., Hewett,D., Hobson,L., Baker,E., Eyre,H.J., Lapsys,N., Le Paslier,D.,
1362 Doggett,N.A., Sutherland,G.R., *et al.* (1997) Human chromosomal fragile site FRA16B is an
1363 amplified AT-rich minisatellite repeat. *Cell*, **88**, 367–374.

1364 72. Nancarrow,J.K., Kremer,E., Holman,K., Eyre,H., Doggett,N.A., Le Paslier,D., Callen,D.F.,
1365 Sutherland,G.R. and Richards,R.I. (1994) Implications of FRA16A structure for the mechanism
1366 of chromosomal fragile site genesis. *Science*, **264**, 1938–1941.

1367 73. Bosco,N., Pelliccia,F. and Rocchi,A. (2010) Characterization of FRA7B, a human common fragile
1368 site mapped at the 7p chromosome terminal region. *Cancer Genet Cytogenet*, **202**, 47–52.

1369 74. Callahan,G., Denison,S.R., Phillips,L.A., Shridhar,V. and Smith,D.I. (2003) Characterization of the
1370 common fragile site FRA9E and its potential role in ovarian cancer. *Oncogene*, **22**, 590–601.

1371 75. Curatolo,A., Limongi,Z.M., Pelliccia,F. and Rocchi,A. (2007) Molecular characterization of the
1372 human common fragile site FRA1H. *Genes Chromosomes Cancer*, **46**, 487–493.

1373 76. Rozier,L., El-Achkar,E., Apiou,F. and Debatisse,M. (2004) Characterization of a conserved
1374 aphidicolin-sensitive common fragile site at human 4q22 and mouse 6C1: possible
1375 association with an inherited disease and cancer. *Oncogene*, **23**, 6872–6880.

1376 77. Becker,N.A., Thorland,E.C., Denison,S.R., Phillips,L.A. and Smith,D.I. (2002) Evidence that
1377 instability within the FRA3B region extends four megabases. *Oncogene*, **21**, 8713–8722.

1378 78. Fechter,A., Buettel,I., Kuehnel,E., Savelyeva,L. and Schwab,M. (2007) Common fragile site
1379 FRA11G and rare fragile site FRA11B at 11q23.3 encompass distinct genomic regions. *Genes*
1380 *Chromosomes Cancer*, **46**, 98–106.

1381 79. Hirst,M.C., Rack,K., Nakahori,Y., Roche,A., Bell,M.V., Flynn,G., Christadoulou,Z., MacKinnon,R.N.,
1382 Francis,M. and Littler,A.J. (1991) A YAC contig across the fragile X site defines the region of
1383 fragility. *Nucleic Acids Research*, **19**, 3283.

1384 80. Verkerk,A.J., Eussen,B.H., Van Hemel,J.O. and Oostra,B.A. (1992) Limited size of the fragile X site
1385 shown by fluorescence in situ hybridization. *Am J Med Genet*, **43**, 187–191.

1386 81. Hirst,M.C., Barnicoat,A., Flynn,G., Wang,Q., Daker,M., Buckle,V.J., Davies,K.E. and Bobrow,M.
1387 (1993) The identification of a third fragile site, FRAXF, in Xq27--q28 distal to both FRAXA and
1388 FRAXE. *Hum Mol Genet*, **2**, 197–200.

1389 82. Ritchie,R.J., Knight,S.J., Hirst,M.C., Grewal,P.K., Bobrow,M., Cross,G.S. and Davies,K.E. (1994) The
1390 cloning of FRAXF: trinucleotide repeat expansion and methylation at a third fragile site in
1391 distal Xqter. *Hum Mol Genet*, **3**, 2115–2121.

1392 83. Abruzzo,M.A., Hunt,P.A., Mayer,M., Jacobs,P.A., Wang,J.C. and Erbe,R.W. (1986) A comparison of
1393 fragile X expression in lymphocyte and lymphoblastoid cultures. *Am J Hum Genet*, **38**, 533–
1394 539.

1395 84. Sutherland,G.R., Baker,E. and Callen,D.F. (1988) A BrdU-enhanceable fragile site or viral
1396 modification site at 11q23.1 in lymphoblastoid cultures. *Cytogenet Cell Genet*, **47**, 201–203.

1397 85. Seki,N., Tsuji,H., Takahashi,E., Yamauchi,M., Saito,T., Hashimoto,T., Yamamoto,K. and Hori,T.
1398 (1992) Induction of a BrdU-enhanceable fragile site-like lesion and sister chromatid
1399 exchanges at 11q23.1 in EBV-transformed lymphoblastoid cell lines. *Cytogenet Cell Genet*, **61**,
1400 95–98.

1401 86. Sutherland,G.R. and Baker,E. (2003) Forgotten fragile sites and related phenomena. *Cytogenet*
1402 *Genome Res*, **100**, 89–91.

1403 87. Li,J.S.Z., Abbasi,A., Kim,D.H., Lippman,S.M., Alexandrov,L.B. and Cleveland,D.W. (2023)
1404 Chromosomal fragile site breakage by EBV-encoded EBNA1 at clustered repeats. *Nature*, **616**,
1405 504–509.

1406 88. McGoldrick,P., Zhang,M., van Blitterswijk,M., Sato,C., Moreno,D., Xiao,S., Zhang,A.B.,
1407 McKeever,P.M., Weichert,A., Schneider,R., *et al.* (2018) Unaffected mosaic C9orf72 case:
1408 RNA foci, dipeptide proteins, but upregulated C9orf72 expression. *Neurology*, **90**, e323–e331.

1409 89. Belzil,V.V., Bauer,P.O., Prudencio,M., Gendron,T.F., Stetler,C.T., Yan,I.K., Pregent,L., Daughrity,L.,
1410 Baker,M.C., Rademakers,R., *et al.* (2013) Reduced C9orf72 gene expression in c9FTD/ALS is

1411 caused by histone trimethylation, an epigenetic event detectable in blood. *Acta Neuropathol*,
1412 **126**, 895–905.

1413 90. Cali,C.P., Patino,M., Tai,Y.K., Ho,W.Y., McLean,C.A., Morris,C.M., Seeley,W.W., Miller,B.L., Gaig,C.,
1414 Vonsattel,J.P.G., *et al.* (2019) C9orf72 intermediate repeats are associated with corticobasal
1415 degeneration, increased C9orf72 expression and disruption of autophagy. *Acta Neuropathol*,
1416 **138**, 795–811.

1417 91. Tassone,F., Hagerman,R.J., Taylor,A.K., Gane,L.W., Godfrey,T.E. and Hagerman,P.J. (2000)
1418 Elevated Levels of FMR1 mRNA in Carrier Males: A New Mechanism of Involvement in the
1419 Fragile-X Syndrome. *The American Journal of Human Genetics*, **66**, 6–15.

1420 92. Eberhart,D.E. and Warren,S.T. (1996) Nuclease sensitivity of permeabilized cells confirms altered
1421 chromatin formation at the fragile X locus. *Somat. Cell Mol. Genet.*, **22**, 435–441.

1422 93. Beverstock,G.C., Mol,A. and Wienhofer,E. (1985) Absence of significant autosomal lesions in
1423 Huntington's disease. *Ann Hum Genet*, **49**, 283–290.

1424 94. Krupina,K., Goginashvili,A. and Cleveland,D.W. (2021) Causes and consequences of micronuclei.
1425 *Curr Opin Cell Biol*, **70**, 91–99.

1426 95. Utani,K., Okamoto,A. and Shimizu,N. (2011) Generation of micronuclei during interphase by
1427 coupling between cytoplasmic membrane blebbing and nuclear budding. *PLoS One*, **6**,
1428 e27233.

1429 96. Fenech,M., Kirsch-Volders,M., Natarajan,A.T., Surralles,J., Crott,J.W., Parry,J., Norppa,H.,
1430 Eastmond,D.A., Tucker,J.D. and Thomas,P. (2011) Molecular mechanisms of micronucleus,
1431 nucleoplasmic bridge and nuclear bud formation in mammalian and human cells.
1432 *Mutagenesis*, **26**, 125–132.

1433 97. Fenech,M. (2007) Cytokinesis-block micronucleus cytome assay. *Nat Protoc*, **2**, 1084–1104.

1434 98. Shimizu,N., Itoh,N., Utiyama,H. and Wahl,G.M. (1998) Selective entrapment of
1435 extrachromosomally amplified DNA by nuclear budding and micronucleation during S phase.
1436 *J Cell Biol*, **140**, 1307–1320.

1437 99. Guttenbach,M. and Schmid,M. (1994) Exclusion of specific human chromosomes into micronuclei
1438 by 5-azacytidine treatment of lymphocyte cultures. *Exp Cell Res*, **211**, 127–132.

1439 100. Bjerregaard,V.A., Garribba,L., McMurray,C.T., Hickson,I.D. and Liu,Y. (2018) Folate deficiency
1440 drives mitotic missegregation of the human FRAXA locus. *Proc Natl Acad Sci U S A*, **115**,
1441 13003–13008.

1442 101. Duncan,A.M. (1986) Enhanced sensitivity of lymphoblastoid cells from individuals carrying the
1443 mutation for the fragile X syndrome to the clastogenic effects of FUdR. *Mutat Res*, **173**, 201–
1444 205.

1445 102. Shah,P., Wolf,K. and Lammerding,J. (2017) Bursting the Bubble - Nuclear Envelope Rupture as a
1446 Path to Genomic Instability? *Trends Cell Biol*, **27**, 546–555.

1447 103. Srivastava,N., Nader,G.P. de F., Williart,A., Rollin,R., Cuvelier,D., Lomakin,A. and Piel,M. (2021)
1448 Nuclear fragility, blaming the blebs. *Curr Opin Cell Biol*, **70**, 100–108.

1449 104. Stephens,A.D., Liu,P.Z., Banigan,E.J., Almassalha,L.M., Backman,V., Adam,S.A., Goldman,R.D.
1450 and Marko,J.F. (2018) Chromatin histone modifications and rigidity affect nuclear
1451 morphology independent of lamins. *Mol Biol Cell*, **29**, 220–233.

1452 105. Bercht Pfleghaar,K., Taimen,P., Butin-Israeli,V., Shimi,T., Langer-Freitag,S., Markaki,Y.,
1453 Goldman,A.E., Wehnert,M. and Goldman,R.D. (2015) Gene-rich chromosomal regions are
1454 preferentially localized in the lamin B deficient nuclear blebs of atypical progeria cells.
1455 *Nucleus*, **6**, 66–76.

1456 106. Niedernhofer,L.J., Gurkar,A.U., Wang,Y., Vijg,J., Hoeijmakers,J.H.J. and Robbins,P.D. (2018)
1457 Nuclear Genomic Instability and Aging. *Annu Rev Biochem*, **87**, 295–322.

1458 107. Fitchett,M. and Seabright,M. (1984) Deleted X chromosomes in patients with the fragile X
1459 syndrome. *J Med Genet*, **21**, 373.

1460 108. Verdyck,P., Berckmoes,V., De Vos,A., Verpoest,W., Liebaers,I., Bonduelle,M. and De Rycke,M.
1461 (2015) Chromosome fragility at FRAXA in human cleavage stage embryos at risk for fragile X
1462 syndrome. *Am J Med Genet A*, **167A**, 2306–2313.

1463 109. Polleys,E.J. and Freudenreich,C.H. (2018) Methods to Study Repeat Fragility and Instability in
1464 Saccharomyces cerevisiae. *Methods Mol Biol*, **1672**, 403–419.

1465 110. Wenger,S.L., Hennessey,J.C. and Steele,M.W. (1987) Increased sister chromatid exchange
1466 frequency at Xq27 site in affected fragile X males. *Am J Med Genet*, **26**, 909–914.

1467 111. van Wietmarschen,N., Merzouk,S., Halsema,N., Spierings,D.C.J., Guryev,V. and Lansdorp,P.M.
1468 (2018) BLM helicase suppresses recombination at G-quadruplex motifs in transcribed genes.
1469 *Nat Commun*, **9**, 271.

1470 112. Chan,K.L., Palmai-Pallag,T., Ying,S. and Hickson,I.D. (2009) Replication stress induces sister-
1471 chromatid bridging at fragile site loci in mitosis. *Nat Cell Biol*, **11**, 753–760.

1472 113. Chaganti,R.S., Schonberg,S. and German,J. (1974) A manyfold increase in sister chromatid
1473 exchanges in Bloom's syndrome lymphocytes. *Proc Natl Acad Sci U S A*, **71**, 4508–4512.

1474 114. Cunniff,C., Bassetti,J.A. and Ellis,N.A. (2017) Bloom's Syndrome: Clinical Spectrum, Molecular
1475 Pathogenesis, and Cancer Predisposition. *Mol Syndromol*, **8**, 4–23.

1476 115. Gratia,M., Rodero,M.P., Conrad,C., Bou Samra,E., Maurin,M., Rice,G.I., Duffy,D., Revy,P., Petit,F.,
1477 Dale,R.C., *et al.* (2019) Bloom syndrome protein restrains innate immune sensing of
1478 micronuclei by cGAS. *J Exp Med*, **216**, 1199–1213.

1479 116. Suzuki,T., Yasui,M. and Honma,M. (2016) Mutator Phenotype and DNA Double-Strand Break
1480 Repair in BLM Helicase-Deficient Human Cells. *Mol Cell Biol*, **36**, 2877–2889.

1481 117. Warren,S.T., Schultz,R.A., Chang,C.C., Wade,M.H. and Trosko,J.E. (1981) Elevated spontaneous
1482 mutation rate in Bloom syndrome fibroblasts. *Proc Natl Acad Sci U S A*, **78**, 3133–3137.

1483 118. Wenger,S.L. (1995) Chemical induction of sister chromatid exchange at fragile sites. *Cancer*
1484 *Genet Cytogenet*, **85**, 72–74.

1485 119. Kumar,J.V., Saraswathi,T., Ranganathan,K., Umadevi,K., Joshua,E. and Rooban,T. (2012) Sister
1486 chromatid exchanges in smokers and smokers with alcohol habit. *J Oral Maxillofac Pathol*, **16**,
1487 338–342.

1488 120. Glover,T.W. and Stein,C.K. (1987) Induction of sister chromatid exchanges at common fragile
1489 sites. *Am J Hum Genet*, **41**, 882–890.

1490 121. Fuster,C., Mirò,R., Templado,C., Barrios,L. and Egozcue,J. (1988) Can sister chromatid
1491 intercrossings be considered as prelesions? *Hum Genet*, **79**, 179–180.

1492 122. Gaddini,L., Pelliccia,F., Limongi,M.Z. and Rocchi,A. (1995) Study of the relationships between
1493 common fragile sites, chromosome breakages and sister chromatid exchanges. *Mutagenesis*,
1494 **10**, 257–260.

1495 123. Gregory,P., Wang,N. and Howard-Peebles,P.N. (1986) Analysis of sister chromatid exchanges in
1496 fra (X) individuals. *Am J Med Genet*, **23**, 563–566.

1497 124. Branda,R.F., Arthur,D.C., Woods,W.G., Danzl,T.J. and King,R.A. (1984) Folate metabolism and
1498 chromosomal stability in the fragile X syndrome. *Am J Med*, **77**, 602–611.

1499 125. Suleĭmanova,D.G. and Kuleshov,N.P. (1987) [Spontaneous and induced chromosome instability
1500 in patients with fragile X syndrome]. *Genetika*, **23**, 504–509.

1501 126. Schmid,M., Feichtinger,W. and Haaf,T. (1987) The fragile site (16)(q22). II. Sister chromatid
1502 exchanges. *Hum Genet*, **76**, 365–368.

1503 127. Hirsch,B. (1991) Sister chromatid exchanges are preferentially induced at expressed and
1504 nonexpressed common fragile sites. *Hum Genet*, **87**, 302–306.

1505 128. Lukusa,T., Meulepas,E., Fryns,J.P., Van den Berghe,H. and Cassiman,J.J. (1991) 'Spontaneous'
1506 FRA16B is a hot spot for sister chromatid exchanges. *Hum Genet*, **87**, 583–586.

1507 129. Recalcati,M.P., Bellini,M., Norsa,L., Ballarati,L., Caselli,R., Russo,S., Larizza,L. and Giardino,D.
1508 (2012) Complex rearrangement involving 9p deletion and duplication in a syndromic patient:
1509 genotype/phenotype correlation and review of the literature. *Gene*, **502**, 40–45.

1510 130. Korbel,J.O. and Campbell,P.J. (2013) Criteria for inference of chromothripsis in cancer genomes.
1511 *Cell*, **152**, 1226–1236.

1512 131. Kinsella,M., Patel,A. and Bafna,V. (2014) The elusive evidence for chromothripsis. *Nucleic Acids*
1513 *Res*, **42**, 8231–8242.

1514 132. Krupina,K., Goginashvili,A. and Cleveland,D.W. (2024) Scrambling the genome in cancer: causes
1515 and consequences of complex chromosome rearrangements. *Nat Rev Genet*, **25**, 196–210.

1516 133. Zhang,C.-Z., Spektor,A., Cornils,H., Francis,J.M., Jackson,E.K., Liu,S., Meyerson,M. and Pellman,D.
1517 (2015) Chromothripsis from DNA damage in micronuclei. *Nature*, **522**, 179–184.

1518 134. Leibowitz,M.L., Papathanasiou,S., Doerfler,P.A., Blaine,L.J., Sun,L., Yao,Y., Zhang,C.-Z., Weiss,M.J.
1519 and Pellman,D. (2021) Chromothripsis as an on-target consequence of CRISPR-Cas9 genome
1520 editing. *Nat Genet*, **53**, 895–905.

1521 135. Urnov,F.D. (2021) CRISPR-Cas9 can cause chromothripsis. *Nat Genet*, **53**, 768–769.

1522 136. Pattamatta,A., Nguyen,L., Olafson,H.R., Scotti,M.M., Laboissonniere,L.A., Richardson,J.,
1523 Berglund,J.A., Zu,T., Wang,E.T. and Ranum,L.P.W. (2021) Repeat length increases disease
1524 penetrance and severity in C9orf72 ALS/FTD BAC transgenic mice. *Hum Mol Genet*, **29**,
1525 3900–3918.

1526 137. Semenov,M. (2021) Proliferative Capacity of Adult Mouse Brain. *Int J Mol Sci*, **22**, 3449.

1527 138. Bordiuk,O.L., Smith,K., Morin,P.J. and Semënov,M.V. (2014) Cell proliferation and neurogenesis
1528 in adult mouse brain. *PLoS One*, **9**, e111453.

1529 139. Lui,J.C. and Baron,J. (2011) Mechanisms limiting body growth in mammals. *Endocr Rev*, **32**, 422–
1530 440.

1531 140. Sanz,M.M., Jenkins,E.C., Brown,W.T., Davisson,M.T., Kevin,M.J., Roderick,T.H., Silverman,W.P.
1532 and Wisniewski,H.M. (1986) Mouse chromosome fragility. *Am J Med Genet*, **23**, 491–509.

1533 141. Kähkönen,M., Tengström,C., Alitalo,T., Matilainen,R., Kaski,M. and Airaksinen,E. (1989)
1534 Population cytogenetics of folate-sensitive fragile sites. II. Autosomal rare fragile sites. *Hum*
1535 *Genet*, **82**, 3–8.

1536 142. Vasta,R., Chia,R., Traynor,B.J. and Chiò,A. (2022) Unraveling the complex interplay between
1537 genes, environment, and climate in ALS. *EBioMedicine*, **75**, 103795.

1538 143. Goncharova,P.S., Davydova,T.K., Popova,T.E., Novitsky,M.A., Petrova,M.M., Gavrilyuk,O.A., Al-
1539 Zamil,M., Zhukova,N.G., Nasyrova,R.F. and Shnayder,N.A. (2021) Nutrient Effects on Motor
1540 Neurons and the Risk of Amyotrophic Lateral Sclerosis. *Nutrients*, **13**, 3804.

1541 144. Cingam,S.R., Koshy,N., Veillon,D. and Peddi,P. (2017) Reversal of isolated 20q deletion with
1542 vitamin B12 replacement in a patient with pernicious anaemia. *BMJ Case Rep*, **2017**,
1543 bcr2016218689.

1544 145. Wollman,M.R., Penchansky,L. and Shekhter-Levin,S. (1996) Transient 7q- in association with
1545 megaloblastic anemia due to dietary folate and vitamin B12 deficiency. *J Pediatr Hematol*
1546 *Oncol*, **18**, 162–165.

1547 146. Goh,K. (1981) Vitamin B12 deficiency in an 18p--patient. *Arch Pathol Lab Med*, **105**, 164.

1548 147. Parmentier,S., Meinel,J., Oelschlaegel,U., Mohr,B., Ehninger,G., Schaich,M. and Platzbecker,U.
1549 (2012) Severe pernicious anemia with distinct cytogenetic and flow cytometric aberrations
1550 mimicking myelodysplastic syndrome. *Ann Hematol*, **91**, 1979–1981.

1551 148. Chintagumpala,M.M., Dreyer,Z.A., Steuber,C.P. and Cooley,L.D. (1996) Pancytopenia with
1552 chromosomal fragility: vitamin B12 deficiency. *J Pediatr Hematol Oncol*, **18**, 166–170.

1553 149. Maltby,E.L. and Higgins,S. (1987) Folate sensitive site at 10q23 and its expression as a deletion.
1554 *J Med Genet*, **24**, 299.

1555 150. Morel,C.F., Duncan,A.M.V. and Désilets,V. (2005) A fragile site at 10q23 (FRA10A) in a
1556 phenytoin-exposed fetus: a case report and review of the literature. *Prenat Diagn*, **25**, 318–
1557 321.

1558 151. De Leon-Luis,J., Santolaya-Forgas,J., May,G., Tonk,V., Shelton,D. and Galan,I. (2005) Prenatal
1559 diagnosis of FRA10A: a case report and literature review. *Am J Med Genet A*, **136**, 63–65.

1560 152. Ozisik,Y.Y., Meloni,A.M., Stone,J.F., Sandberg,A.A. and Surti,U. (1994) Spontaneous expression
1561 of the chromosome fragile site at 10q23 in leiomyoma. *Cancer Genet Cytogenet*, **74**, 73–75.

1562 153. Sarafidou,T., Kahl,C., Martinez-Garay,I., Mangelsdorf,M., Gesk,S., Baker,E., Kokkinaki,M.,
1563 Talley,P., Maltby,E.L., French,L., *et al.* (2004) Folate-sensitive fragile site FRA10A is due to an
1564 expansion of a CGG repeat in a novel gene, FRA10AC1, encoding a nuclear protein. *Genomics*,
1565 **84**, 69–81.

1566 154. Sashindran,V.K., Aggarwal,V. and Khera,A. (2022) Prevalence of Vitamin B12 deficiency in
1567 elderly population (>60 years) presenting with dementia to outpatient department. *Med J*
1568 *Armed Forces India*, **78**, 94–98.

1569 155. Pinto,W.B.V. de R., Souza,P.V.S. de, Rogério,R.M., Pedroso,J.L. and Barsottini,O.G.P. (2014)
1570 Vitamin B12 deficiency mimicking neuroimaging features of motor neuron disease. *Arq*
1571 *Neuropsiquiatr*, **72**, 85.

1572 156. Chen,A.T., Reidy,J.A., Annest,J.L., Welty,T.K. and Zhou,H.G. (1989) Increased chromosome
1573 fragility as a consequence of blood folate levels, smoking status, and coffee consumption.
1574 *Environ Mol Mutagen*, **13**, 319–324.

1575 157. Barale,R., Chelotti,L., Davini,T., Del Ry,S., Andreassi,M.G., Ballardin,M., Bulleri,M., He,J.,
1576 Baldacci,S., Di Pede,F., *et al.* (1998) Sister chromatid exchange and micronucleus frequency
1577 in human lymphocytes of 1,650 subjects in an Italian population: II. Contribution of sex, age,
1578 and lifestyle. *Environ Mol Mutagen*, **31**, 228–242.

1579 158. Maffei,F., Fimognari,C., Castelli,E., Stefanini,G.F., Forti,G.C. and Hrelia,P. (2000) Increased
1580 cytogenetic damage detected by FISH analysis on micronuclei in peripheral lymphocytes
1581 from alcoholics. *Mutagenesis*, **15**, 517–523.

1582 159. Demirhan,O. and Tastemir,D. (2008) Cytogenetic effects of ethanol on chronic alcohol users.
1583 *Alcohol Alcohol*, **43**, 127–136.

1584 160. Ueda,K., Sakai,C., Ishida,T., Morita,K., Kobayashi,Y., Horikoshi,Y., Baba,A., Okazaki,Y.,
1585 Yoshizumi,M., Tashiro,S., *et al.* (2023) Cigarette smoke induces mitochondrial DNA damage
1586 and activates cGAS-STING pathway: application to a biomarker for atherosclerosis. *Clin Sci*
1587 *(Lond)*, **137**, 163–180.

1588 161. Hesdorffer,C.S. and Longo,D.L. (2015) Drug-Induced Megaloblastic Anemia. *N Engl J Med*, **373**,
1589 1649–1658.

1590 162. Czuppa,M., Dhingra,A., Zhou,Q., Schludi,C., König,L., Scharf,E., Farny,D., Dalmia,A., Täger,J.,
1591 Castillo-Lizardo,M., *et al.* (2022) Drug screen in iPSC-Neurons identifies nucleoside analogs as
1592 inhibitors of (G4C2)n expression in C9orf72 ALS/FTD. *Cell Rep*, **39**, 110913.

1593 163. Chiurazzi,P., Pomponi,M.G., Pietrobono,R., Bakker,C.E., Neri,G. and Oostra,B.A. (1999)
1594 Synergistic effect of histone hyperacetylation and DNA demethylation in the reactivation of
1595 the FMR1 gene. *Hum Mol Genet*, **8**, 2317–2323.

1596 164. Lamparska,K., Clark,J., Babilonia,G., Bedell,V., Yip,W. and Smith,S.S. (2012) 2'-
1597 Deoxyriboguanylurea, the primary breakdown product of 5-aza-2'-deoxyribocytidine, is a
1598 mutagen, an epimutagen, an inhibitor of DNA methyltransferases and an inducer of 5-
1599 azacytidine-type fragile sites. *Nucleic Acids Res*, **40**, 9788–9801.

1600 165. Feichtinger,W. and Schmid,M. (1989) Increased frequencies of sister chromatid exchanges at
1601 common fragile sites (1)(q42) and (19)(q13). *Hum Genet*, **83**, 145–147.

1602 166. Rodríguez-Reyes,R. and Morales-Ramírez,P. (2011) The in vivo induction of sister chromatid
1603 exchange by the demethylating agent 5-aza-2'-deoxycytidine. *Mutagenesis*, **26**, 551–554.

1604 167. Haaf,T., Ott,G. and Schmid,M. (1986) Differential inhibition of sister chromatid condensation
1605 induced by 5-azadeoxycytidine in human chromosomes. *Chromosoma*, **94**, 389–394.

1606 168. Davidson,S., Crowther,P., Radley,J. and Woodcock,D. (1992) Cytotoxicity of 5-aza-2'-
1607 deoxycytidine in a mammalian cell system. *Eur J Cancer*, **28**, 362–368.

1608 169. Gijselinck,I., Van Mossevelde,S., van der Zee,J., Sieben,A., Engelborghs,S., De Bleecker,J.,
1609 Ivanoiu,A., Deryck,O., Edbauer,D., Zhang,M., *et al.* (2016) The C9orf72 repeat size correlates
1610 with onset age of disease, DNA methylation and transcriptional downregulation of the
1611 promoter. *Mol. Psychiatry*, **21**, 1112–1124.

1612 170. Kojak,N., Kuno,J., Fittipaldi,K.E., Khan,A., Wenger,D., Glasser,M., Donnianni,R.A., Tang,Y.,
1613 Zhang,J., Huling,K., *et al.* (2024) Somatic and intergenerational G4C2 hexanucleotide repeat
1614 instability in a human C9orf72 knock-in mouse model. *Nucleic Acids Res*, **52**, 5732–5755.

1615 171. Russ,J., Liu,E.Y., Wu,K., Neal,D., Suh,E., Irwin,D.J., McMillan,C.T., Harms,M.B., Cairns,N.J.,
1616 Wood,E.M., *et al.* (2015) Hypermethylation of repeat expanded C9orf72 is a clinical and
1617 molecular disease modifier. *Acta neuropathologica*, **129**, 39–52.

1618 172. Zhang,M., Tartaglia,M.C., Moreno,D., Sato,C., McKeever,P., Weichert,A., Keith,J., Robertson,J.,
1619 Zinman,L. and Rogaeva,E. (2017) DNA methylation age-acceleration is associated with
1620 disease duration and age at onset in C9orf72 patients. *Acta Neuropathol.*, **134**, 271–279.

1621 173. Zhang,M., McKeever,P.M., Xi,Z., Moreno,D., Sato,C., Bergsma,T., McGoldrick,P., Keith,J.,
1622 Robertson,J., Zinman,L., *et al.* (2020) DNA methylation age acceleration is associated with
1623 ALS age of onset and survival. *Acta Neuropathol*, **139**, 943–946.

1624 174. Galkin,F., Kovalchuk,O., Koldasbayeva,D., Zhavoronkov,A. and Bischof,E. (2023) Stress, diet,
1625 exercise: Common environmental factors and their impact on epigenetic age. *Ageing Res Rev*,
1626 **88**, 101956.

1627 175. Fitzgerald,K.N., Hodges,R., Hanes,D., Stack,E., Cheishvili,D., Szyf,M., Henkel,J., Twedt,M.W.,
1628 Giannopoulou,D., Herdell,J., *et al.* (2021) Potential reversal of epigenetic age using a diet and
1629 lifestyle intervention: a pilot randomized clinical trial. *Aging (Albany NY)*, **13**, 9419–9432.

1630 176. Sae-Lee,C., Corsi,S., Barrow,T.M., Kuhnle,G.G.C., Bollati,V., Mathers,J.C. and Byun,H.-M. (2018)
1631 Dietary Intervention Modifies DNA Methylation Age Assessed by the Epigenetic Clock. *Mol*
1632 *Nutr Food Res*, **62**, e1800092.

1633 177. Liu,Y., Huang,Z., Liu,H., Ji,Z., Arora,A., Cai,D., Wang,H., Liu,M., Simko,E.A.J., Zhang,Y., *et al.* (2023)
1634 DNA-initiated epigenetic cascades driven by C9orf72 hexanucleotide repeat. *Neuron*, **111**,
1635 1205-1221.e9.

1636 178. Rapkin,L.M., Ahmed,K., Dulev,S., Li,R., Kimura,H., Ishov,A.M. and Bazett-Jones,D.P. (2015) The
1637 histone chaperone DAXX maintains the structural organization of heterochromatin domains.
1638 *Epigenetics Chromatin*, **8**, 44.

1639 179. He,Q., Kim,H., Huang,R., Lu,W., Tang,M., Shi,F., Yang,D., Zhang,X., Huang,J., Liu,D., *et al.* (2015)
1640 The Daxx/Atrx Complex Protects Tandem Repetitive Elements during DNA Hypomethylation
1641 by Promoting H3K9 Trimethylation. *Cell Stem Cell*, **17**, 273–286.

1642 180. Scott,W.A., Dhanji,E.Z., Dyakov,B.J.A., Dreseris,E.S., Asa,J.S., Grange,L.J., Mirceta,M.,
1643 Pearson,C.E., Stewart,G.S., Gingras,A.-C., *et al.* (2021) ATRX proximal protein associations
1644 boast roles beyond histone deposition. *PLoS Genet*, **17**, e1009909.

1645 181. van Blitterswijk,M., Mullen,B., Nicholson,A.M., Bieniek,K.F., Heckman,M.G., Baker,M.C.,
1646 DeJesus-Hernandez,M., Finch,N.A., Brown,P.H., Murray,M.E., *et al.* (2014) TMEM106B
1647 protects C9ORF72 expansion carriers against frontotemporal dementia. *Acta Neuropathol*,
1648 **127**, 397–406.

1649 182. van Blitterswijk,M., Mullen,B., Heckman,M.G., Baker,M.C., DeJesus-Hernandez,M., Brown,P.H.,
1650 Murray,M.E., Hsiung,G.-Y.R., Stewart,H., Karydas,A.M., *et al.* (2014) Ataxin-2 as potential
1651 disease modifier in C9ORF72 expansion carriers. *Neurobiol Aging*, **35**, 2421.e13–17.

1652 183. van Blitterswijk,M., Mullen,B., Wojtas,A., Heckman,M.G., Diehl,N.N., Baker,M.C., DeJesus-
1653 Hernandez,M., Brown,P.H., Murray,M.E., Hsiung,G.-Y.R., *et al.* (2014) Genetic modifiers in
1654 carriers of repeat expansions in the C9ORF72 gene. *Mol Neurodegener*, **9**, 38.

1655 184. Pliner,H.A., Mann,D.M. and Traynor,B.J. (2014) Searching for Grendel: origin and global spread
1656 of the C9ORF72 repeat expansion. *Acta Neuropathol*, **127**, 391–396.

1657 185. Biasiotto,G. and Zanella,I. (2019) The effect of C9orf72 intermediate repeat expansions in
1658 neurodegenerative and autoimmune diseases. *Mult Scler Relat Disord*, **27**, 42–43.

1659 186. Burberry,A., Suzuki,N., Wang,J.-Y., Moccia,R., Mordes,D.A., Stewart,M.H., Suzuki-Uematsu,S.,
1660 Ghosh,S., Singh,A., Merkle,F.T., *et al.* (2016) Loss-of-function mutations in the C9ORF72
1661 mouse ortholog cause fatal autoimmune disease. *Sci Transl Med*, **8**, 347ra93.

1662 187. Béland,L.-C., Markovinovic,A., Jakovac,H., De Marchi,F., Bilic,E., Mazzini,L., Kriz,J. and Munitic,I.
1663 (2020) Immunity in amyotrophic lateral sclerosis: blurred lines between excessive
1664 inflammation and inefficient immune responses. *Brain Commun*, **2**, fcaa124.

1665 188. Burberry,A., Wells,M.F., Limone,F., Couto,A., Smith,K.S., Keaney,J., Gillet,G., van Gastel,N.,
1666 Wang,J.-Y., Pietilainen,O., *et al.* (2020) C9orf72 suppresses systemic and neural inflammation
1667 induced by gut bacteria. *Nature*, **582**, 89–94.

1668 189. Burgess,R.C., Burman,B., Kruhlak,M.J. and Misteli,T. (2014) Activation of DNA damage response
1669 signaling by condensed chromatin. *Cell Rep*, **9**, 1703–1717.

1670 190. Jacome,A. and Fernandez-Capetillo,O. (2011) Lac operator repeats generate a traceable fragile
1671 site in mammalian cells. *EMBO Rep*, **12**, 1032–1038.

1672 191. Soutoglou,E., Dorn,J.F., Sengupta,K., Jasin,M., Nussenzweig,A., Ried,T., Danuser,G. and Misteli,T.
1673 (2007) Positional stability of single double-strand breaks in mammalian cells. *Nat Cell Biol*, **9**,
1674 675–682.

1675 192. Soutoglou,E. and Misteli,T. (2008) Activation of the cellular DNA damage response in the
1676 absence of DNA lesions. *Science*, **320**, 1507–1510.

1677 193. Freaney,J.E., Zhang,Q., Yigit,E., Kim,R., Widom,J., Wang,J.-P. and Horvath,C.M. (2014) High-
1678 density nucleosome occupancy map of human chromosome 9p21-22 reveals chromatin
1679 organization of the type I interferon gene cluster. *J Interferon Cytokine Res*, **34**, 676–685.

1680 194. Apostolou,E. and Thanos,D. (2008) Virus Infection Induces NF-kappaB-dependent
1681 interchromosomal associations mediating monoallelic IFN-beta gene expression. *Cell*, **134**,
1682 85–96.

1683 195. Pang,W. and Hu,F. (2021) Cellular and physiological functions of C9ORF72 and implications for
1684 ALS/FTD. *J Neurochem*, **157**, 334–350.

1685 196. Quinodoz,S.A., Ollikainen,N., Tabak,B., Palla,A., Schmidt,J.M., Detmar,E., Lai,M.M., Shishkin,A.A.,
1686 Bhat,P., Takei,Y., *et al.* (2018) Higher-Order Inter-chromosomal Hubs Shape 3D Genome
1687 Organization in the Nucleus. *Cell*, **174**, 744-757.e24.

1688 197. Jagannathan,M. and Yamashita,Y.M. (2017) Function of Junk: Pericentromeric Satellite DNA in
1689 Chromosome Maintenance. *Cold Spring Harb Symp Quant Biol*, **82**, 319–327.

1690 198. Jagannathan,M., Cummings,R. and Yamashita,Y.M. (2018) A conserved function for
1691 pericentromeric satellite DNA. *Elife*, **7**, e34122.

1692 199. Malachowski,T., Chandradoss,K.R., Boya,R., Zhou,L., Cook,A.L., Su,C., Pham,K., Haws,S.A.,
1693 Kim,J.H., Ryu,H.-S., *et al.* (2023) Spatially coordinated heterochromatinization of long
1694 synaptic genes in fragile X syndrome. *Cell*, **186**, 5840-5858.e36.

1695 200. Droppelmann,C.A., Campos-Melo,D., Moszczynski,A.J., Amzil,H. and Strong,M.J. (2019) TDP-43
1696 aggregation inside micronuclei reveals a potential mechanism for protein inclusion
1697 formation in ALS. *Sci Rep*, **9**, 19928.

1698 201. Fritsch,L.E., Ju,J., Gudenschwager Basso,E.K., Soliman,E., Paul,S., Chen,J., Kaloss,A.M.,
1699 Kowalski,E.A., Tuhy,T.C., Somaiya,R.D., *et al.* (2022) Type I Interferon Response Is Mediated
1700 by NLRX1-cGAS-STING Signaling in Brain Injury. *Front Mol Neurosci*, **15**, 852243.

1701 202. Song,X., Ma,F. and Herrup,K. (2019) Accumulation of Cytoplasmic DNA Due to ATM Deficiency
1702 Activates the Microglial Viral Response System with Neurotoxic Consequences. *J Neurosci*,
1703 **39**, 6378–6394.

1704 203. Quek,H., Luff,J., Cheung,K., Kozlov,S., Gatei,M., Lee,C.S., Bellingham,M.C., Noakes,P.G., Lim,Y.C.,
1705 Barnett,N.L., *et al.* (2017) Rats with a missense mutation in Atm display neuroinflammation
1706 and neurodegeneration subsequent to accumulation of cytosolic DNA following unrepaired
1707 DNA damage. *J Leukoc Biol*, **101**, 927–947.

1708 204. Lupski,J.R. (2023) Somatic cell structural variant mutagenesis and neurologic disease. *Cell*
1709 *Genom*, **3**, 100376.

1710 205. Schuy,J., Grochowski,C.M., Carvalho,C.M.B. and Lindstrand,A. (2022) Complex genomic
1711 rearrangements: an underestimated cause of rare diseases. *Trends Genet*, **38**, 1134–1146.

1712 206. Campbell,I.M., Shaw,C.A., Stankiewicz,P. and Lupski,J.R. (2015) Somatic mosaicism: implications
1713 for disease and transmission genetics. *Trends Genet*, **31**, 382–392.

1714 207. Coffee,B., Ikeda,M., Budimirovic,D.B., Hjelm,L.N., Kaufmann,W.E. and Warren,S.T. (2008)
1715 Mosaic FMR1 deletion causes fragile X syndrome and can lead to molecular misdiagnosis: a
1716 case report and review of the literature. *Am J Med Genet A*, **146A**, 1358–1367.

1717 208. Gómez-Rodríguez,M.J., Morales-Conejo,M., Arteche-López,A., Sánchez-Calvín,M.T., Quesada-
1718 Espinosa,J.F., Gómez-Manjón,I., Palma-Milla,C., Lezana-Rosales,J.M., Pérez de la Fuente,R.,
1719 Martin-Ramos,M.-L., *et al.* (2022) Fragile X Syndrome Caused by Maternal Somatic
1720 Mosaicism of FMR1 Gene: Case Report and Literature Review. *Genes (Basel)*, **13**, 1609.

1721 209. Gonçalves,T.F., dos Santos,J.M., Gonçalves,A.P., Tassone,F., Mendoza-Morales,G., Ribeiro,M.G.,
1722 Kahn,E., Boy,R., Pimentel,M.M.G. and Santos-Rebouças,C.B. (2016) Finding FMR1 mosaicism
1723 in Fragile X syndrome. *Expert Rev Mol Diagn*, **16**, 501–507.

1724 210. Hensel,C.H., Vanzo,R.J., Martin,M.M., Ling,L., Aliaga,S.M., Bui,M., Francis,D.I., Twede,H.,
1725 Field,M.H., Morison,J.W., *et al.* (2019) Abnormally Methylated FMR1 in Absence of a
1726 Detectable Full Mutation in a U.S.A Patient Cohort Referred for Fragile X Testing. *Sci Rep*, **9**,
1727 15315.

1728 211. Prawer,Y., Hunter,M., Cronin,S., Ling,L., Aliaga Vera,S., Fahey,M., Gelfand,N., Oertel,R.,
1729 Bartlett,E., Francis,D., *et al.* (2018) Prenatal Diagnosis of Fragile X Syndrome in a Twin
1730 Pregnancy Complicated by a Complete Retraction. *Genes (Basel)*, **9**, 287.

1731 212. Pandelache,A., Francis,D., Oertel,R., Dickson,R., Sachdev,R., Ling,L., Gamage,D. and Godler,D.E.
1732 (2021) Detection of Cryptic Fragile X Full Mutation Alleles by Southern Blot in a Female and
1733 Her Foetal DNA via Chorionic Villus Sampling, Complicated by Mosaicism for
1734 45,X0/46,XX/47,XXX. *Genes (Basel)*, **12**, 798.

1735 213. Mätlik,K., Baffuto,M., Kus,L., Deshmukh,A.L., Davis,D.A., Paul,M.R., Carroll,T.S., Caron,M.-C.,
1736 Masson,J.-Y., Pearson,C.E., *et al.* (2023) Cell Type Specific CAG Repeat Expansions and
1737 Toxicity of Mutant Huntingtin in Human Striatum and Cerebellum. *bioRxiv*,
1738 10.1101/2023.04.24.538082.

1739 214. Pressl,C., Mätlik,K., Kus,L., Darnell,P., Luo,J.-D., Paul,M.R., Weiss,A.R., Liguore,W., Carroll,T.S.,
1740 Davis,D.A., *et al.* (2023) Selective Vulnerability of Layer 5a Corticostriatal Neurons in
1741 Huntington's Disease. *bioRxiv*, 10.1101/2023.04.24.538096.

1742 215. Albert,S.M. (2010) Neurodegenerative disease and cancer: a critical role for melanoma?
1743 *Neuroepidemiology*, **35**, 305–306.

1744 216. Baade,P.D., Herrero Hernández,E., Freedman,D.M., Smithers,B.M. and Fritschi,L. (2010) No role
1745 for melanoma treatment in the association between melanoma and amyotrophic lateral
1746 sclerosis or Parkinson's disease. *Neuroepidemiology*, **35**, 303–304.

1747 217. Baade,P.D., Fritschi,L. and Freedman,D.M. (2007) Mortality due to amyotrophic lateral sclerosis
1748 and Parkinson's disease among melanoma patients. *Neuroepidemiology*, **28**, 16–20.

1749 218. Freedman,D.M., Curtis,R.E., Daugherty,S.E., Goedert,J.J., Kuncl,R.W. and Tucker,M.A. (2013) The
1750 association between cancer and amyotrophic lateral sclerosis. *Cancer Causes Control*, **24**,
1751 55–60.

1752 219. Freedman,D.M., Travis,L.B., Gridley,G. and Kuncl,R.W. (2005) Amyotrophic lateral sclerosis
1753 mortality in 1.9 million US cancer survivors. *Neuroepidemiology*, **25**, 176–180.

1754 220. Akimoto,C., Volk,A.E., van Blitterswijk,M., Van den Broeck,M., Leblond,C.S., Lumbroso,S.,
1755 Camu,W., Neitzel,B., Onodera,O., van Rheenen,W., *et al.* (2014) A blinded international
1756 study on the reliability of genetic testing for GGGGCC-repeat expansions in C9orf72 reveals
1757 marked differences in results among 14 laboratories. *J Med Genet*, **51**, 419–424.

1758 221. Van Mossevelde,S., van der Zee,J., Cruts,M. and Van Broeckhoven,C. (2017) Relationship
1759 between C9orf72 repeat size and clinical phenotype. *Curr Opin Genet Dev*, **44**, 117–124.

1760 222. DeJesus-Hernandez,M., Mackenzie,I.R., Boeve,B.F., Boxer,A.L., Baker,M., Rutherford,N.J.,
1761 Nicholson,A.M., Finch,N.A., Flynn,H., Adamson,J., *et al.* (2011) Expanded GGGGCC
1762 hexanucleotide repeat in noncoding region of C9ORF72 causes chromosome 9p-linked FTD
1763 and ALS. *Neuron*, **72**, 245–256.

1764 223. Takahashi,E., Hori,T. and Murata,M. (1988) Population cytogenetics of rare fragile sites in Japan.
1765 *Hum Genet*, **78**, 121–126.

1766 224. Migliore,L., Coppedè,F., Fenech,M. and Thomas,P. (2011) Association of micronucleus
1767 frequency with neurodegenerative diseases. *Mutagenesis*, **26**, 85–92.

1768 225. Fenech,M., Kirsch-Volders,M., Natarajan,A.T., Surralles,J., Crott,J.W., Parry,J., Norppa,H.,
1769 Eastmond,D.A., Tucker,J.D. and Thomas,P. (2011) Molecular mechanisms of micronucleus,
1770 nucleoplasmic bridge and nuclear bud formation in mammalian and human cells.
1771 *Mutagenesis*, **26**, 125–132.

1772 226. Dingwall,C., Lomonossoff,G.P. and Laskey,R.A. (1981) High sequence specificity of micrococcal
1773 nuclease. *Nucleic Acids Res*, **9**, 2659–2673.

1774 227. Hörz,W. and Altenburger,W. (1981) Sequence specific cleavage of DNA by micrococcal nuclease.
1775 *Nucleic Acids Res*, **9**, 2643–2658.

1776 228. Bastepe,M. and Xin,W. (2015) Huntington Disease: Molecular Diagnostics Approach. *Curr Protoc*
1777 *Hum Genet*, **87**, 9.26.1-9.26.23.

1778 229. Nutter,C.A., Bubenik,J.L., Oliveira,R., Ivankovic,F., Sznajder,Ł.J., Kidd,B.M., Pinto,B.S., Otero,B.A.,
1779 Carter,H.A., Vitriol,E.A., *et al.* (2019) Cell-type-specific dysregulation of RNA alternative
1780 splicing in short tandem repeat mouse knockin models of myotonic dystrophy. *Genes Dev*,
1781 **33**, 1635–1640.

1782 230. Love,M.I., Huber,W. and Anders,S. (2014) Moderated estimation of fold change and dispersion
1783 for RNA-seq data with DESeq2. *Genome Biol*, **15**, 550.

1784 231. Patro,R., Duggal,G., Love,M.I., Irizarry,R.A. and Kingsford,C. (2017) Salmon provides fast and
1785 bias-aware quantification of transcript expression. *Nat Methods*, **14**, 417–419.

232. Angelosanto,F.A. (1995) Tissues other than bone marrow that can be used for cytogenetic analyses. *Environ Mol Mutagen*, **25**, 338–343.

233. Bayani,J. and Squire,J.A. (2004) Preparation of cytogenetic specimens from tissue samples. *Curr Protoc Cell Biol*, **Chapter 22**, Unit 22.2.

234. Krawczun,M.S., Lele,K.P., Jenkins,E.C. and Brown,W.T. (1986) Fragile X expression increased by low cell-culture density. *Am J Med Genet*, **23**, 467–473.

235. Fonatsch,C. and Schwinger,E. (1983) Frequency of fragile X chromosomes, fra(X), in lymphocytes in relation to blood storage time and culture techniques. *Hum Genet*, **64**, 39–41.

236. Brookwell,R., Daniel,A., Turner,G. and Fishburn,J. (1982) The fragile X(q27) form of X-linked mental retardation: FUdR as an inducing agent for fra(X)(q27) expression in lymphocytes, fibroblasts, and amniocytes. *Am J Med Genet*, **13**, 139–148.

237. Daniel,A., Ekblom,L. and Phillips,S. (1984) Constitutive fragile sites 1p31, 3p14, 6q26, and 16q23 and their use as controls for false-negative results with the fragile(X). *Am J Med Genet*, **18**, 483–491.

238. Bertrand,A., Wen,J., Rinaldi,D., Houot,M., Sayah,S., Camuzat,A., Fournier,C., Fontanella,S., Routier,A., Couratier,P., Pasquier,F., Habert,M.O., Hannequin,D., Martinaud,O., Caroppo,P., Levy,R., Dubois,B., Brice,A., Durrleman,S., Colliot,O., Le Ber,I.; Predict to Prevent Frontotemporal Lobar Degeneration and Amyotrophic Lateral Sclerosis (PREV-DEMALS) Study Group. (2018) Early Cognitive, Structural, and Microstructural Changes in Presymptomatic C9orf72 Carriers Younger Than 40 Years. *JAMA Neurol*, **75**, 236-245.

239. Querin,G., Bede,P., El Mendil,M.M., Li,M., Pélégrini-Issac,M., Rinaldi,D., Catala,M., Saracino,D., Salachas,F., Camuzat,A., Marchand-Pauvert,V., Cohen-Adad,J., Colliot,O., Le Ber,I., Pradat,P.F.; Predict to Prevent Frontotemporal Lobar Degeneration and Amyotrophic Lateral Sclerosis Study Group, (2019) Presymptomatic spinal cord pathology in c9orf72 mutation carriers: A longitudinal neuroimaging study. *Ann Neurol*, **86**(2):158-167.

ACKNOWLEDGEMENTS

This study is dedicated to the memory of Dr. Stephen T. Warren (1953-2021), a pioneer and advocate of Fragile X syndrome, a mentor, and friend. We thank Robert H. Brown for providing a YAC-*C9orf72* clone, John Volpe, Shamima Keka Islam for counting micronuclei, Lazar Joksimovic, and Raymond Wong for his expertise in the preparation of metaphase spreads. We thank Olivia Beck and Lieve Wiericx for sharing their expertise in cytogenetic fragile site recognition and Edwin Reyniers and Stephen W. Scherer, Jeff MacDonald, Mehdi Zarrei, Mehdi Layeghifard, and Bhooma Thiruvahindrapuram for help with the der-Chr9 data, and Michael Fenech for support regarding micronuclei, NBuds, and NBlebs.

DATA AVAILABILITY

Datasets generated during the current study supporting its findings have been deposited or made available as indicated:

- RNASeq gene expression data - available on Gene Expression Ombinus (GEO), accession #GSE262674.
- Whole genome sequencing data in the form of a CRAM file is available upon request to the corresponding author.

INCLUSION AND ETHICS STATEMENT

All collaborators of this study who have fulfilled the criteria for authorship required by *NAR Molecular Medicine* and Oxford University Press journals are included as authors. Each author's contribution is detailed in the Author Contributions list. Expectations for collaborators were agreed upon ahead of the study's initiation, and authorship placement was agreed upon by each collaborator. This study was conducted in collaboration with researchers and physicians from distinct cultural, ethnic, and racial backgrounds. The findings of this

study apply to members of the population globally, as well as locally in the regions where patient recruitment occurred. The research does not result in stigmatization, incrimination, discrimination, or personal risk to participants who provided samples. Local and regional research publications relevant to our study was considered and included in our bibliography.

The Hospital for Sick Children Research Ethics Board oversight and approval for the herein study was obtained. REB for human tissue, cell and animal studies: #1000056560.

AUTHOR CONTRIBUTIONS

Conceptualization: CEP and RFK

Fig. 1: CEP

Fig. 2: ML, MDW, CEP

Fig. 3: MM, MHMS, CEP, PAD, GAR, EK, MZ

Fig. 4: MM, IvdW, SS, RFK, CEP

Fig. 5: MHMS, TKP, CEP (sample collection by LZ, JK, AA, PMcG, PMcK, JR)

Fig. 6: MM*, MHMS, NS, SL, KY, MM†, MK, RKCY, PMcK, JR, LS, MSS, CEP

Fig. 7: NS, BM (training by MM*, MHMS, TKP)

Table 1: MM* , MK, and CEP

Fig. S1: ML, MDW, CEP

Fig. S2: MM*, MZ, ER, MHMS

Fig. S3: MM*, IvdW, SS, RFK

Fig. S4: MHMS

Fig. S5: MM*

Fig. S6: MM*, MM†, SL, NS, KY, MHMS, CEP

Fig. S7: TA, EAP, CHF

Fig. S8: RKCY, RFK, MM*, LS

Fig. S9: NS

Fig. S10: BM (training by MM*)

Table S1: MHMS

Table S2: LZ, JK, AA, PMcG, PMcK, JR, CEP

Table S3: LS, MK, PMcK, RKCY, JR, CEP

Table S4: MK, RKCY

BAC DNA for patient *C9orf72* provided by: CJ, PJdeJ

ALS patient cells provided by: PAD, GAR

Autopsy tissues prepared by: LZ, PMK, JR

Intellectual input and experimental design: CEP, RFK, EC, RW, MDW, MSS, ER

Supervision: CEP and RFK

Writing – original draft: MM*, CEP

Writing – review & editing: CEP, MHMS, NS, MSS, MM†

All authors provided feedback on the manuscript.

MM* = Mila Mirceta

MM† = Mohiuddin Mohiuddin

FUNDING

This work was supported by the ALS Canada-Brain Canada 2020 Discovery Grant [HSC0005599 to C.E.P., E.R., G.A.R.]; ALS Canada Doctoral Research Award 2016 [to M.H.M.S.]; the Weston Family Foundation [TR202268 to C.E.P.]; the W. Garfield Weston Foundation [CNV0001757 to C.E.P.]; the National Institutes of Health [GM122880 to C.H.F.]; and the National Natural Science Foundation of China [82071430 to M.Z., E.R.]; James Hunter and Family ALS Initiative [J.R. and E.R.]; Canadian Consortium on Neurodegeneration in Aging [to G.A.R. and E.R.].

COMPETING INTERESTS

The authors declare no competing interests.

SUPPLEMENTARY INFORMATION

Supplementary information is available for this paper by request.

MATERIALS AVAILABILITY

Correspondence and requests for materials should be addressed to Dr. Christopher E. Pearson (mail to: cepearson.sickkids@gmail.com). Mouse models presented in this study are commercially available from Jackson Laboratories (FVB/NJ-Tg(C9orf72)500Lpwr/J).